MODELING AND EXPERIMENTAL VERIFICATION OF DYNAMIC CHARACTERISTICS OF THE ANTENNA STRUCTURE UNDER MECHANICAL SHOCK USING MDOF MODELS

A THESIS SUBMITTED TO
THE GRADUATE SCHOOL OF NATURAL AND APPLIED SCIENCES
OF
MIDDLE EAST TECHNICAL UNIVERSITY

BY

YUNUS EMRE ÖZÇELİK

IN PARTIAL FULFILLMENT OF THE REQUIREMENTS
FOR
THE DEGREE OF MASTER OF SCIENCE
IN
MECHANICAL ENGINEERING

DECEMBER 2015

Approval of the thesis:

MODELIN AND EXPERIMENTAL VERIFICATION OF DYNAMIC CHARACTERISTIC OF THE ANTENNA STRUCTURE UNDER MECHANICAL SHOCK USING MDOF MODELS

submitted by **YUNUS EMRE ÖZÇELİK** in partial fulfillment of the requirements for the degree of **Master of Science in Mechanical Engineering Department, Middle East Technical University by,**

Prof. Dr. Gülbin Dural Ünver
Dean, Graduate School of **Natural and Applied Sciences** _____

Prof. Dr. Tuna Balkan
Head of Department, **Mechanical Engineering** _____

Assoc. Prof. Ender Ciğeroğlu
Supervisor, **Mechanical Engineering Dept., METU** _____

Prof. Dr. Mehmet Çalışkan
Co-Supervisor, **Mechanical Engineering Dept., METU** _____

Examining Committee Members:

Assoc. Prof. Dr. Yiğit Yazıcıoğlu
Mechanical Engineering Dept., METU _____

Assoc. Prof. Dr. Ender Ciğeroğlu
Mechanical Engineering Dept., METU _____

Prof. Dr. Mehmet Çalışkan
Mechanical Engineering Dept., METU _____

Assist. Prof. Dr. O. Gökhan Özgen
Mechanical Engineering Dept., METU _____

Assist. Prof. Dr. Mehmet Bülent Özer
Mechanical Engineering Dept., TOBB ETU _____

Date: _____

I hereby declare that all information in this document has been obtained and presented in accordance with academic rules and ethical conduct. I also declare that, as required by these rules and conduct, I have full cited and referenced all material and results that are not original to this work.

Name, Last name : Yunus Emre ÖZÇELİK
Signature :

ABSTRACT

MODELING AND EXPERIMENTAL VERIFICATION OF DYNAMIC CHARACTERISTICS ANTENNA STRUCTURE UNDER MECHANICAL SHOCK USING MDOF MODEL

Özçelik, Yunus Emre

M.S., Department of Mechanical Engineering

Supervisor: Assoc. Prof. Dr. Ender Ciğeroğlu

Co-supervisor: Prof. Dr. Mehmet Çalışkan

December 2015, 118 pages

Antenna structures used in electronic warfare, radar, naval, satellite, spacecraft systems encounter mechanical shock from various sources such as near miss under water explosion, pyrotechnic and ballistic shocks. Since most antenna structures have larger dimension in longitudinal direction and experience high frequency, high amplitude shock energy, geometric nonlinearity becomes crucial to predict dynamic behavior in real life. In this thesis, an antenna structure is modeled by Euler-Bernoulli beam theory including geometrical and inertia nonlinearities. The resulting partial differential equations of motions are converted into a set of nonlinear ordinary differential equations (ODEs) by using Galerkin's Method, which are solved by Newmark and Backward Euler time integration methods. The results for the linear system obtained from time integration and approximate methods such as Absolute Method, Square Root of Sum of Squares (SRSS), Naval Research Method, Combined Quadratic Combination (CQC) and Shock Response Spectrum Method (SRS) are compared to the nonlinear ones. Moreover, these results are compared with the ones obtained from commercial Finite Element software as well as experimental results from a drop test table.

Keywords: Antenna Structure, Mechanical Shock, Nonlinear Dynamic Analysis, Finite Element Method, Mechanical Shock Testing

ÖZ

MEKANİK ŞOK ALTINDAKİ ANTENLERİN DİNAMİK KARAKTERİSTİĞİNİN ÇOKLU SERBESTLİK DERECESİNE SAHİP SİSTEMLERLE MODELLENMESİ VE DENEY İLE DOĞRULANMASI

Özçelik, Yunus Emre
Yüksek Lisans, Makina Mühendisliği Bölümü
Tez Yöneticisi: Doç. Dr. Ender Ciğeroğlu
Ortak Tez Yöneticisi:Prof. Dr. Mehmet Çalışkan
Aralık 2015, 118 sayfa

Anten yapıları elektronik harp, radar, deniz, uydu ve uzay sistemlerinde sıklıkla kullanılmaktadır. Belirtilen uygulama alanlarında kullanılan anten yapıları temassız deniz altı patlaması, piroteknik ve balistik patlama gibi faktörlerden dolayı mekanik şoka maruz kalmaktadır. Anten yapılarının çoğunun boyu uzun ve bu yapılar yüksek frekans ve büyüklükte mekanik şoka maruz kaldıklarından dolayı, geometrik ve ataletsel doğrusal olmamama durumunun matematiksel modellemeye dâhil edilmesi daha gerçekçi sonuç verecektir. Bu tezde anten yapısı Euler-Bernoulli kiriş teorisi kullanarak geometrik ve ataletsel doğrusal olmama durumu da göz önünde bulundurularak sürekli biçimde modellenmiştir. Oluşan doğrusal olmayan kısmi diferansiyel denklemler Galerkin metodu kullanılarak doğrusal olmayan bayağı diferansiyel denklemlere dönüştürüldü. Bu denklemler Newmark ve geriye Euler zaman integrasyon metotları yardımıyla çözülür. Ayrıca anten yapısında oluşan maksimum ivme ve göreceli sehim, Mutlak Metot, Karelerinin Toplamının Karekökü, Naval Araştırma Metodu, Birleşik Karasel Kombinasyonu gibi yaklaşık

sonuç veren metotlar ile karşılaştırılmıştır. Dahası, bu sonuçlar ticari sonlu elemanlar yazılımı ve düşürme tablası ile yapılan deney sonuçları ile karşılaştırıldı.

Anahtar Kelimeler: Anten Yapıları, Mekanik Şok, Doğrusal Olmayan Dinamik Analiz, Sonlu Elemanlar Metodu, Mekanik Şok Testi

To Seherim

ACKNOWLEDGEMENTS

I would like to express my sincere gratitude to my supervisor Assoc. Prof. Dr. Ender CİĞEROĞLU and my co-supervisor Prof. Dr. Mehmet ÇALIŞKAN for their excellent supervision and leading guidance from the beginning to the end of my thesis work which made this study possible.

I am grateful to my dear mother Naciye ÖZÇELİK, my dear father Ramazan ÖZÇELİK , my dear brother Hasan Yasin ÖZÇELİK and my dear sister Şevval ÖZÇELİK for their endless love and vulnerable support throughout my life.

I would also like to express my sincere appreciation for Evren Kutlu, Mehmet Emre Demir, Yusuf Başıbüyük for their valuable friendship, motivation and help.

I would like to thank TÜBİTAK for providing financial support during the study.

TABLE OF CONTENTS

LIST OF TABLES

TABLES

LIST OF FIGURES

FIGURES

LIST OF SYMBOLS

m	: Mass per unit length
ω_n	: Natural frequency
$\phi(x)$	: Assumed mode shape function
l	: Length of an antenna structure
ρ	: Density of an antenna's material
A	: Cross section of an antenna
EI	: Flexural rigidity
$w(x)$	: Assumed displacement function
k_{eq}	: Equivalent stiffness
m_{eq}	: Equivalent mass
c_{eq}	: Equivalent damping
$\dot{y}$	: Velocity of base
y	: Displacement of base
z	: Relative displacement
$\dot{z}$	: Relative velocity
$\ddot{z}$	: Relative acceleration
$w(x,t)$	: Transverse deflection of an antenna
c	: Viscous damping coefficient
$F(x,t)$	: Distributed force
T	: Time scale parameter
β	: Frequency parameter
a_{max}	: Maximum value of mechanical shock
a_{pulse}	: Unit mechanical shock profile
c_{non}	: Nondimensional damping term
F_{non}	: Nondimensional forcing term

$u_i(t)$: Generalized coordinate

n : Number of modes

ζ_i : Modal damping ratio of i^{th} mode

α_{in} : Nondimensional inertia term

Δt : Time step

$\Delta t_{critical}$: Critical time step

τ_n : Natural period of a system

$\mathbf{M}$: Mass matrix

$\mathbf{C}$: Damping matrix

$\mathbf{p}$: External load vector

$\mathbf{f}_d$: Internal damping force vector

$\mathbf{f}_s$: Internal spring vector

k_t : Tangent stiffness matrix

w_{max} : Maximum relative displacement

x_{stat} : Maximum static deformation

Γ_n : Modal participation factor

CHAPTER 1

INTRODUCTION

1.1 Introduction to the Problem

In all around the world, approximately 40 % of the total world population uses the internet [1] and cell phones are used by around 97 people out of every 100 people [2], which can provide a valid evidence for the idea that wireless communication is commonly used worldwide. These infrastructures communicate with each other via antennas. In other words, the Internet and cell phones services are not functional without antennas. Thus, it can be said that the antenna structure is an irreplaceable component of electronic systems. IEEE defines what antenna does as “transmitting or receiving electromagnetic waves”. In other words, the antenna structure converts electrical signal into electromagnetic or electrical signal (see Figure 1.1) [3].

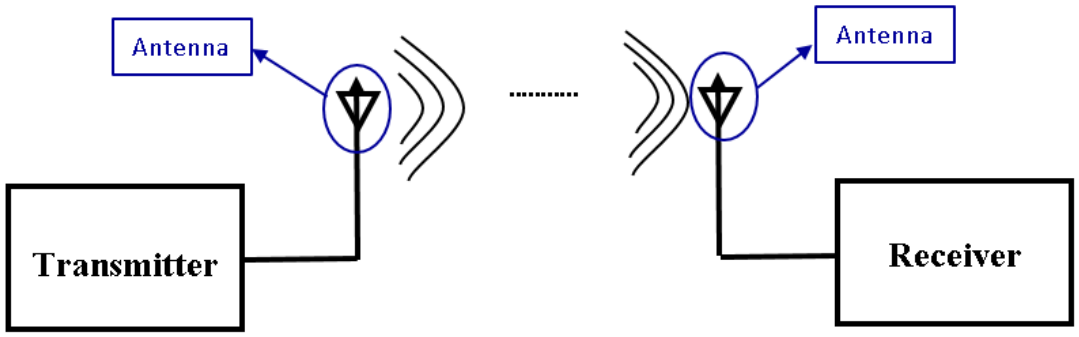

Figure 1.1 Wireless communication using antenna

For military applications, the antenna structures are used in electronic warfare (EW), radar, naval, satellite and spacecraft systems so that the devices and vehicles including these systems can communicate with each other (see Figure 1.2). For

example, a warplane can track other warplanes via the antenna structure in the radar systems.

Figure 1.2 Military communication system [4]

Some antenna types being used in civilian and military systems are listed below [3];

- Wire Antenna
    - Dipole Antennas
    - Monopoles Antennas (see Figure 1.3)
    - Loops Antennas
    - Helix Antennas
- Aperture Antennas
- Antenna Array
- Frequency-Independent Antennas
- Microstrip Patch Antennas
- Fractal Antennas
- Genetically Designed Antennas
- Active Antennas

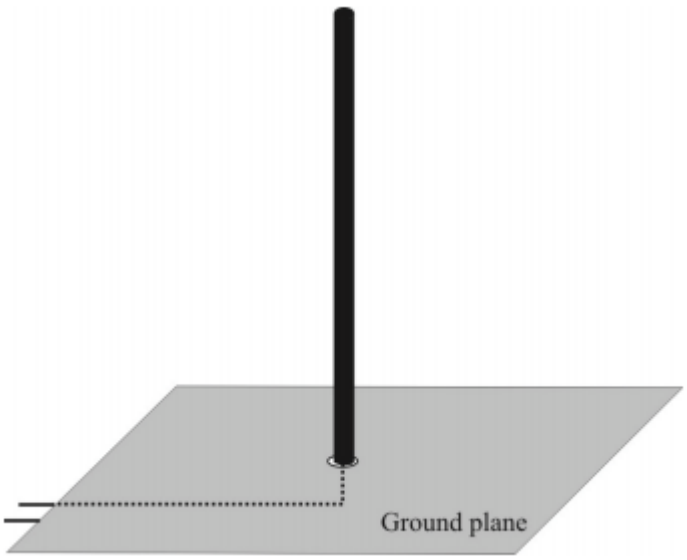

Figure 1.3 Monopole antenna structure [3]

The antenna structures are generally made up of high conductive materials, since the performance of antenna structure is proportional to conductivity of the material [5]. Table 1.1 below summarizes the most widely used materials in antenna structures.

Table 1.1 Conductivity of some common materials [5]

Material	**Conductivity (S/m)**	**Material**	**Conductivity (S/m)**
Silver	6.30E+07	Zinc	1.70E+07
Copper	5.80E+07	Brass	1.00E+07
Gold	4.10E+07	Phosphor Bronze	1.00E+07
Aluminum	3.50E+07	Tin	9.00E+06
Tungsten	1.80E+07	Lead	5.00E+06

However, the antenna structures being used in military and civilian systems can encounter many mechanical shocks from various sources such as near miss under water explosion, ballistic shock due explosion of mine, pyrotechnic shock, and so forth. Mechanical shock can be described as “a sudden and violent change in the state of motion of the component parts or particles of a body or medium resulting from sudden application of a relatively large external force, such as a blow or impact” according to first Shock and Vibration Symposium in 1947 [6]. Generally mechanical shocks contain high amplitude and rich frequency energy since the

duration of mechanical shock is measured in milliseconds and the amplitude may be as high as 10000 G (see Figure 1.4)

Therefore, even if only one of the antennas in the electronic warfare and communication systems shown in Figure 1.2 is broken down due to a mechanical shock which it receives, the whole system will be unable to function well. For example, a printed circuit board (PCB), which is printed on the antenna structure, may be damaged due to exposure of a high level of mechanical shock, and as a result of this, the system becomes dysfunctional. Therefore, the antenna structures must be designed to withstand mechanical shocks to ensure its reliability.

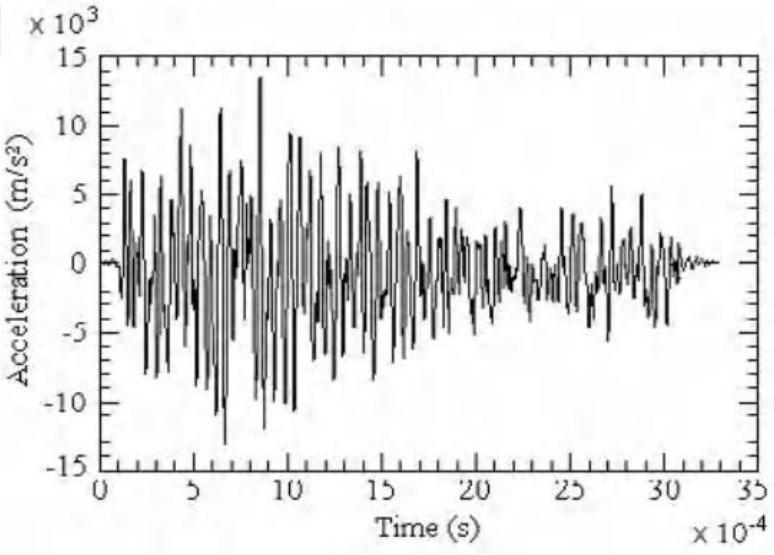

Figure 1.4 Time history of mechanical shock [7]

Especially in military, it is vital that all electronic and mechanical systems should withstand mechanical shock types which are explained briefly below.

1.1.1 Transportation and Handling Shock

Electronic and mechanical systems used in military and civilian applications may experience mechanical shocks during the transportation and handling of materials due to human errors. For instance, while a military armored vehicle is running over a bump at unwary speed, all systems including antennas are exposed to mechanical shocks. Therefore, in military applications, all systems are designed to withstand the

mechanical shocks. During the qualification procedure, some military standards are used to check the endurance of systems when they encounter any transportation and handling shocks. For example, Table 1.2 and Figure 1.5 allow a better understanding of what test qualification values of transportation and material handling shocks are according to MIL-STD-810G

Table 1.2 Terminal peak sawtooth pulse parameters for transportation and material handling [8]

	Peak Value [g]		**Nominal Duration [ms]**	
	Flight Vehicle Equipment	**Ground Equipment**	**Flight Vehicle Equipment**	**Ground Equipment**
Transportation and Material Handling Shock	20	40	11	11

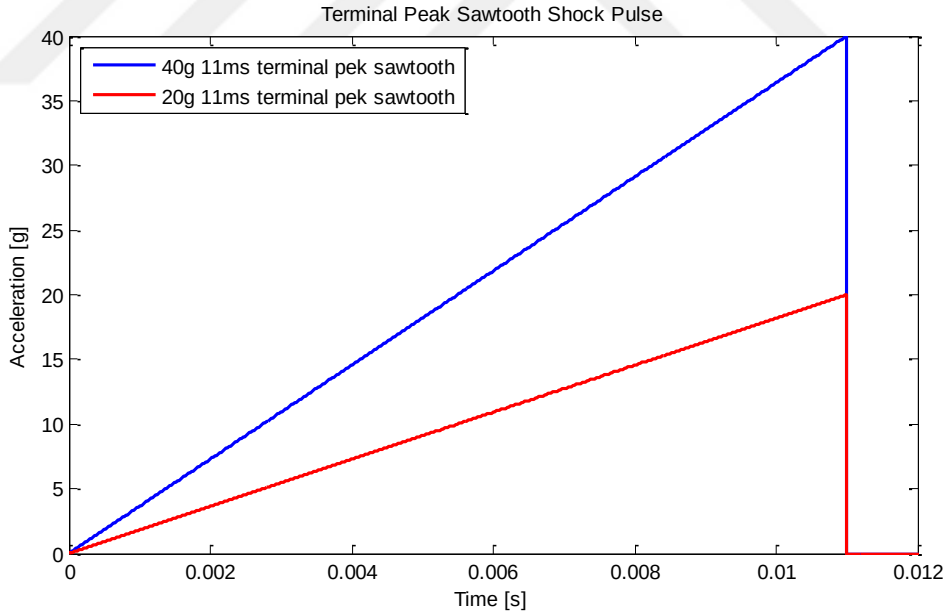

Figure 1.5 Time history of terminal peak sawtooth shock pulse [8]

1.1.2 Ballistic Shock

Ballistic shock is a shock containing high amplitude and high frequency which is mainly caused by the impact of non-perforating mine blasts, projectiles or ordnances

on armored vehicles [8]. Figure 1.6 displays the ballistic shock response taken on outer surface M113 armored personnel carrier. As seen in Figure 1.6, while shock amplitude is very high, the duration of shock is very short.

Some physical properties of ballistic shock are given below [8];

- Ballistic shock can cause high strain rates
- The frequency contents is high, broadbanding from10 Hz to 1,000,000 Hz. since the duration of ballistic shock is very short.
- High acceleration input (300 g – 1,000,000 g) is developed, since ballistic shock contains high level energy. As a result, high acceleration, velocity and displacement responses are observed on electronic and mechanical systems which are exposed to ballistic shock (see Figure 1.6).

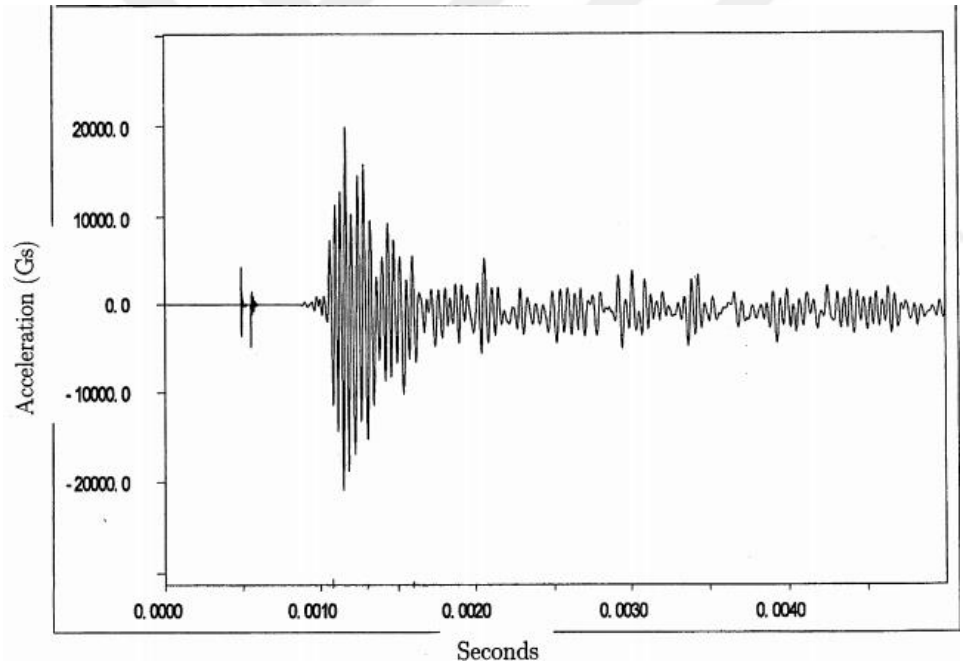

Figure 1.6 Time history of ballistic shock [9]

1.1.3 Pyrotechnic Shock

Pyrotechnical shock, which is usually referred as pyroshock, is the response of a system to high-magnitude and high-frequency stress waves generated as a results of explosive charges in order to separate two stages of a rocket [10]. Physical properties of pyrotechnical shock are listed below [7];

- Acceleration and frequency contents of pyrotechnical shock are as high as ballistic shock's (see Figure 1.7).
- Since pyroshock has rich frequency content, the electronic system can be broken down.
- Shock level in three orthogonal directions is similar to each other.

The characterization of pyrotechnical shock strongly depends on the distance from source. Table 1.3 shows that acceleration amplitude and frequency range is about 1,000 g - 300,000 g and 10,000 Hz – 100,000 Hz, respectively.

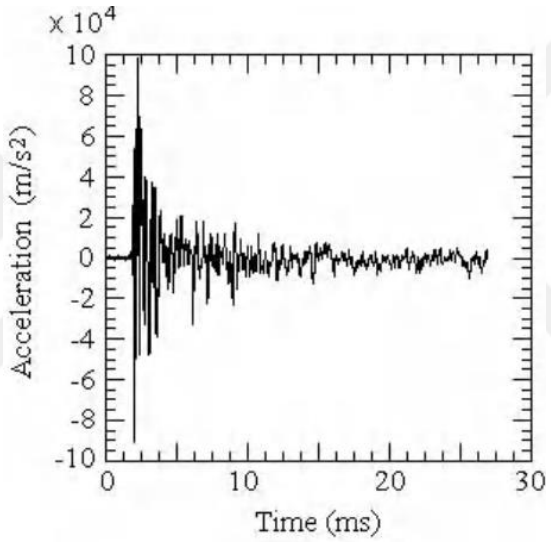

Figure 1.7 Time history of pyrotechnical shock

Table 1.3 Characterization pyrotechnical shock

Type of Field	Distance from the source	Shock Amplitude	Frequency
Near Field	<7.5 cm	5 000 g-300 000 g	>100 000 Hz
Far Field	>7.5 cm	1 000 g- 5 000 g	> 10 000 Hz

1.1.4 Gunfire Shock

According to MIL-STD-810G, gunfire shock is defined as a mechanical shock that has a high repetitive rate and a substantial wave originated from [8];

- air-borne where system is affected muzzle blast pressure,
- structure-borne shock transmitted from gun mechanisms to systems.
- combination of air-borne and structure-borne effects.

In this section, what antenna structure and mechanical shock do was summarized. Importance of the antenna structure was highlighted by military and civilian examples. In addition to that types of mechanical shock were briefly introduced.

1.2 Literature Survey

In literature, the nonlinear dynamic characteristics of antenna structures which is exposed to mechanical shocks is limited, since most of the studies investigated the effects of static and dynamic loads on antenna such as modal and random vibrations analyses rather than the effects of mechanical shock on it.

Concerning the linear dynamic analyses of antenna structure, the simulation was carried thanks to commercial finite element programs such as ABAQUS® and NASTRAN®. Also, the static and dynamic analyses of dipoloop antenna radome was simulated by using a linear finite element analysis by Reddy and Hussain [11]. Mechanical shock analysis was done thanks to ABAQUS®. In this study, only stresses were evaluated on the dipoloop antenna radome. Lopatin and Morozov [12] studied the free vibration of thin-walled composite spoke of an umbrella-type deployable space antenna. The composite spoke of the deployable space antenna was modeled as a cantilever beam via considering the effects of transverse shear.

Moreover, the nonlinear dynamic response of the antenna structure under dynamic loads is characterized by a few researchers. Random and modal analyses of a gimbaled antenna including gap nonlinearity resulting from small clearances in the joints have been studied by Su [13] who linearized this nonlinearity and solved it by a commercial finite element software. Also, Sreekantamurthy et al. [14] investigated static and dynamic loads such as inflation pressure, gravity and pretension loads on a parabolic reflector antenna by using a commercial finite element software. In their

work, geometric nonlinearity was included to the model, since the deformation of parabolic reflector antenna was large.

Although the nonlinear dynamic characteristic of antenna structure under mechanical shock is different from the linear ones when the amplitude of the applied shock is high, as in the ballistic and pyrotechnical shocks, there appears almost no study on this specific topic. However, especially in micro and nanoscale areas, many researchers investigated the dynamics response of micro electro mechanical systems, micro beams, micro switches and so forth which are under mechanical shock even by considering nonlinearities. As a beginning, some authors used single degree of freedom assumption to get a rough estimation of the dynamic response of micro systems. For example, Younis et al. [15] studied the performance of capacitive switches modeled as a single degree of freedom (SDOF) system under mechanical shock through including the effects of squeeze-film damping and electrostatic forces. Moreover, Li and Shemansky [16] treated the micro-machined structure as a single degree of freedom system as well as a distributed parameter model. For more accurate analysis, many authors used continuous beam models to simulate the response of micro systems to a mechanical shock. As an example, Younis et al. [17] investigated the simultaneous effects of mechanical shock and electrostatic forces on microstructures simulated as cantilever and clamped-clamped beams. In this study, reduced order model results based on Galerkin's Method were compared with the ones obtained from commercial finite element software. Due to the large deformation of micro systems resulted from the applied mechanical shock, some researchers included nonlinearity to the models to predict the dynamic behaviors in real life. For instance, Younis and Arafat included both geometric and inertia nonlinearities into their studies while analyzing the response of the cantilever microbeam activated by mechanical shock and electrostatic forces [18]. In this work, they analyzed the effects of cubic geometric and inertia nonlinearities on the cantilever microbeam by using reduced order model which is based upon Galerkin's Method. In another study of Younis et al.[19], the response of the clamped-clamped microbeam was investigated through using four modes in the Galerkin based reduced order model including geometric nonlinearity. Moreover, Younis et al. [19] studied the effects of

shape of shock pulse and package on the response of microbeam and they validated the results via a commercial finite element software.

Furthermore, some researchers employed approximate solutions to the response of systems under mechanical shock through frequency domain approaches rather than time domain approach which is computationally expensive. As an example, Liang et al. [20] estimated shock response of the mast in ships using frequency domain method such as square root of the sum of squares (SRSS), complete quadratic combination method (CQC), naval research laboratory method (NRL) and absolute summation method (ABS). Alexander [21] mentioned the frequency domain methods which are applied to the nonlinear systems as well. Younis and Pitarresi [22] emphasized synthetic methods utilizing the static response and shock spectrum based on maximum responses of many single degree of freedom systems. In this study [22], linear and nonlinear response of microbeam found in synthetic method and Galerkin-based reduced order method employing six modes were compared in terms of different values of shock amplitude.

Mechanical shock excitation is inherently applied to the base of structures. In literature, mechanical shock was simulated for continuous systems by base excitation which is either applied to the fixed boundary condition ([23,24]) or distributed force applied through length of a structure ([17,18,19,22]).

1.3 Objective

Antenna structures used for military and civilian applications are vital components of electronic systems. These antenna structures are subjected to mechanical shock from various environments such as transportation, ballistic, pyrotechnic shocks. Therefore, correct modeling of dynamic characteristic of the antenna structure under mechanical shock is needed because of performance of the antenna structure. Inherently, most of the antenna structures have slender shape, larger dimension in longitudinal direction. Moreover, they are subjected to high amplitude mechanical shock. Thus, mathematical modeling of the antenna structure through linear theory give incorrect

result, since the antenna structures experience large deformation, where nonlinear effects dominate shock response of the antenna structure. In other words, nonlinearities due to large deformation must be included in order to predict dynamic behavior in real life.

1.4 Scope of the Thesis

The outline of the thesis is given as follows:

In Chapter 2, equivalent lumped mass method is introduced in order to get dynamic response of the antenna structure. Moreover, linear continuous beam model is given to simulate dynamic behavior of the antenna structure under mechanical shock. In addition to that continuous beam model including geometric nonlinearity is explained. Furthermore, the brief information about Galerkin's method that is used in this thesis is given to get reduced order model. In addition to that shock response of the antenna structure obtained from commercial finite element software is discussed.

In Chapter 3, numerical integration methods used to solve both linear and nonlinear differential equations are introduced in order to capture dynamic behavior of the antenna structure. Firstly, central difference method is given to solve equation of motion that is obtained from equivalent lumped mass model. In addition to that a nonlinear differential solver is written by Newmark and backward Euler methods, since nonlinear solvers of MATLAB diverge while solving a set of nonlinear differential equations.

In Chapter 4, linear and nonlinear approximate methods are studied. In the linear approximation methods, modal and shock response spectrum parameters are combined with statistical methods in order to get maximum shock response of the antenna structure. Moreover, the nonlinear shock response of the antenna structure is computed by combination of nonlinear static response and shock response spectrum.

In Chapter 5, experimental studies are introduced. In that chapter, firstly, modal testing of the antenna structure is studied in order to obtain modal damping ratios. After that mechanical shock testing of the antenna structure is discussed.

In Chapter 6, shock response of the antenna structure is discussed by linear and nonlinear reduced order models, finite element method and experiment results.

In Appendix A, technical papers of the equipment that was used during modal and shock testing are presented. In appendix B, the conference paper that will be presented in 34th IMAC conference held in Orlando/USA is supplied.

CHAPTER 2

THEORY

2.1 Introduction

In this chapter, mathematical modeling of the antenna structure under mechanical shock is proposed by linear and nonlinear theories. In Section 2.2, the antenna structure is modeled as an equivalent spring mass system. In Section 2.3, free and forced response of the antenna structure is represented by linear Euler-Bernoulli beam theory. In Section 2.4, shock response of an antenna structure including geometric nonlinearity is presented. In Section 2.5, dynamic characteristic of an antenna structure is obtained by ANSYS 15.0, commercial finite element software.

2.2 Equivalent Lumped Mass Model

In this section, an antenna structure is treated as a single degree of freedom system by using an equivalent lumped mass model. Basically, most antenna structures such as monopole antennas (see Figure 1.3) have a cantilever beam structure, since one end is fixed to the antenna hub while the other end is free to transmit or receive electromagnetic waves (see Figure 1.3).

Consider a cantilever type antenna structure with uniform density and constant cross section as shown in Figure 2.1. The equivalent mass of the antenna structure is computed by Rayleigh's method which requires assumed displacement function [25]. According to definition of Rayleigh's method, maximum potential and kinetic energy are equal to each other.

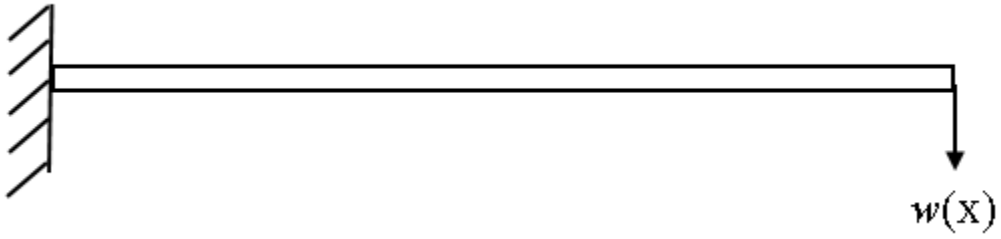

Figure 2.1 Cantilever beam type the antenna structure

Total kinetic energy and potential energy (usually referred as strain energy for continuous system) equations are expressed as follows

$$T = \frac{1}{2} m\omega^2 \int_0^L \phi(x)\,\mathrm{d}x, \tag{2.1}$$

$$P = \frac{EI}{2} \int_0^L \left(\frac{d^2\phi(x)}{dx^2} \right) dx, \tag{2.2}$$

where m is the mass per length, ω_n is the natural frequency of the antenna structure, $\phi(x)$ is the assumed mode shaped, EI is the flexural rigidity of the antenna structure. Assumed displacement function which needs to satisfy geometric boundary conditions is selected as

$$w(\mathrm{x}) = \mathrm{w}_0 \left(1 - \cos\left(\frac{\pi x}{2L} \right) \right). \tag{2.3}$$

Substituting Eq. (2.3) into Eq. (2.1) and Eq. (2.2), equating the resultants of Eq. (2.1) and Eq. (2.2) square of the fundamental frequency is obtained as

$$\omega^2 = \frac{\dfrac{\pi^4 EI}{L^3}}{16mL\left(3 - \dfrac{8}{\pi} \right)}. \tag{2.4}$$

For the cantilever beam, an equivalent stiffness at the free end is given as [26]

$$k_{eq} = \frac{3EI}{L^3}. \tag{2.5}$$

Square of the natural frequency of the equivalent lumped mass system is

$$\omega^2 = \frac{k_{eq}}{m_{eq}}. \tag{2.6}$$

After equating Eq. (2.4) and Eq. (2.6), equivalent mass can be computed as [25]

$$m_{eq} = 0.2235mL\ . \tag{2.7}$$

After finding the equivalent mass and stiffness, one can write an equation of motion of the equivalent lumped mass system with base excitation as (see Figure 2.2)

$$m_{eq}\ddot{x} + c_{eq}\dot{x} + k_{eq}x = c_{eq}\dot{y} + k_{eq}y, \tag{2.8}$$

where, m_{eq}, c_{eq}, k_{eq} are equivalent mass, damping and stiffness of the system, respectively. $\dot{y}$ and y are velocity and displacement of the base due to mechanical shock.

Considering the relative displacement of the mass with respect to the base, a new variable can be defined as

$$z = x - y, \tag{2.9}$$

Eq. (2.8) can be written in the following form

$$m_{eq}\ddot{z} + c_{eq}\dot{z} + k_{eq}z = -m_{eq}\ddot{y}\ . \tag{2.10}$$

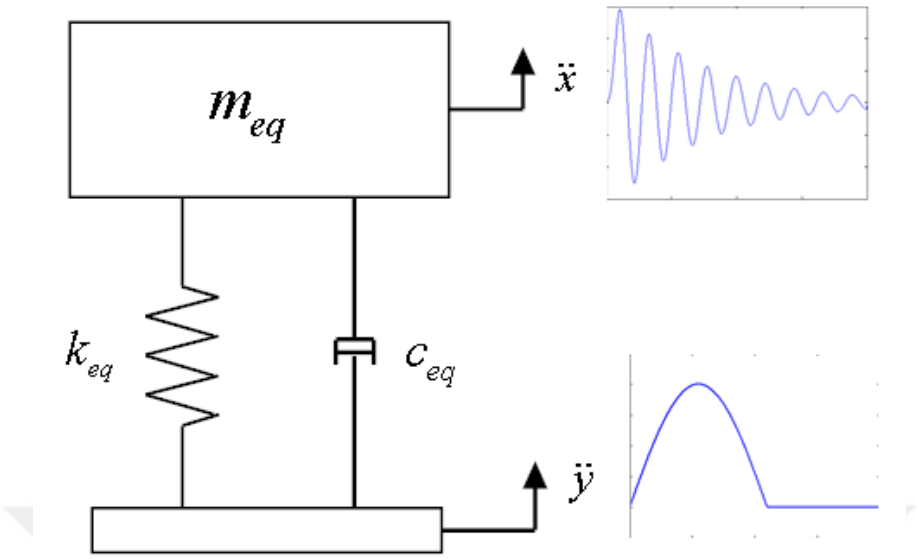

Figure 2.2 Equivalent lumped mass system with base excitation

Here, $\dot{z}$ and $\ddot{z}$ are the relative velocity and acceleration of the equivalent mass with respect to base, respectively.

Eq. (2.10) does not have a closed form solution if $\ddot{y}$ is an arbitrary function Inherently, most mechanical shocks such as ballistic, gunfire shock and etc. cannot be expressed in terms of mathematical functions. Therefore, numerical integration methods are widely used to solve Eq.(2.10), known as convolution integral. In the literature, a plenty of numerical methods are available to calculate the convolution integral in the case of an arbitrary base acceleration. In this part, the convolution integral is calculated by central difference algorithm (see Section 3.2) which is a fundamental numerical integration method due to its easy implementation for single degree of freedom systems [27]. The algorithm of the central difference method is detailed in Section 3.2.

As an example, assume an antenna structure with $L = 350mm$, $EI = 1.867Nm^2$ and $m = 0.216kg/m$. Therefore, the equivalent lumped mass and stiffness of the antenna structure, shown in Figure 2.3, are $0.0169kg$ and $130.6N/mm$, respectively. Assuming a damping ratio of 0.05, the relative displacement and acceleration

responses of the antenna structure exposed to $50g$, $10ms$ half sine mechanical shock are given in the Figure 2.4 and Figure 2.5, respectively.

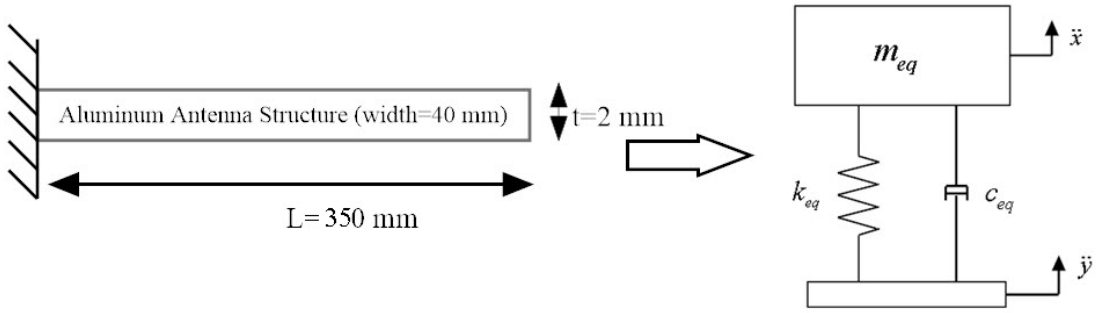

Figure 2.3 Equivalent lumped mass model of the antenna structure

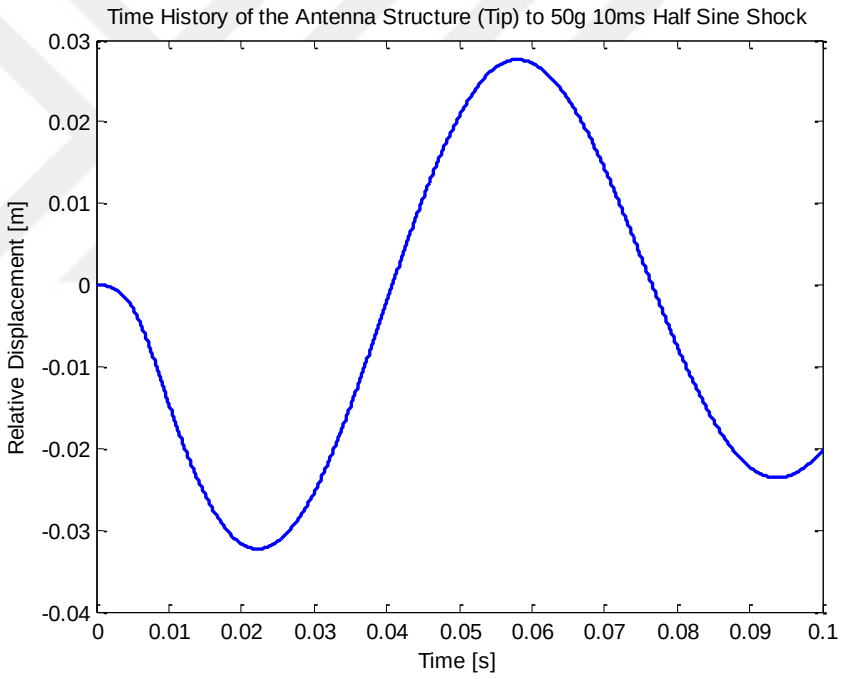

Figure 2.4 Relative displacement of the antenna structure (tip) under $50g$, $10ms$ half sine mechanical shock

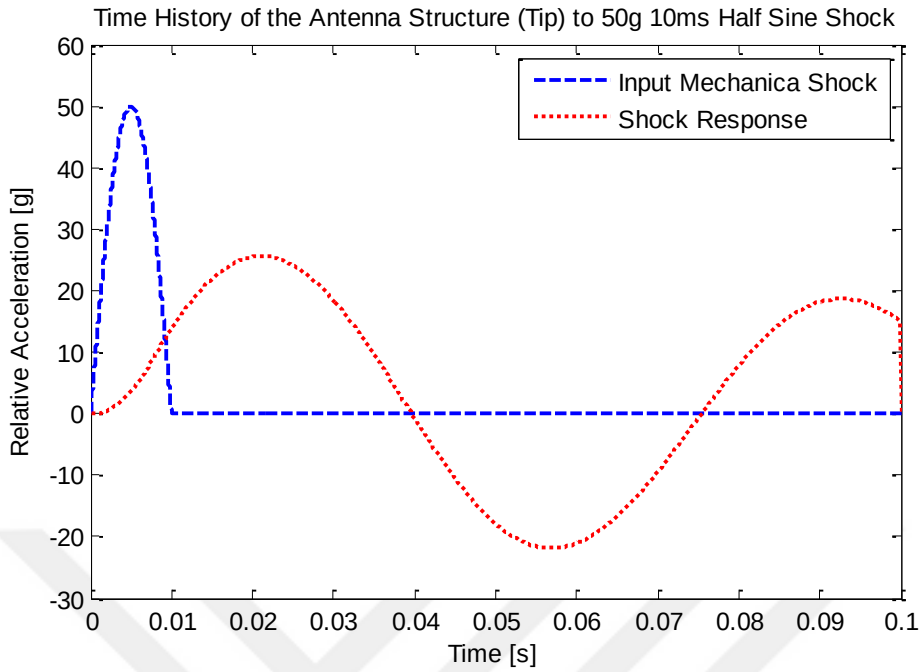

Figure 2.5 Relative acceleration response of the antenna structure (tip) under $50g$, $10ms$ half sine mechanical shock

In Section 2.2, equivalent lumped mass model is summarized for an antenna structure. Although lumped mass model is a fundamental and computationally efficient model, it is not applicable for the cases where contribution of the modes higher than the first mode cannot be neglected. Therefore, continuous beam modeling by using Euler-Bernoulli beam theory results in highly accurate results due to the fact that the effects of higher modes can as well be retained in the solution.

2.3 Linear Continuous Beam Model

In this section, an antenna structure is modeled by using Euler Bernoulli beam theory. In this section, firstly, free vibration of an antenna structure is investigated. Then, modeling of the antenna structure under mechanical shock is introduced.

In literature, Euler Bernoulli beam theory is widely used to model slender beam like structures [15, 17, 18, 19, 22, 23]. However, due to inherent assumptions of the theory, accuracy of the results is poor when the ratio of thickness to length is larger

than 10%; in which case Timoshenko beam model is required to get accurate results [28]. Those assumptions that are valid for Euler Bernoulli beam theory are given as,

- Shear deformations are neglected [29].
- Cross section plane which is normal to the longitudinal axis of a beam remain plane and normal to the longitudinal axis after beam deforms [29].

Consider the antenna structure, whose length, density, cross sectional area and flexural rigidity are represented by l, ρ, A and EI, respectively. As can be seen in Figure 2.6, the transverse deflection of the antenna structure is defined by $w(x,t)$, where x is axial position and t represents time. Equation of motion of the antenna structure can be written as [30]

$$\frac{\partial^2}{\partial x^2}\left(EI\left(x\right)\frac{\partial^2 w(x,t)}{\partial x^2}\right)+c\frac{\partial w(x,t)}{\partial t}+\rho A\left(x\right)\frac{\partial^2 w(x,t)}{\partial t^2}=F\left(x,t\right), \qquad (2.11)$$

where, c is the viscous damping coefficient and $F\left(x,t\right)$ is the distributed force acting on the antenna structure.

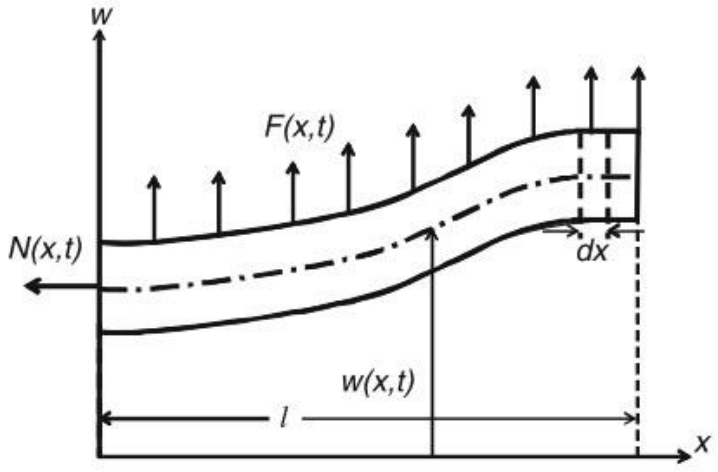

Figure 2.6 Nomenclatures of the antenna structure in bending direction [30]

It should be note that nondimensionalization (normalization), which converts the equation of motion into nondimensional equations via normalized nondimensional parameters, has many advantages over the dimensional one. First advantage is that the normalization reveals hidden properties of some variables. Furthermore, normalization helps to reduce number of variables in the equation by generating universal variables, suitable for general systems rather than specific ones [30]. In this thesis, nondimensional parameters are preferred due to the advantages listed above.

2.3.1 Free Vibration Analysis of the Antenna Structure

In this part, natural frequencies and mode shapes of the antenna structure are analyzed via normalized equation of motion.

For free vibrations, external forcing and damping terms in Eq. (2.11) are neglected and constant cross section is assumed. In the light of the above information, Eq. (2.11) is reduced to

$$EI\frac{\partial^4 w(x,t)}{\partial x^4}+\rho A\frac{\partial^2 w(x,t)}{\partial t^2}=0\ . \tag{2.12}$$

Introducing the following nondimensional variables

$$\hat{x}=\frac{x}{l},\ \hat{w}=\frac{w}{l},\ \hat{t}=\frac{t}{T}\ , \tag{2.13}$$

where T is time scale parameters [30] and substituting Eq. (2.13) into Eq. (2.12) , is the following nondimensional equation is obtained

$$\frac{\partial^4 \hat{w}}{\partial \hat{x}^4}+\frac{\rho A l^4}{EIT^4}\frac{\partial^2 \hat{w}}{\partial \hat{t}^2}=0\ . \tag{2.14}$$

Defining the time scale parameter T as

$$T = \sqrt{\frac{\rho A l^4}{EI}} \ . \tag{2.15}$$

Eq. (2.14) becomes

$$\frac{\partial^4 \hat{w}}{\partial \hat{x}^4} + \frac{\partial^2 \hat{w}}{\partial \hat{t}^2} = 0 \ . \tag{2.16}$$

Solving Eq. (2.16) for fixed-free boundary conditions, the characteristic equation is obtained

$$\cosh(\beta_n l)\cos(\beta_n l) = -1. \tag{2.17}$$

Naturally, most antenna structures have cantilever type configuration, since one end is fixed to the antenna hub while the other end is free to receive or transmit electromagnetic wave. Therefore, nondimensional mode shapes of the antenna structure which satisfy both geometric and natural boundary condition, shown in Figure 2.7, can be written as

$$\begin{aligned}\hat{\phi}_n(\hat{x}) = A_n \frac{\sinh(\beta_n l) + \sin(\beta_n l)}{\cosh(\beta_n l) + \cos(\beta_n l)} (\cosh(\beta_n l\hat{x}) - \cos(\beta_n l\hat{x})) \\ + \sin(\beta_n l\hat{x}) - \sinh(\beta_n l\hat{x})\end{aligned} , \tag{2.18}$$

where β is the frequency parameter obtained from the solution of the characteristic equations defined by Eq. (2.17) and A is an arbitrary constant, for mass normalized mode shapes it is given as

$$A_n = \frac{1}{\sqrt{\int_0^1 \hat{\phi}_n(\hat{x})}} \ . \tag{2.19}$$

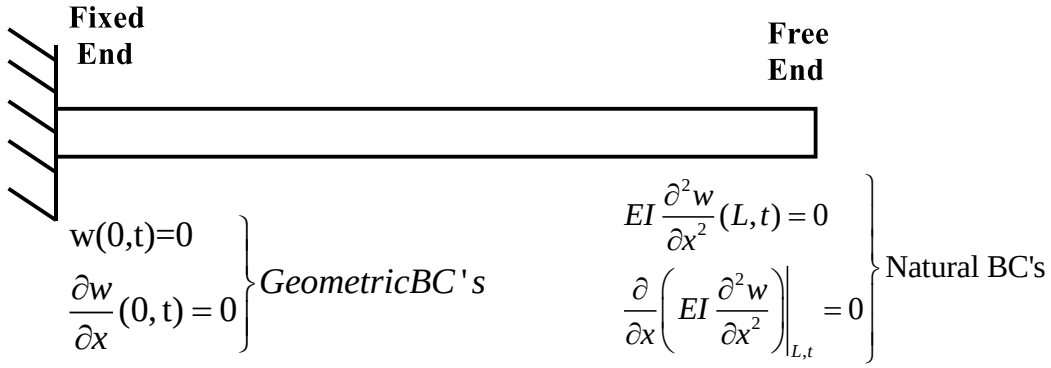

Figure 2.7 Boundary condition of the antenna structure

The nondimensional natural frequency can be calculated as

$$\omega_{non,n} = \beta_n{}^2 l^2 \ . \tag{2.20}$$

$\beta_n l$ values obtained from the solution of Eq. (2.17) are given in Table 2.1.

Table 2.1 The roots of the characteristic equation

n	$\beta_n l$
1	1.87510
2	4.69409
3	7.85476
4	10.99554
n≥5	(2n-1)π/2

The first four nondimensional mode shapes and natural frequencies of the antenna structure are given in Figure 2.8.

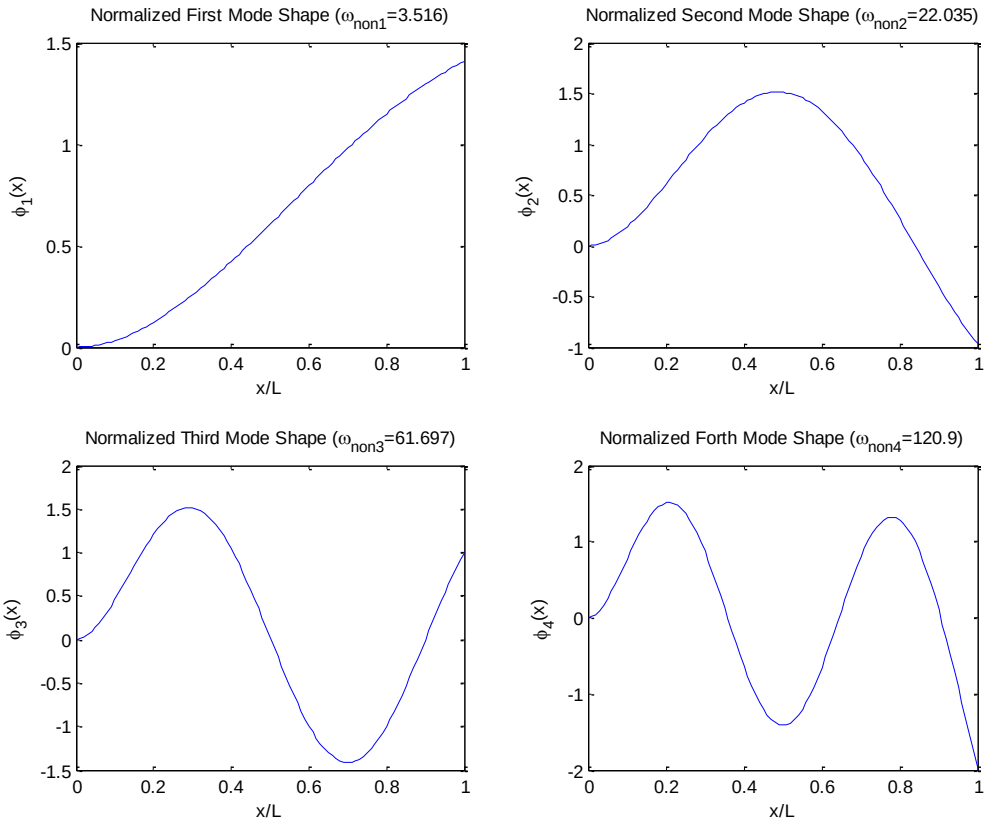

Figure 2.8 Nondimensional mode shapes and natural frequencies of the antenna structure

2.3.2 Forced Vibration Analysis of the Antenna Structure under Mechanical Shock

In this section, shock response of the antenna structure is analyzed by linear Euler-Bernoulli beam theory. The partial differential equation of motion is converted into a set of ordinary differential equations by using Galerkin's method. Inherently, mechanical shock is simulated for continuous systems by base excitation which is either applied to the fixed boundary condition (see Figure 2.9) or considered as a distributed force applied through the structure (see Figure 2.10). In this thesis, mechanical shock is simulated by a distributed force applied on the structure.

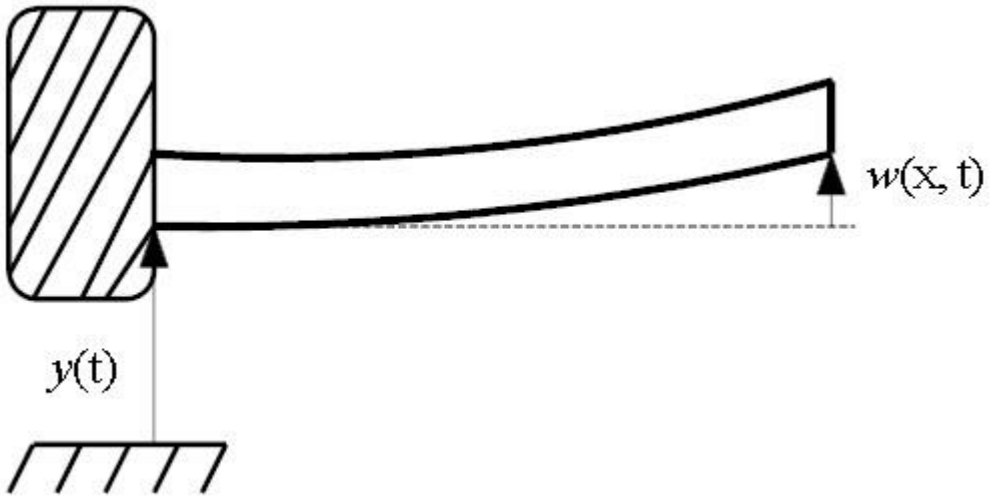

Figure 2.9 Mechanical shock represented as base excitation

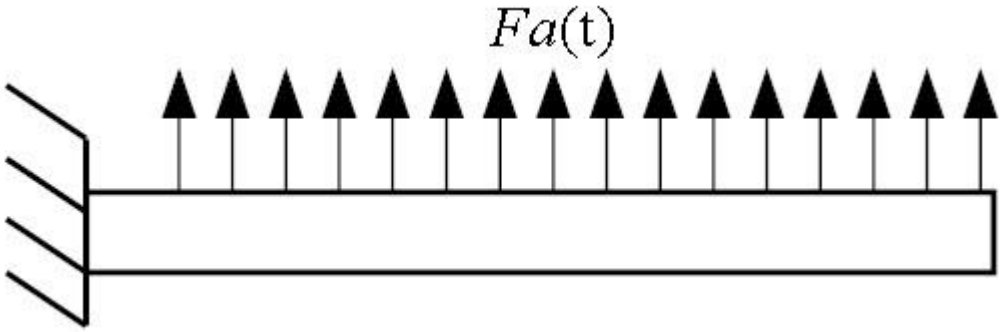

Figure 2.10 Mechanical shock represented as distributed force

Equation of motion of the antenna structure exposed to a mechanical shock, which is considered as a distributed force applied on the structure, is given as follows

$$\frac{\partial^2}{\partial x^2}\left(EI\frac{\partial^2 w(x,t)}{\partial x^2}\right)+c\frac{\partial w(x,t)}{\partial t}+\rho A\frac{\partial^2 w(x,t)}{\partial t^2}=-(\rho \mathrm{A}\, a_{max})a_{pulse}(t)\,, \qquad (2.21)$$

where, a_{max} is the maximum value of mechanical shock and a_{pulse} is a unit mechanical shock profile such as half sine, terminal peak sawtooth etc.. Inserting the nondimensional variables defined in Eq. (2.13) into Eq.(2.21), and dropping the hats for simplicity, the nondimensional equation of motion of a uniform antenna structure becomes

$$\frac{\partial^4 w(x,t)}{\partial t^4} + c_{non}\frac{\partial w(x,t)}{\partial t} + \frac{\partial^2 w(x,t)}{\partial t^2} = F_{non} a_{pulse}(t) \ , \tag{2.22}$$

where, nondimensional damping and forcing terms are

$$c_{non} = \frac{cl^4}{EIT} \ , \mathrm{F}_{non} = \frac{-\rho A a_{\max} l^3}{EI} \ . \tag{2.23}$$

As can be seen in Eq. (2.23), effects of the mechanical shock increase sharply with increasing length and decreasing thickness. This result is in agreement with the experimental results given in the literature [31].

The resulting partial differential equation of motion can be converted into a set of ordinary differential equations by using Galerkin's method. In this approach, the solution of Eq. (2.22) is expressed as

$$w(x,t) = \sum_{i=1}^{n} u_i(t)\phi_i(x) \ , \tag{2.24}$$

where, $\phi_i(x)$ is a comparison function which satisfies both geometric and natural boundary conditions and differentiable at least to the order of the partial differential equation, $u_i(t)$ is generalized coordinate to be determined and n is the number of modes used in the analysis [32]. After substituting Eq. (2.24) into Eq. (2.22), the following equation is obtained

$$\sum_{i=1}^{n} u_i(t)\phi_i''''(x) + c_{non}\sum_{i=1}^{n} \dot{u}_i(t)\phi_i(x) + \sum_{i=1}^{n} \ddot{u}_i(t)\phi_i(x) = \mathrm{F}_{non}\, a_{pulse}(t) \ , \tag{2.25}$$

where, 'prime' and 'dot' refer to derivative with respect to x and t, respectively. Multiplying Eq. (2.25) by $\phi_j(x)$ and integrating from 0 to 1 one obtains

$$\sum_{i=1}^{n} u_i(t)\left(\int_0^1 \phi_j(x)\phi_i''''(x)\,\mathrm{d}x\right) + c_{non}\sum_{i=1}^{n}\dot{u}_i(t)\left(\int_0^1 \phi_j(x)\phi_i(x)\,\mathrm{d}x\right) + \sum_{i=1}^{n}\ddot{u}_i(t)\left(\int_0^1 \phi_j(x)\phi_i(x)\,\mathrm{d}x\right) = \int_0^1 \phi_j(x)\,\mathrm{F}_{non}\,a_{pulse}(t)\,\mathrm{d}x \quad . \tag{2.26}$$

From the spatial differential equation obtained in free vibration analysis, $\phi_i''''(x)$ can be written as

$$\phi_i''''(x) = \omega_{non,i}{}^2\phi_i(x) \quad . \tag{2.27}$$

Moreover, it is noted that integral of $\phi_i(x)\phi_j(x)$ from 0 to 1 is equal to 1 when $i = j$, otherwise it is equal to 0, since the mode shapes of a cantilever beam are orthogonal to each other. In the light of the foregoing findings, Eq. (2.26) reduces to following uncoupled equation of motion in terms of the generalized coordinate as

$$\ddot{u}_j(t) + 2\zeta_j\omega_{non,j}\dot{u}_j(t) + \omega_{non,j}{}^2u(t) = \int_0^1 \phi_j(x)\,\mathrm{F}_{non}\,a_{pulse}(t)\,\mathrm{d}x \quad , \tag{2.28}$$

where, ζ_j is the modal damping ratio of the j^{th} mode which is defined as

$$\zeta_j = \frac{c_{non}}{2\omega_{non,j}} \quad . \tag{2.29}$$

Moreover, it should be noted that damping term in Eq. (2.28) is defined in terms of modal damping ratio, which can be easily obtained by a modal test of the antenna structure.

Another crucial topic is the number of modes that should be used in Eq. (2.28) in order to get an accurate result. In continuous systems, actual solution is represented by infinite number of modes which is practically impossible. Therefore, reduced

order model (ROM) are used to estimate the dynamic characteristic of the antenna structure. In literature, this dilemma is overcome by employing different methods. Some authors claim that use of only few modes (1-6) is enough to capture dynamic characteristic of the structures, since higher modes have weaker effect on the response [30]. Moreover, Tom [33] remarks that the dynamic response of a structure is represented accurately when the analysis includes the number of modes, whose effective total mass is at least 90 % of the actual mass. In other words, the first four modes which satisfy the above requirement are essential to be included in dynamic response calculation of the antenna structure. In reality, however, the number of modes required to represent the dynamic response accurately depends on the frequency content of the input shock.

As an example, consider the antenna structure shown in Figure 2.11 with constant cross section and uniform density. Assume that the antenna structure is subjected to $50g$ $11ms$ half sine mechanical shock, which is defined in IEC-60068-2-27 for transportation shock [34]. Eq. (2.28) is solved by using Newmark method (see Section 3.3) by substituting the values given in Table 2.2. After finding the solution of generalized coordinates ($u(t)$), inverse transformation is necessary to get the physical solution ($w(x)$). The relative displacement and acceleration responses of the antenna structure are given for different number of modes in Figure 2.12 and Figure 2.13 , respectively. In this example, damping ratio ζ is taken as 0.05 for all modes. From these figures it can be seen that relative displacement and acceleration are independent of the number of modes included in the analysis due to of the frequency content of input signal (see Figure 6.5).

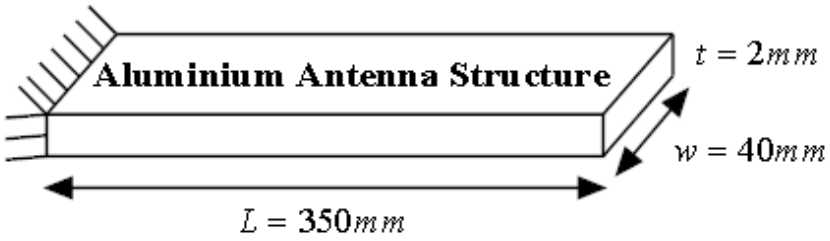

Figure 2.11: Geometric properties of the antenna structure

Table 2.2 The nondimensional natural frequencies and mass normalized mode shape constants for the first six modes

Mode Number (n)	**Nondimensional Natural Frequency $\omega_{non,n}$**	**Mass Normalized Mode Shape Constant A_n**
1	3.516	0.7341
2	22.0345	1.0185
3	61.6972	1.003349
4	120.9019	1.02353985
5	199.8591	1.0000
6	298.5550	1.0000

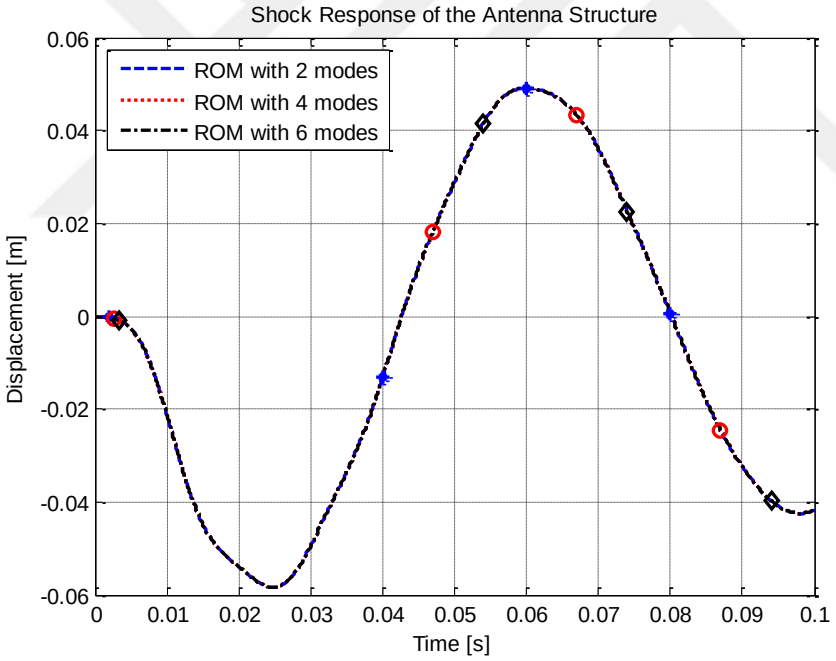

Figure 2.12 Relative displacement of the tip of the antenna structure for different number of modes retained in the solution

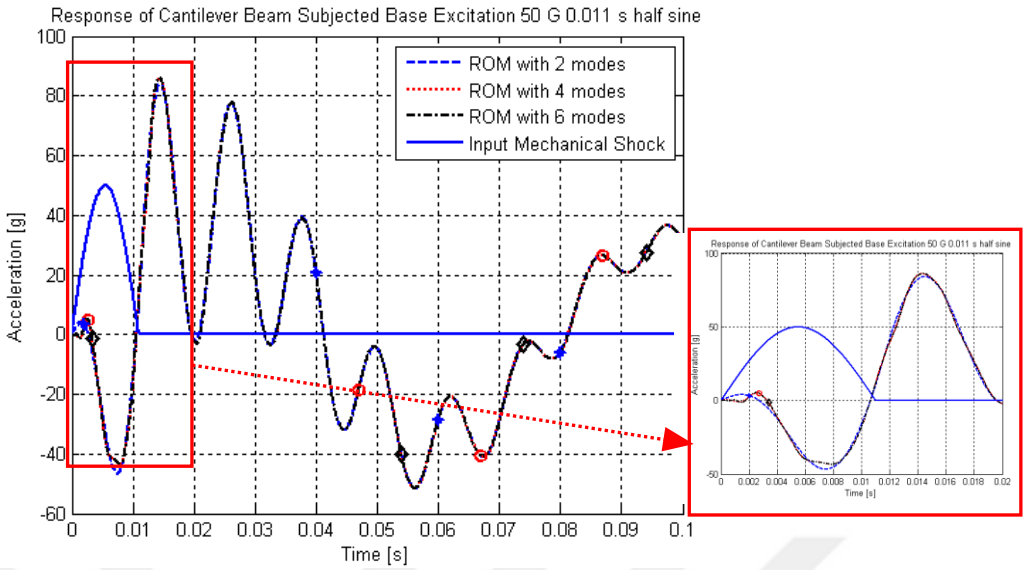

Figure 2.13 Acceleration of the tip of the antenna structure for different number of modes retained in the solution

2.4 Nonlinear Continuous Beam Model

In this section, shock response of an antenna structure considering geometric nonlinearity is studied. Initially, definition, importance and types of nonlinearities are presented. Afterwards, mathematical background of the geometric nonlinearity is discussed.

In real life, response of almost all systems to any forcing is nonlinear, where superposition property of linear systems does not hold. For simplicity, many engineering systems are treated as linear which is a valid assumption in most cases. For instance, in order to obtain linearized equation of motion of an antenna structure under mechanical shock, small deformation is assumed. This assumption gives accurate results if the deformations in the real case are small compared with respect to the thickness of the antenna structure. However, if the deformation is large, small deformation assumption results in highly inaccurate results. Therefore, linear modeling may result in a design which is not optimum and hence, increases weight and cost. In addition to this, estimated acceleration of a PCB on the antenna structure is not accurate, since mechanical shocks result in large deformations, in which case the antenna structure needs to be modeled by including the nonlinear effects.

Nonlinearities common in structures are geometric nonlinearity, damping nonlinearity, inertia nonlinearity, curvature nonlinearity, material nonlinearity and boundary condition nonlinearity. Since, the antenna structure experiences large deformation due to its long and slender structure, curvature and inertia nonlinearities are as well included into the model.

In the light of the foregoing information, equation of motion of the antenna structure including geometric nonlinearity is written as, [30]

$$\begin{aligned} EI\frac{\partial^4 w}{\partial x^4}+c\frac{\partial w}{\partial t}+\rho A\frac{\partial^2 w}{\partial t^2}=-EI\frac{\partial}{\partial x}\left(\frac{\partial w}{\partial x}\frac{\partial}{\partial x}\left(\frac{\partial w}{\partial x}\frac{\partial^2 w}{\partial x^2}\right)\right) \\ -\frac{1}{2}\rho A\frac{\partial}{\partial x}\left(\frac{\partial w}{\partial x}\int_L^x\left(\frac{\partial^2}{\partial t^2}\int_0^x\left(\frac{\partial w}{\partial x}\right)^2 dx\right)dx\right)-(\rho \mathrm{A}\, a_{max})a_{pulse}(t) \end{aligned}, \tag{2.30}$$

where, the first term on the right hand side of the equation is due to geometric curvature while the second term of right hand side of the equation is known as the inertia nonlinearity. Substituting the nondimensional parameters defined in Eq. (2.13) into Eq. (2.30) and drop "hats" for the sake of simplicity, the following normalized equation is obtained

$$\begin{aligned} \frac{\partial^4 w}{\partial x^4}+C_{non}\frac{\partial w}{\partial t}+\frac{\partial^2 w}{\partial t^2}=-\frac{\partial}{\partial x}\left(\frac{\partial w}{\partial x}\frac{\partial}{\partial x}\left(\frac{\partial w}{\partial x}\frac{\partial^2 w}{\partial x^2}\right)\right) \\ -\alpha_{in}\frac{\partial}{\partial x}\left(\frac{\partial w}{\partial x}\int_1^x\left(\frac{\partial^2}{\partial t^2}\int_0^x\left(\frac{\partial w}{\partial x}\right)^2 dx\right)dx\right)+F_{non}a_{pulse}(t) \end{aligned}, \tag{2.31}$$

where, damping, inertia and forcing nondimensional parameters are introduced respectively as

$$c_{non}=\frac{cl^4}{EIT}\ ,\ \alpha_{in}=\frac{l^4\rho A}{2T^2EI},\ \mathrm{F}_{non}=\frac{-\rho A a_{\max} l^3}{EI}. \tag{2.32}$$

The nondimensional equation of motion defined in Eq. (2.31) is nonlinear because of the first and the second terms on the right hand side of the equation. Furthermore, as can be seen from the above equation, these nonlinear terms are of cubic order.

Eq. (2.31) can be converted into a set of nonlinear ordinary differential equations in order to predict the dynamic characteristic of the antenna structure by using a reduced order model based on Galerkin's Method. Nowadays, reduced order models are frequently used in literature to solve nonlinear transient problems ([17,18,19,22]).

In this thesis, Galerkin's method is used in order to obtain a set of ordinary differential equations. Thus, Eq. (2.24) is substituted into Eq. (2.31), and the following result is obtained

$$\begin{aligned}&\sum_{i=1}^{n} u_i(t)\phi_i''''(x) + c_{non}\sum_{i=1}^{n}\dot{u}_i(t)\phi_i(x) + \sum_{i=1}^{n}\ddot{u}_i(t)\phi_i(x) = \\ &-\left(\left(\sum_{i=1}^{n} u_i\phi_i''\right)^2 + 4\left(\sum_{i=1}^{n} u_i\phi_i'\right)\left(\sum_{i=1}^{n} u_i\phi_i''\right)\left(\sum_{i=1}^{n} u_i\phi_i'''\right) + \left(\sum_{i=1}^{n} u_i\phi_i'\right)^2\left(\sum_{i=1}^{n} u_i\phi_i''''\right)\right), \\ &-\alpha_{in}\frac{\partial}{\partial x^2}\left(\left(\sum_{i=1}^{n} u_i\phi_i'\right)\int_1^x\left(\frac{\partial^2}{\partial t^2}\int_0^x\left(\sum_{i=1}^{n} u_i\phi_i'\right)^2 dx\right)dx\right) + \mathrm{F}_{non}\, a_{pulse}(t)\end{aligned} \quad (2.33)$$

where $\phi_i(x)$ is a comparison function which satisfies both geometric and natural boundary conditions and differentiable at least to the order of the partial differential equation. Therefore, mode shape functions of the antenna structure are selected as the trial comparison functions, since they satisfy above requirements. Moreover, when Eq. (2.33) is multiplied by $\phi_j(x)$, and integrated from 0 to 1 the following result is obtained

$$\sum_{i=1}^{n} u_i \int_0^1 \phi_j \phi_i'''' \, \mathrm{d}x + c_{non} \sum_{i=1}^{n} \dot{u}_i \int_0^1 \phi_j \phi_i \, \mathrm{d}x + \sum_{i=1}^{n} \ddot{u}_i \int_0^1 \phi_j \phi_i \, \mathrm{d}x =$$

$$-\int_0^1 \phi_j \left(\left(\sum_{i=1}^{n} u_i \phi_i'' \right)^2 + 4 \left(\sum_{i=1}^{n} u_i \phi_i' \right) \left(\sum_{i=1}^{n} u_i \phi_i'' \right) \left(\sum_{i=1}^{n} u_i \phi_i''' \right) + \left(\sum_{i=1}^{n} u_i \phi_i' \right)^2 \left(\sum_{i=1}^{n} u_i \phi_i'''' \right) \right) dx \,. \quad (2.34)$$

$$-\alpha_{in} \int_0^1 \phi_j \left(\frac{\partial}{\partial x^2} \left(\left(\sum_{i=1}^{n} u_i \phi_i' \right) \int_1^x \left(\frac{\partial^2}{\partial t^2} \int_0^x \left(\sum_{i=1}^{n} u_i \phi_i' \right)^2 dx \right) dx \right) \right) dx + \int_0^1 \phi_j \, \mathrm{F}_{non} \, a_{pulse}$$

Eq.(2.34) can be represented in matrix form, where in this study MUPAD® available in MATLAB® is used for the symbolic calculations.

The solution to a set of nonlinear differential equations is another arduous issue. Therefore, a computer code is written by using Newmark method and Backward Euler method in order to get dynamic characteristic of the antenna structure under mechanical shock, since MATLAB ode integrators do not solve nonlinear ordinary differential equations of the antenna structure. Detailed information on ode integrators is given in Chapter 3 Sections 3.4, 3.5 and 3.6.

Nonlinear mathematical model used in this study is validated by considering the results given by Younis et al. [18], where authors [18] studied nonlinear response of cantilever MEMS under mechanical shock. The maximum nondimensional deflection versus shock amplitude plot given in [18] is considered to validate the nonlinear mathematical model used in this study. Consider the cantilever MEMS, whose length, thickness and width are $L = 100\mu\text{m}$, $h = 0.1\mu\text{m}$ and $b = 10\mu\text{m}$, respectively. The cantilever MEMS is made up of silicon, whose density and Young's modulus are $2332 kg/m^3$ and $169 GPa$, respectively. The results obtained (see Figure 2.14) are compared with the ones given in [18] (see Figure 2.15) which are in well agreement with the ones given in [18]; hence, the nonlinear model and the solution method used are validated.

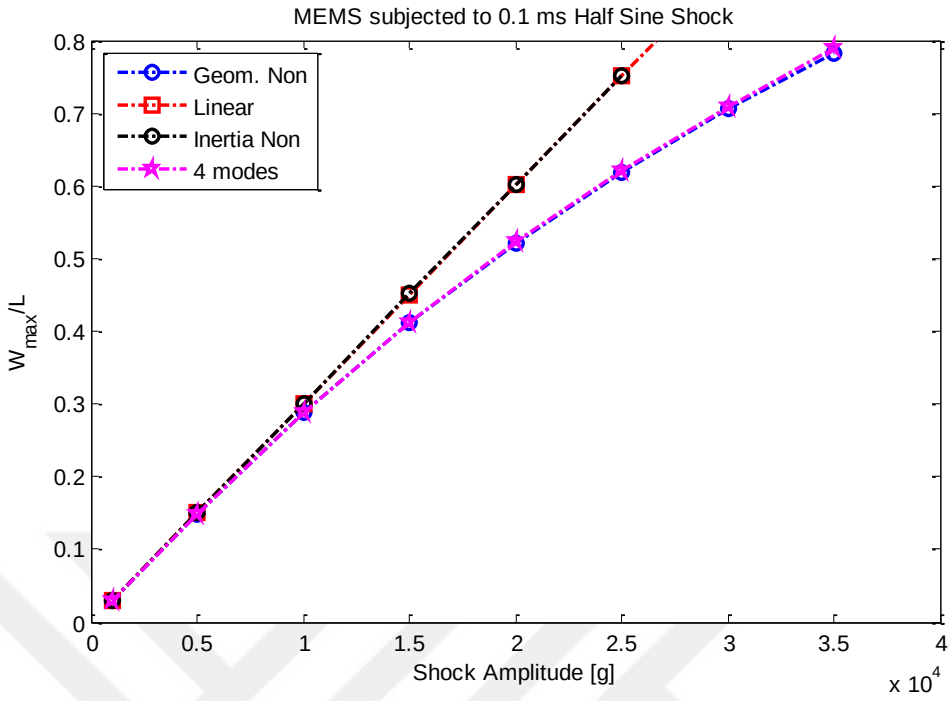

Figure 2.14 Calculated shock response of the cantilever MEMS

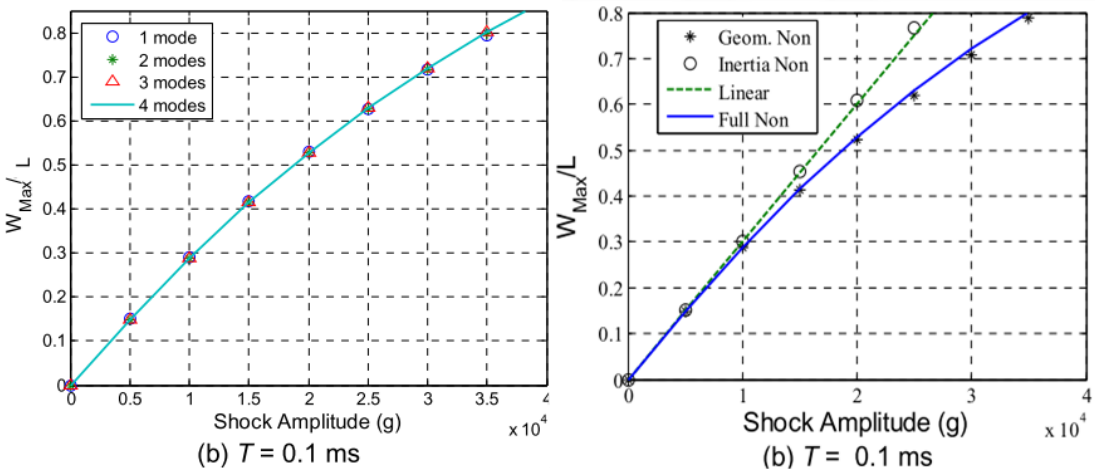

Figure 2.15 The paper shock response of the cantilever beam [18]

2.5 Finite Element Method

In this section, the shock response of the antenna structure is obtained by using ANSYS commercial finite element software.

Consider the antenna structure given in Figure 2.16 with constant cross section and uniform density. The antenna structure is made up of aluminum, whose density and

Young's modulus are $2700 kg/m^3$ and $70 GPa$, respectively. Moreover, "*Transient Structural*" module of the antenna structure is used to get shock response of the antenna structure. Furthermore, the antenna structure is modeled by 3D 2 Node beam element known as BEAM188 (see in Figure 2.17). This element type is used to analyze slender beam like structures. Moreover, this element has six degrees of freedom which are three translation degrees of freedom in X, Y and Z directions and three rotational degrees of freedom about X, Y and Z directions. Moreover, this element is also suitable for modeling stress stiffening and large deformation effects. This element is built upon Timoshenko beam theory which includes shear deformation [35]. Furthermore, in this particular case, 88 elements and 177 nodes are used to get the shock response of the antenna structure. Time step used in the simulation is critical for transient analysis which should be selected as [35];

$$\Delta t = \frac{1}{20} f_{highest} , \tag{2.35}$$

where $f_{highest}$ is the highest natural frequency of interest. The highest natural frequency of interest depends on the frequency content of the input signal. In this case study, $50g$ $11ms$ half sine mechanical shock is used and its fast Fourier transform (FFT) is given in Figure 2.18. Therefore, $500Hz$ can be chosen as the highest natural frequency of interest. Moreover, for nonlinear systems, time step should be selected as follows [7];

$$\Delta t = (0.2 - 0.9)\Delta t_{linear} . \tag{2.36}$$

Consequently, for this case study, time step is chosen as 0.00002 to meet the requirements defined above.

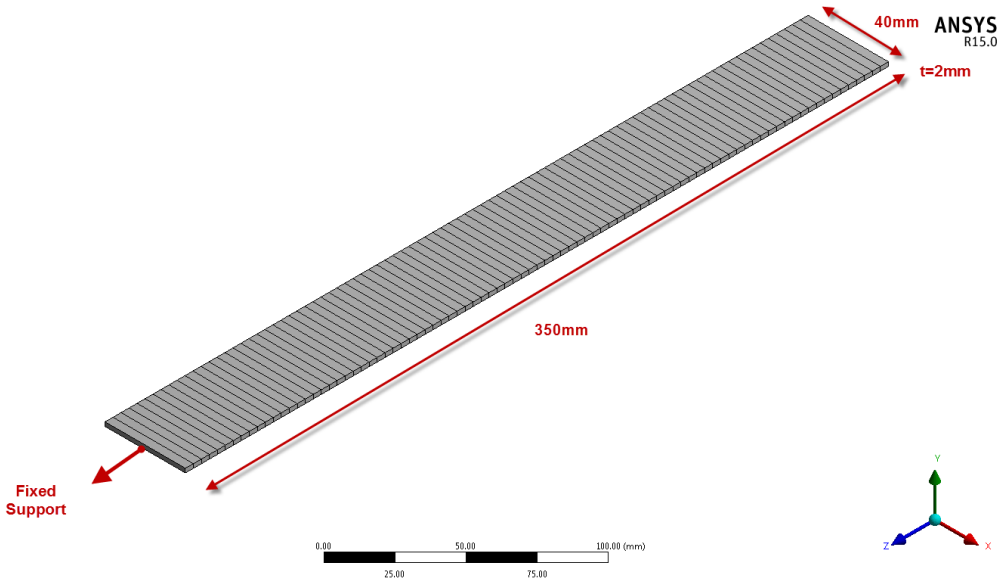

Figure 2.16 Geometric properties of the antenna structure

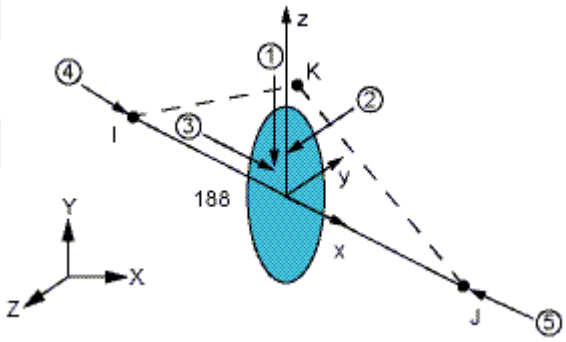

Figure 2.17 Geometry of BEAM188 [35]

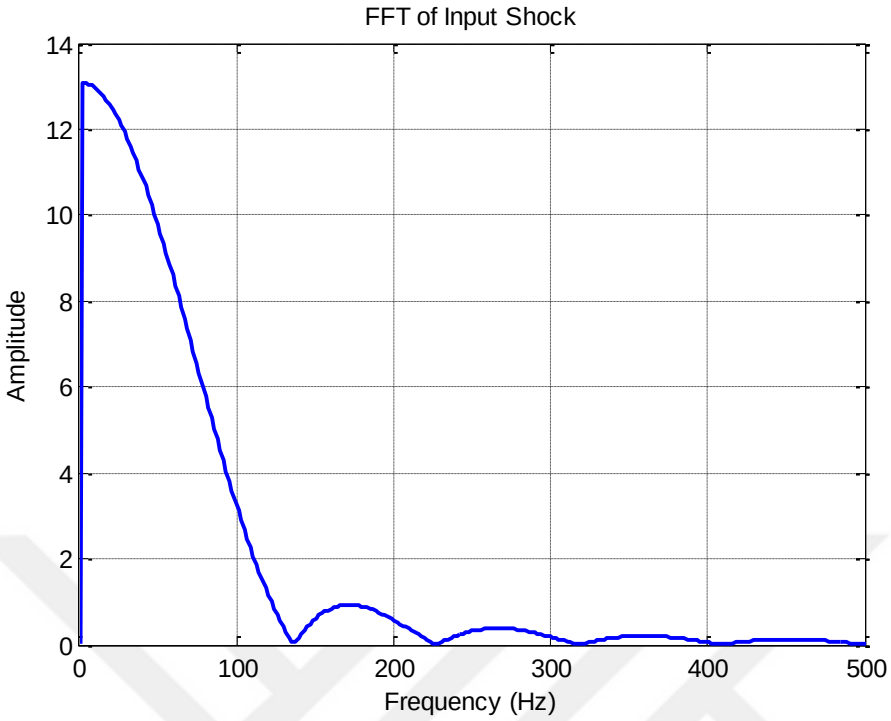

Figure 2.18 FFT of $50g$ $11ms$ half sine mechanical shock

ANSYS Workbench does not possess tools for mechanical shock simulation, since mechanical shocks are applied to a structure from its base. In literature, Application Customization Toolkit exists for transient base excitation analysis. However, this toolkit is applicable for only linear transient analysis. Consequently, ANSYS Parametric Design Language (APDL) is used to simulate mechanical shock. The APDL code which is embedded into "Transient Structural" module is written by "ACCEL" command. This command specifies acceleration to the selected nodes. Furthermore, Rayleigh damping is used to model the damping which is defined as

$$[C] = \alpha_m [M] + \beta_m [K] , \tag{2.37}$$

where α and β are mass and stiffness constant, respectively. In this example, 5% damping ratio is used for all the modes. Shock responses of the antenna structure obtained from ANSYS and reduced order Euler-Bernoulli beam model are compared in Figure 2.19. As can be seen from the figure, shock responses of the antenna structure obtained from both methods are in good agreement.

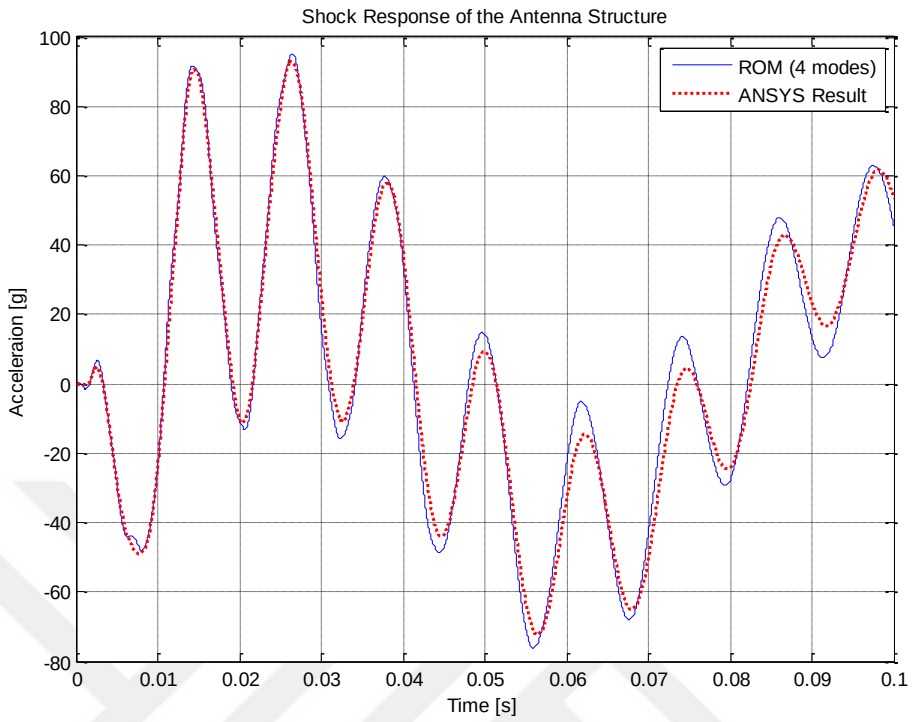

Figure 2.19 Shock response of the antenna structure

In nonlinear finite element analysis, there are some drawbacks which affect shock response of an antenna structure. One of them is Rayleigh damping, which depends on mass and stiffness matrices defined by Eq. (2.37). Using constant β_m leads to undesirable results in the nonlinear analysis, since ANSYS updates stiffness matrix for each iteration. Therefore, when β_m is included in nonlinear transient analysis, damping matrix is updated at every step. As a result of this, damping also becomes nonlinear. Consequently, β_m constant cannot be used in the nonlinear analysis.

CHAPTER 3

NUMERICAL INTEGRATION METHODS

3.1 Introduction

In this chapter, numerical integration methods to solve both linear and nonlinear differential equations are introduced. In Section 3.2, the algorithm of central difference method is given in order to solve the equation of motion for single degree of freedom systems. In Section 3.3, Newmark method is proposed to get shock response of the antenna structure. MATLAB ODE solvers are illustrated in Section 3.4 for the solution of the nonlinear equation of motion. In Section 3.5, backward Euler method is proposed in order to get shock response of the antenna structure including geometric nonlinearity. Section 3.6 presents Newmark method for the nonlinear system, given as an alternative to the backward Euler method.

To begin with, equation of motion of an antenna structure generally does not have a closed form solution under the excitation of an input shock which may not been represented in terms of mathematical functions. Moreover, the equation of motion may be nonlinear, which prevents the application of analytical methods. Thus, numerical integration methods are needed to solve the equation of motion of the antenna structure. In literature, various numerical integration methods are available. Some of these methods are finite difference, Runge-Kutta, backward Euler, Newmark and Wilson methods. Moreover, in some of these methods, the solution or the current displacement is found by using previously determined displacement, velocity and acceleration. These methods are categorized under explicit integration methods [27]. Finite difference and Runge-Kutta methods are examples of explicit integration methods. In Newmark, Wilson and backward Euler methods, the current equation of motion is integrated by synthetic difference equations in order to find the current solution [27]. These methods are listed under implicit integration methods.

Generally, these time integration methods have two basic characteristics [27]. Firstly, the numerical integration methods do not satisfy equation of motion at all times except at small discrete time intervals. Secondly, each numerical integration method has special relations between displacements, velocity and accelerations within successive time intervals.

In this thesis, central difference, Newmark and backward Euler methods are used to solve the equation of motion of the antenna structure.

3.2 Central Difference Method

The Central difference method, which is a special case of finite difference methods, is the basic explicit numerical integration method. The theory behind the central difference method is the Taylor series expansion which is used to approximate the current displacement. Flowchart of the central difference method is given in Figure 3.1.

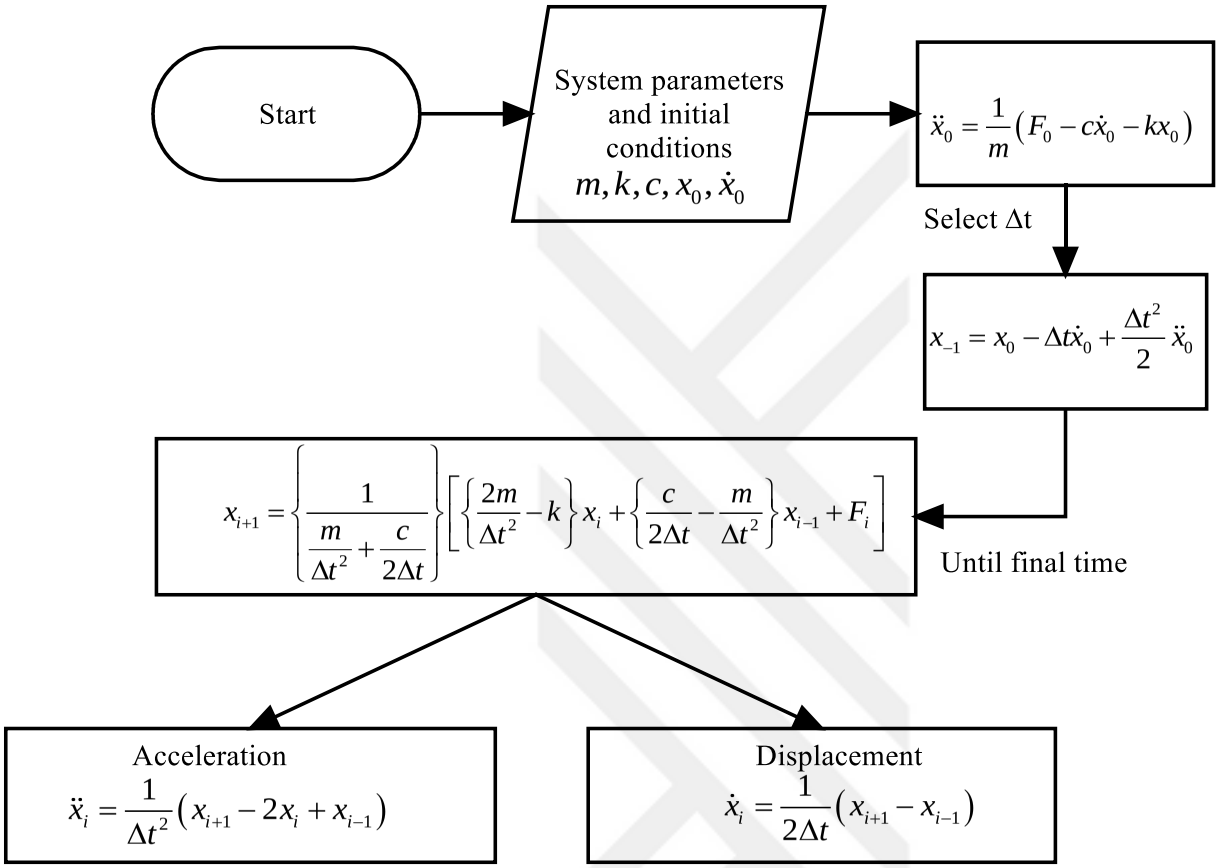

Figure 3.1 Flowchart of the central difference methods

Critical issue in central difference method is the choice of time step. The time step should be chosen smaller than critical time step in order obtain a stable algorithm. The critical time step is defined as

$$\Delta t_{critical} = \frac{\tau_n}{\pi} \ , \tag{3.1}$$

where τ_n is the natural period of the system. Furthermore, the accuracy of the method is determined by how small the time step, Δt, is chosen. Response of the equivalent lumped mass model of the antenna structure is obtained by using central difference method, since Saieni [36] claims that the central difference method is the least computationally expensive method for single degree of freedom systems. As an example, equivalent lumped mass system given in Figure 2.3 is subjected to $40g$ $500ms$ half sine shock. Relative acceleration response of the antenna structure is given Figure 3.2 and Figure 3.3 for various time steps. As can be seen from Figure 3.2, the response is unstable if the time step is selected twice of the critical time step. On the other hand, Figure 3.3, if time step is chosen smaller than critical time step, response of the single degree of freedom system is stable as expected.

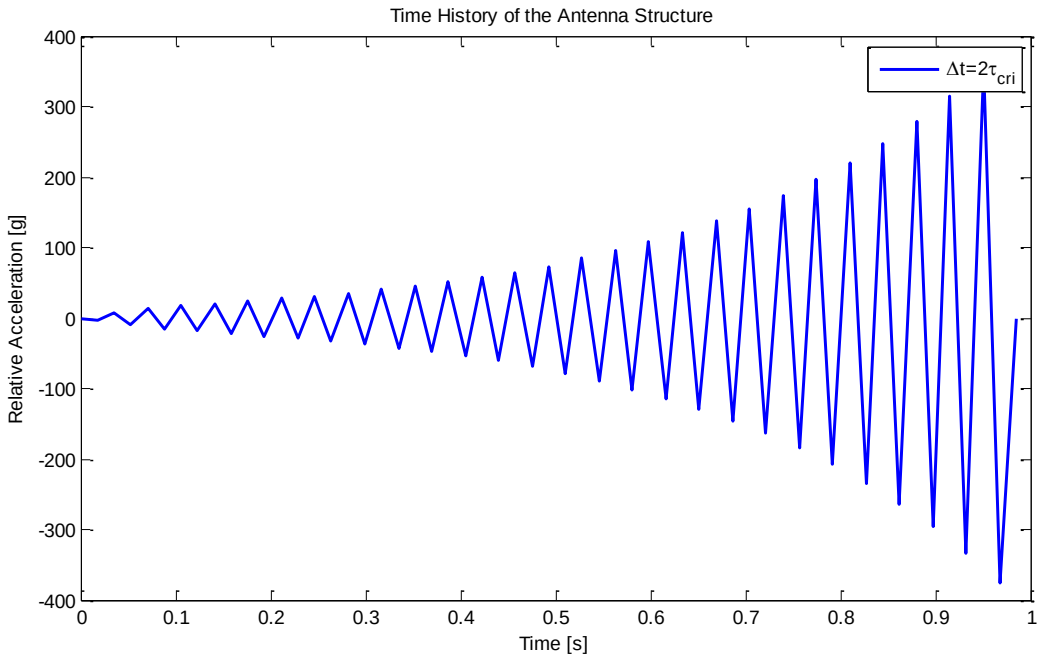

Figure 3.2 Unstable shock response of the antenna structure

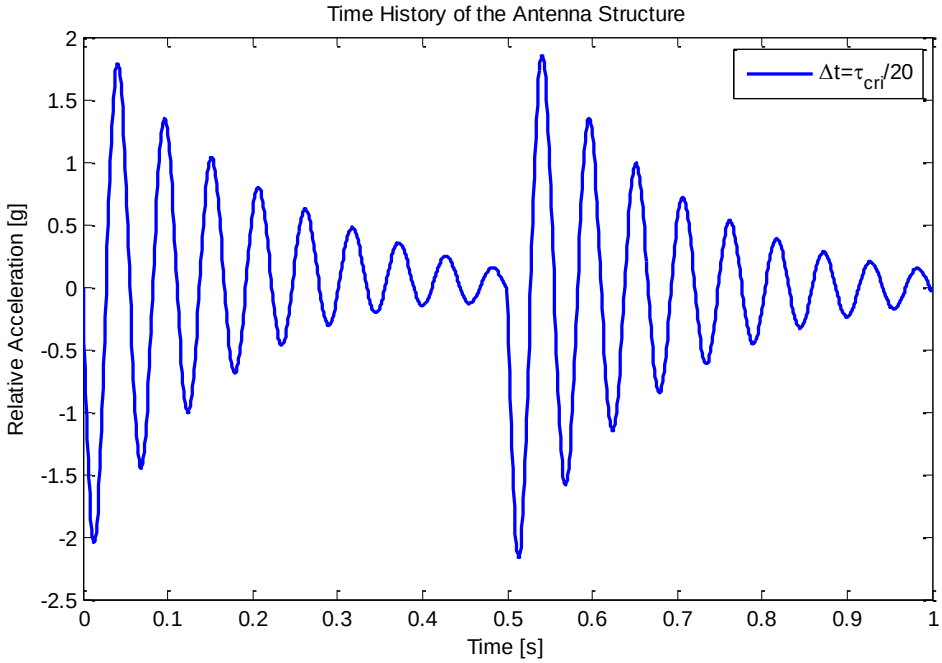

Figure 3.3 Response of the antenna structure using central difference method

In this Section, the central difference algorithm is summarized for single degree of freedom systems. In addition to that importance of selection of time step is mentioned.

In central difference method, time step is chosen smaller to get stable solution. This results in drawbacks for multi degree of freedom systems in terms of computation time. Therefore, implicit methods such as Newmark method where time step may be selected larger than the explicit methods are implemented for the solution of continuous and multi degree of freedom systems [36]

3.3 Newmark Methods for Linear Systems

Newmark Method, which is a single step implicit numerical integration method, is one of the most popular numerical integration method to analyze response of dynamic systems [37]. Newmark introduced this integration method in 1959 for both

blast and seismic loading [38]. Newmark method is based on velocity and displacement equations [27] given as

$$\dot{x}_{i+1} = \dot{x}_i + \left[(1-\beta)\ddot{x}_i + \beta \ddot{x}_{i+1} \right] \Delta t \ , \tag{3.2}$$

$$x_{i+1} = x_i + \Delta t \dot{x}_i + \left[(0.5-\alpha)\ddot{x}_i + \alpha \ddot{x}_{i+1} \right] \Delta t^2 \quad , \tag{3.3}$$

where α and β are artificial parameters of Newmark method. These parameters determine acceleration variation, stability and accuracy of the method. For example, if $\alpha = 1/6$ and $\beta = 0.5$ are chosen, this special case is called as linear acceleration methods. Moreover, if $\alpha = 0.25$ and $\beta = 0.5$ are chosen, this special case is called as constant average method [27]. Linear ordinary differential equations are solved by using the algorithm flowchart of which is given in Figure 3.4.

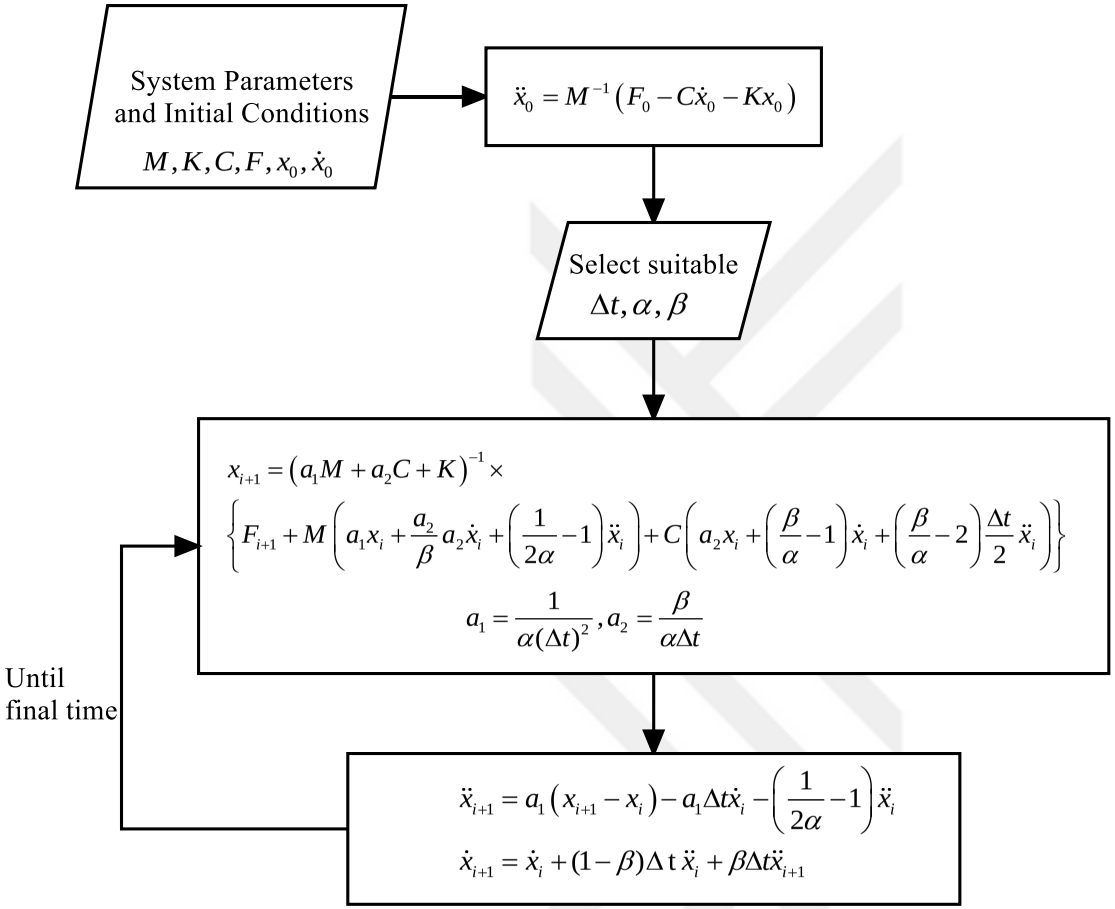

Figure 3.4 Flowchart of Newmark method for linear systems

One of the main advantages of Newmark method is that it is unconditionally stable when the following inequality is satisfied [27]

$$\beta \geq \frac{1}{2} \quad \alpha \geq \frac{1}{4}\left(\beta + \frac{1}{2}\right)^2 . \tag{3.4}$$

Moreover, Newmark method may bring artificial damping, known as algorithmic damping, to filter out higher frequency component of the system responses. This damping is proportional to $(\beta - 1/2)$. Thus, algorithmic damping may induce negative and positive damping. In the case of negative damping, vibration level of the system is higher than the expected response. In the case of positive damping, however, vibration is damped out more quickly than the expected response. For instance, consider the antenna structure given in Figure 2.11. The antenna structure, which is exposed to 100 g 1ms half sine mechanical shock, is modeled by including six modes. As can be seen in Figure 3.5, the result obtained from positive algorithmic damping is lower than the one obtained from negative algorithmic damping.

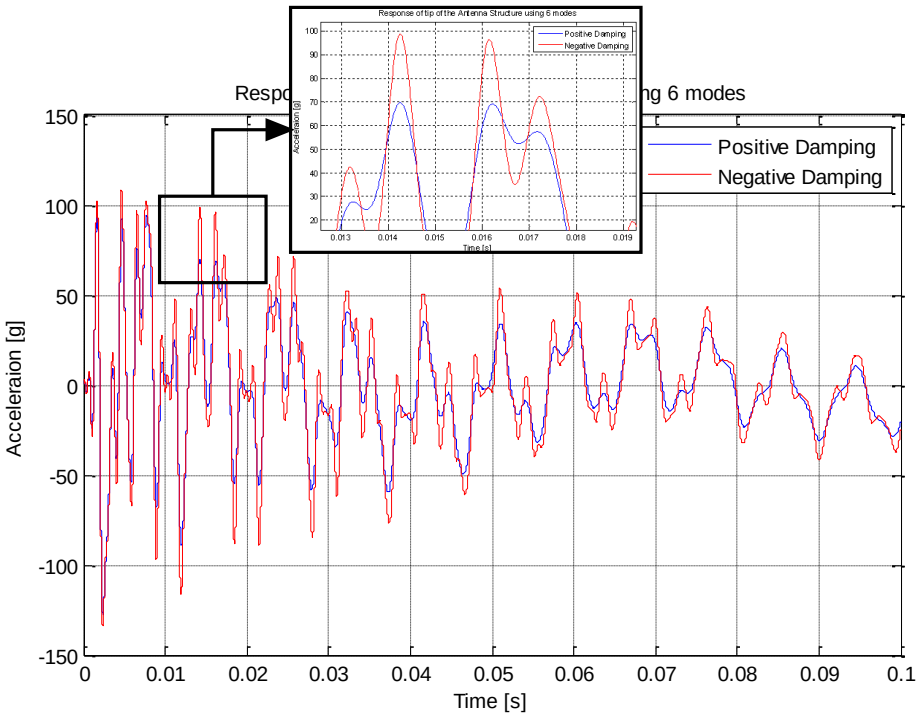

Figure 3.5 Effect of algorithmic damping on response of the antenna structure

3.4 MATLAB Ordinary Differential Equation (ODE) Solvers

In this Section, MATLAB® ordinary differential equation solvers are introduced to solve the resulting nonlinear ordinary differential equations.

In Section 3.3, linear response of the antenna structure is obtained from Newmark method. However, when the system is nonlinear, solution of the nonlinear differential equations of motion is a troublesome task. MATLAB®, powerful tool for engineering computation, has a lot of solvers, which are summarized in Table 3.1, for both linear and nonlinear ordinary differential equations.

Table 3.1 MATLAB® ODE solvers [39]

Solver	Problem Type	Order of Accuracy	Method	When to Use
ode45	Nonstiff	Medium	Runge-Kutta	Should be first solver
ode23	Nonstiff	Low	Runge-Kutta	Should be used for solving moderately stiff problems
ode113	Nonstiff	Low to high	Adams	Should be used for solving computationally expensive problems
ode15s	Stiff	Low to medium	NDFs (BDFs)	Should be used for stiff problems
ode23s	Stiff	Low	Rosenbrock	Should be used for stiff problems
ode23t	Moderately Stiff	Low	Trapezoidal rule	Should be used for moderately stiff problems without numerical damping
ode23tb	Stiff	Low	TR-BDF2	Should be used for stiff problems

Firstly, in order to use these solvers, nonlinear ordinary differential equations are converted to state space representation where systems are represented by first order

differential equations rather than second order. As an example, consider the antenna structure given in Figure 2.11. Responses of the antenna structure under the half sine mechanical shocks having various magnitudes are investigated by using both MATLAB® ODE solvers and Newmark method (see Section 3.6). Figure 3.6 shows acceleration response of the tip point of the antenna structure including geometric nonlinearity. Nonlinear result obtained from Newmark method is in agreement with the results obtained from ODE 23t, which is generally used for moderately stiff problems. As can be seen from Figure 3.7 and Figure 3.8, however, if the magnitude of the mechanical shock increases, the difference between nonlinear responses obtained from Newmark method and MATLAB® ODE solvers starts to increase dramatically. This significant change is mainly due to numerical error. As shown in Figure 3.8, if the magnitude of the mechanical shock continues to increase, dramatic responses are obtained from not only ODE 23t but also other stiff MATLAB® ODE solvers.

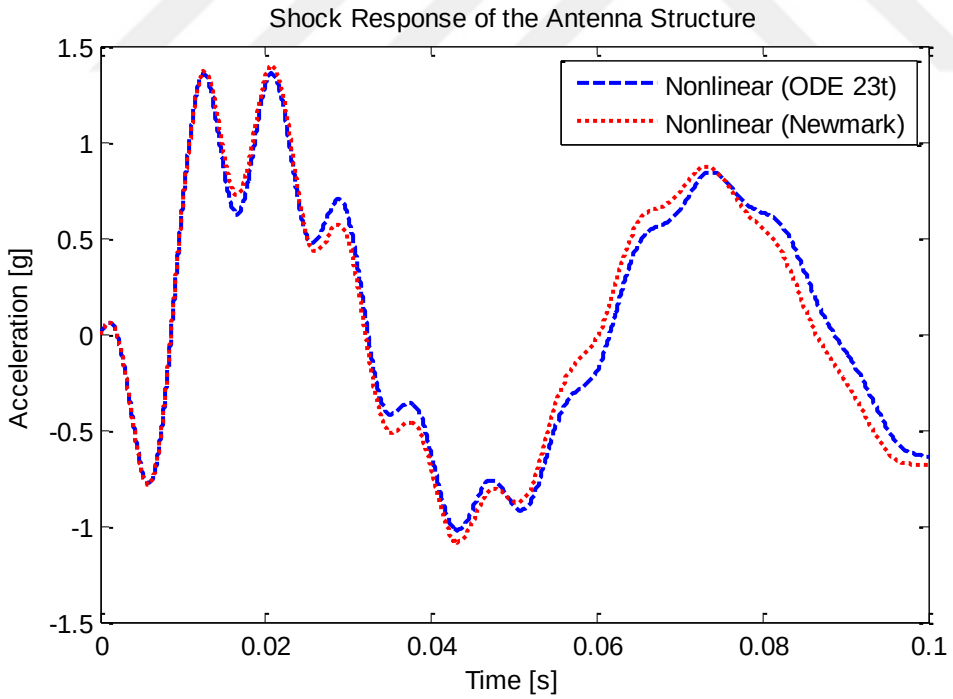

Figure 3.6 Response of tip point of the antenna structure including geometric nonlinearity for $1g$ $11ms$ half sine shock

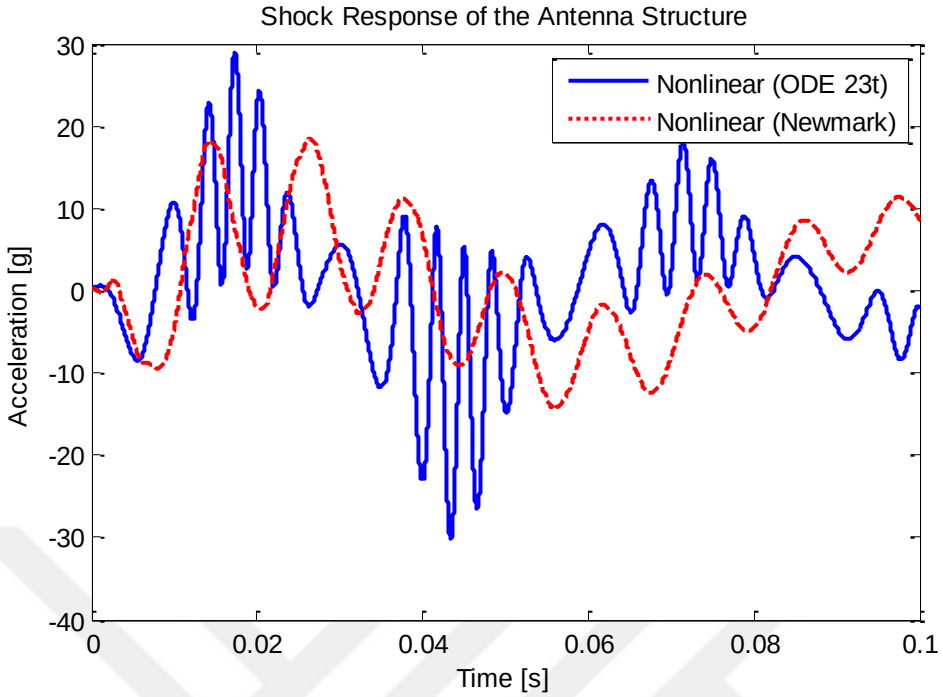

Figure 3.7 Response of tip point of the antenna structure including geometric nonlinearity for $10g$ $11ms$ half sine shock

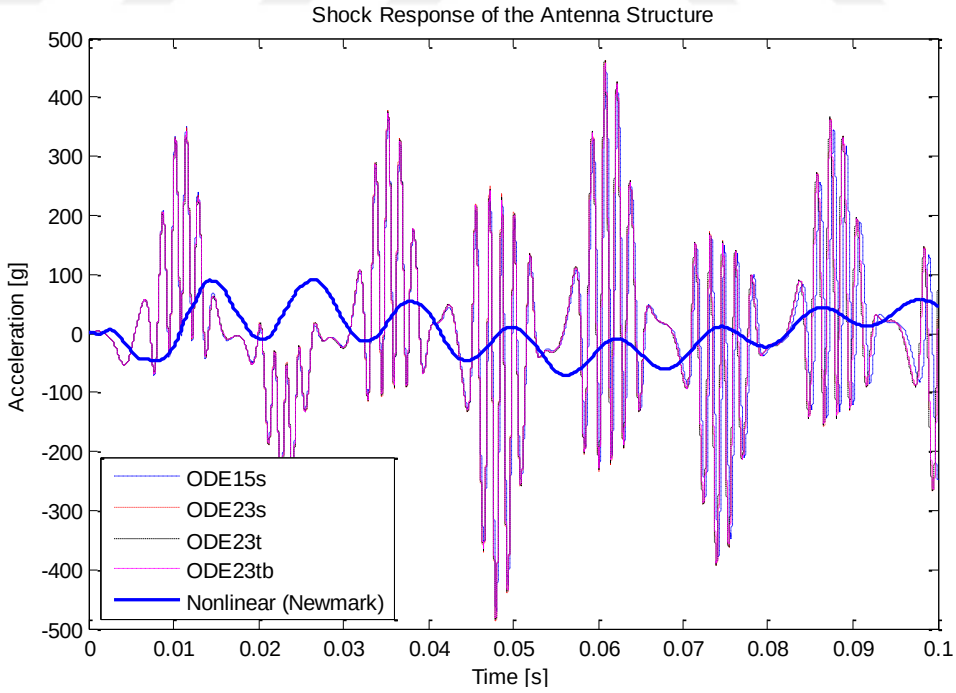

Figure 3.8 Response of the antenna structure obtained from stiff MATLAB® ODE solvers for $50g$ $11ms$ half sine shock

According to above figures, although MATLAB® ODE solvers have a capability to solve linear equation of motion of the antenna structure, the equation of motion of the antenna structure including geometric nonlinearity under mechanical shock cannot be solved. Therefore, a computer code based on other integration methods must be written to determine the dynamic characteristic of an antenna structure under mechanical shock. In this thesis, backward Euler and Newmark methods are used to predict shock response of an antenna structure including geometric nonlinearity.

3.5 Backward Euler Method

In this section, backward Euler method is explained in detail. Backward Euler method is one of the implicit methods to solve both linear and nonlinear ordinary differential equations and it is one of the most fundamental numerical integration method for structural dynamics. One of the advantage of this method is that backward Euler method damps out effects of artificial higher modes on system response [40]. In addition to that backward Euler method does not involve artificial parameters. Moreover, computational cost of backward Euler method is the same as trapezoidal rule, which can be unstable for solving nonlinear systems. Although trapezoidal method is a self-starting method, backward Euler method is a two-step method.

For this algorithm, equation of motion of nonlinear dynamic problem is written as [40]

$$\mathbf{M}\ddot{\mathbf{x}}=\mathbf{p}-\mathbf{f}_d-\mathbf{f}_s\,, \tag{3.5}$$

where, $\mathbf{M}$ is mass matrix, $\mathbf{p}$ is external load vector, $\mathbf{f}_d$ is internal damping force vector and $\mathbf{f}_s$ is internal spring force vector. The flowchart of backward Euler method based on Eq. (3.5) is given Figure 3.9.

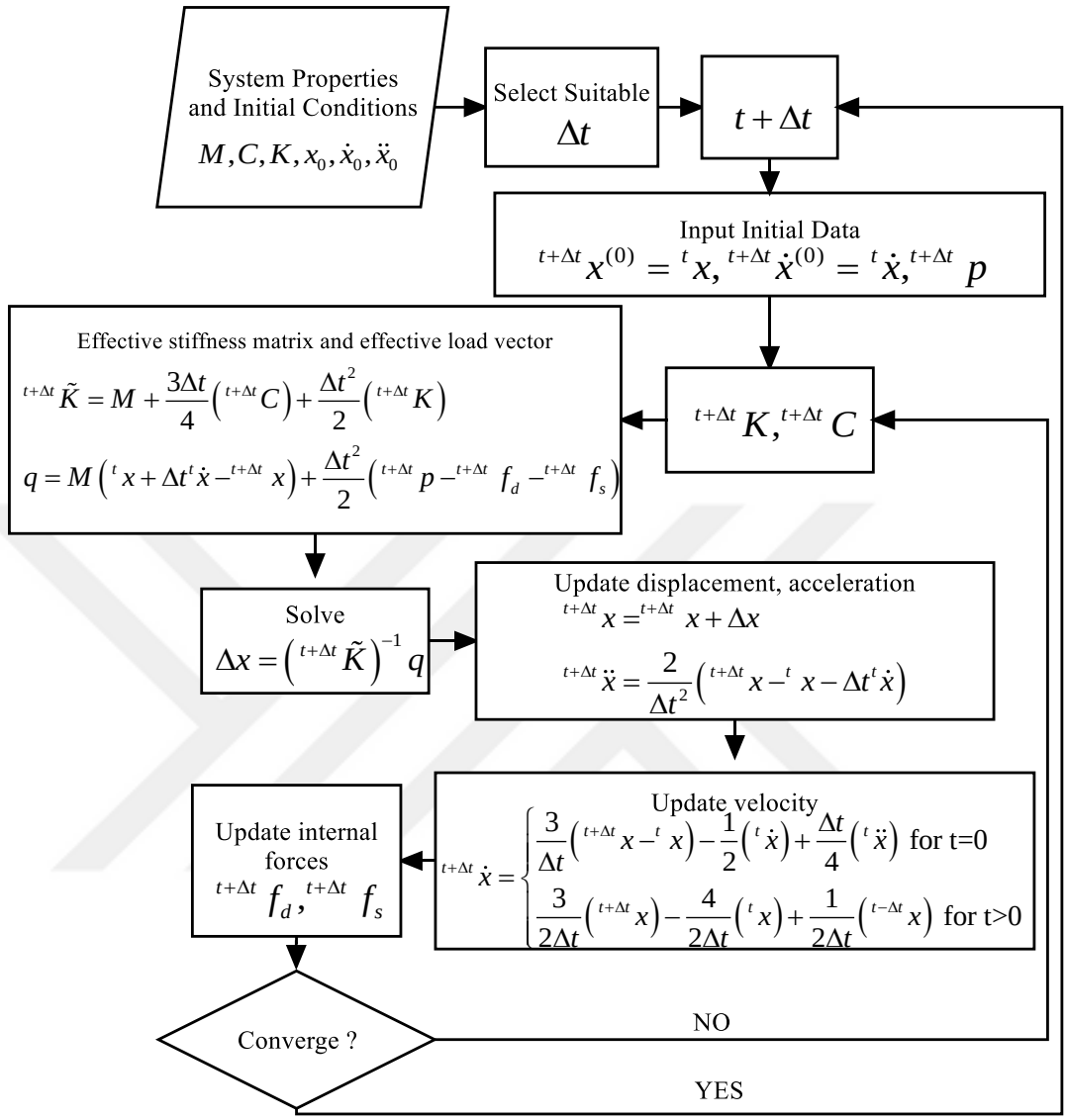

Figure 3.9 Flowchart of backward Euler Method

3.6 Newmark Method for Nonlinear Systems

Newmark method is an implicit numerical integration method to solve both linear and nonlinear structural dynamic problems as mentioned in Section 3.3. In this Section, solution of both linear and nonlinear structural dynamics problems is considered by using Newmark method.

Consider the general equation of motion of a dynamic problem as [41]

$$\mathbf{M}\ddot{\mathbf{x}}+\mathbf{C}\dot{\mathbf{x}}+\mathbf{f}_s=\mathbf{p}\ , \tag{3.6}$$

where, **M** and **C** are mass and damping matrices, respectively. $\mathbf{f}_s$ is vector of internal spring forces, which is nonlinear, and **p** is the external load vector. In this method, Newton-Raphson method is used to find the rate of change of stiffness in infinitesimal displacement increment. Therefore, Jacobian matrix or tangent stiffness matrix of internal spring force is written as

$$k_T=\begin{bmatrix} \dfrac{\partial f_{s_1}}{\partial x_1} & \cdots & \dfrac{\partial f_{s_1}}{\partial x_n} \\ \vdots & \ddots & \vdots \\ \dfrac{\partial f_{s_n}}{\partial x_1} & \cdots & \dfrac{\partial f_{s_n}}{\partial x_n} \end{bmatrix}. \tag{3.7}$$

Flowchart of Newmark method is given [41] in Figure 3.10.

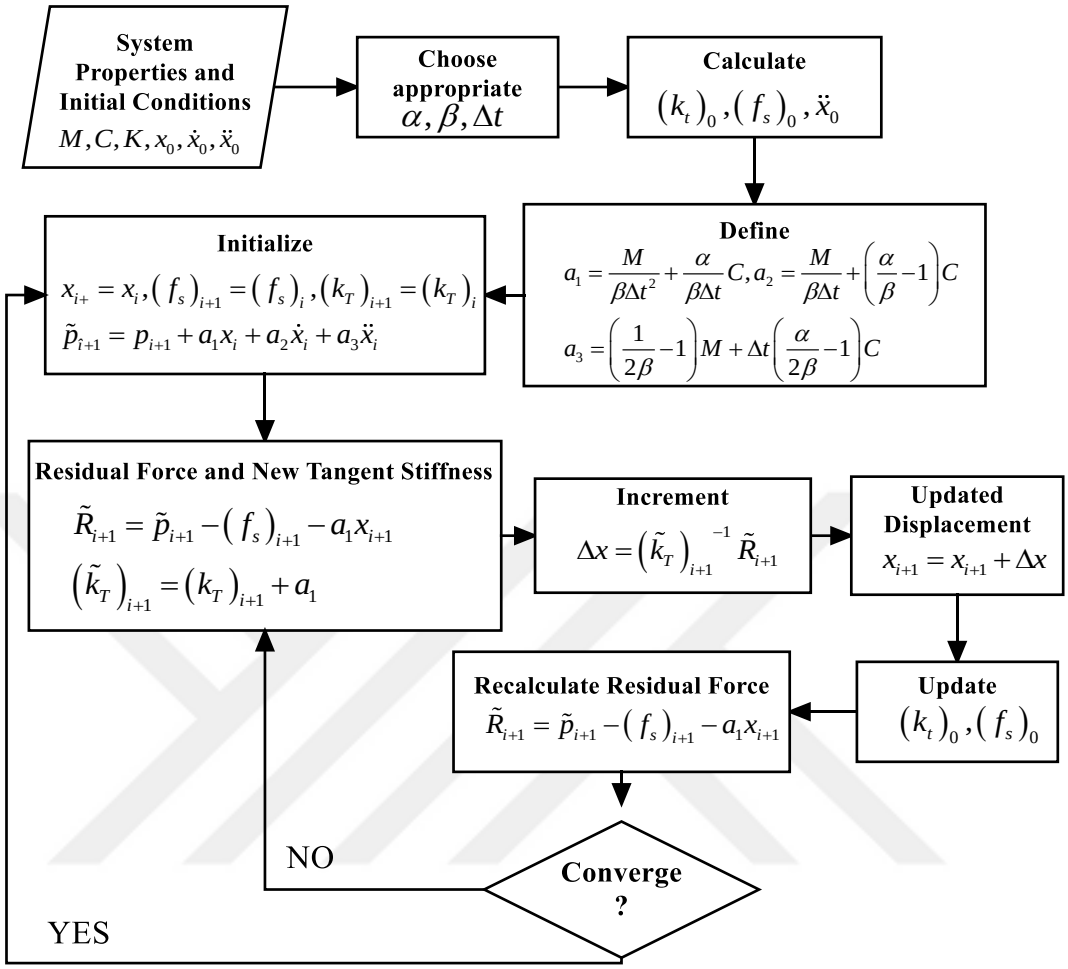

Figure 3.10 Flowchart of Newmark method for nonlinear systems

In this method, numerical damping is again adjusted by Newmark constants α and β. This brings the control of algorithmic damping, which filters out artificial component of higher modes. Moreover, Newmark method is a single step method while backward Euler method is a two-step method. On the other hand, Newmark method introduces artificial parameters such as α and β.

As an example, consider the antenna structure given in Figure 2.11 with constant cross section and uniform density. Shock response of the antenna structure is given Figure 3.11. As can be seen from the figure, the result of backward Euler method is in agreement with the result of Newmark method.

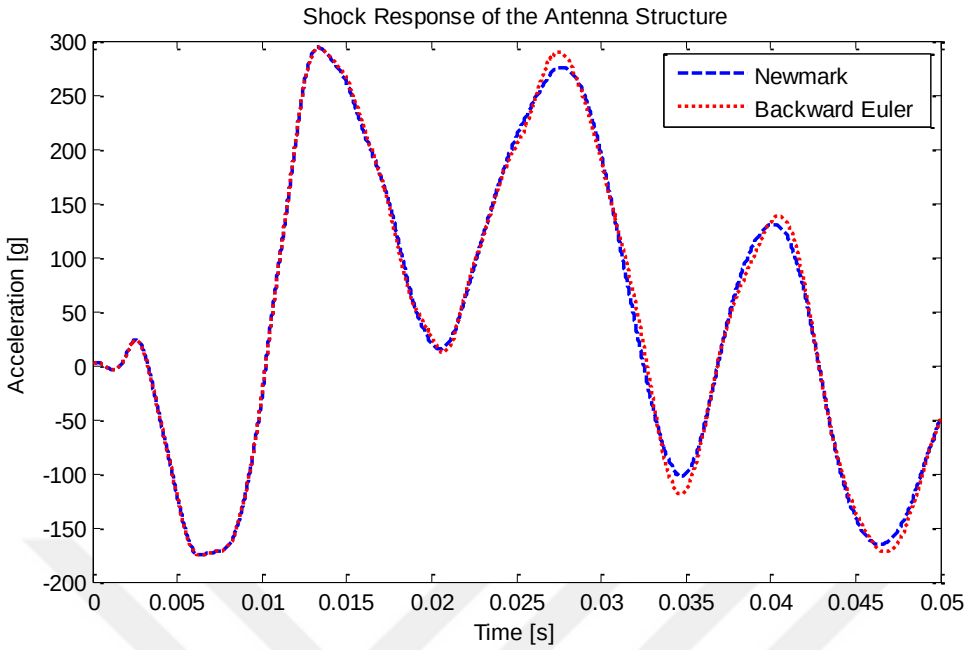

Figure 3.11 Comparison of Newmark and backward Euler methods

In this chapter, numerical integration methods are presented in order to solve both linear and nonlinear ordinary differential equations. Central difference and Newmark methods are briefly introduced for linear systems. A computer code based on Newmark and backward Euler methods is written to capture shock response of an antenna structure including nonlinearity, since MATLAB® ODE solvers are not capable of solving these equations.

CHAPTER 4

APPROXIMATE METHODS FOR SHOCK RESPONSE CALCULATION

4.1 Introduction

In this chapter, approximate methods are studied to estimate maximum shock response of the antenna structure. Up to this chapter, shock response of the antenna structure is investigated by solving linear or nonlinear equation of motion at each time interval which is computationally expensive procedure. Therefore, approximate methods are developed to estimate shock response of antenna structures. In Section 4.2, a brief introduction to shock response spectrum, which is widely used in approximate methods, is presented. In Section 4.2.1, approximate methods based on static combination are introduced for both linear and nonlinear models. Moreover, in Section 4.3, approximate methods based on modal combination are examined.

4.2 Shock Response Spectrum

A shock response spectrum, introduced by Maurice Biot in 1932, involves peak responses of single degree of freedom systems, where natural frequency is the independent variable [6]. In shock response spectrum plots, Y axis shows peak responses of systems exposed to any arbitrary shock while X axis represents natural frequencies of the infinite number of single degree of freedom systems. Figure 4.1 shows construction of the shock response spectrum. Shock response spectrum is developed for mechanical shocks that have complex time history such as ballistic and pyrotechnic shocks. Thus, they cannot be easily reproduced for a qualification test. For example, a qualification test of military systems such as an antenna structure exposed to a ballistic shock is practically impossible, since reproduction of the ballistic shock is not an easy task. In addition to this, effects of complex shock pulses on dynamic systems are not studied, since they cannot be expressed in terms of

mathematical functions. As a result of this, shock response spectrum is developed for both determination of qualification of shock level and understanding the effect of mechanical shocks [42]. Therefore, shock response spectrum is widely used in many military and civilian standards. For example, MIL-STD-810G uses shock response spectrum for analysis and testing of the military systems that are exposed to mechanical shocks.

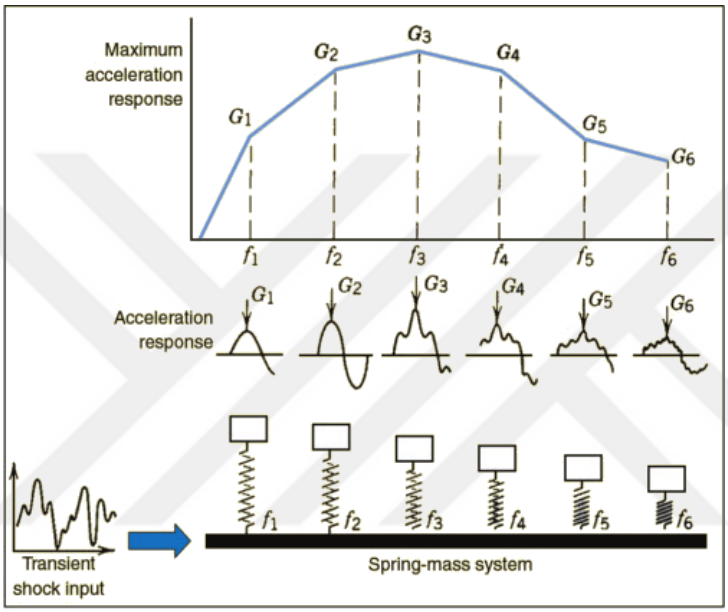

Figure 4.1 Construction of shock response spectrum [6]

Moreover, the shock response spectrum may be presented in several forms such as;

- Maximax spectrum, where maximum absolute responses is plotted as a function of natural frequency [6],
- Maximum positive spectrum , where maximum positive response is plotted as a function of natural frequency [6],
- Maximum negative spectrum, where maximum negative response is plotted as a function of natural frequency [6],
- Relative displacement spectrum, where relative displacement between the base and structure is plotted as a function of natural frequency [42].

Maximax acceleration spectrum is the most accepted form of shock response spectrum for the analysis of mechanical shock according to military standard MIL-

STD-810 G [8]. For example, consider a half sine mechanical shock shown in Figure 4.2. Maximax peak acceleration shock response spectrum of mechanical shocks is given in Figure 4.3 by assuming a damping ratio, ζ , of 0.05. It should be noted that shock response spectrum plots are obtained by using central difference method.

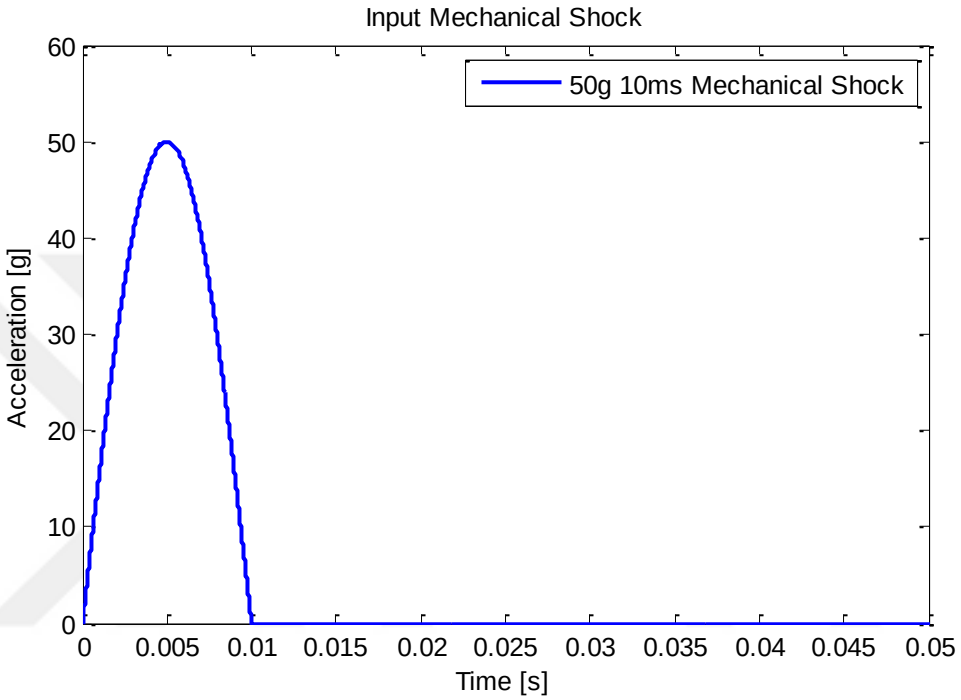

Figure 4.2 Input mechanical shock (50g 10ms)

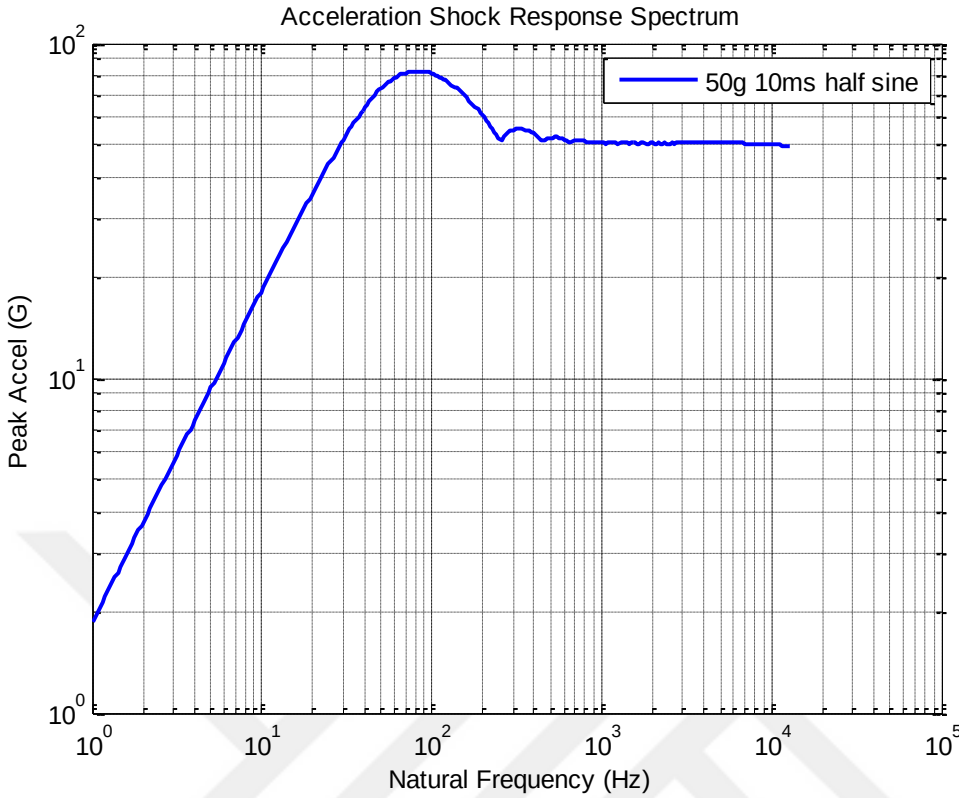

Figure 4.3 Maximax acceleration shock response spectrum of 50 g 11ms half sine and mechanical shocks

4.2.1 An Approximate Method based on Static Combination

In this Section, one of the approximate methods used to estimate the maximum deformation of the antenna structure under mechanical shock by means of combination of static response and shock response spectrum is examined. Calculation of maximum shock response of the antenna structure is the primary objective in most of the time, since the antenna structure may experience functional and structural failure at these peak responses due to high acceleration. Therefore, approximate methods to estimate maximum response of the antenna structure are required.

In one of the approximate methods, according to Younis [30], the maximum displacement of the antenna structure under mechanical shock can be estimated by multiplying the maximum static response with dynamic factor obtained from a shock

response spectrum. Firstly, relative displacement shock response spectrum is plotted where Y axis of the shock response spectrum is the ratio of relative displacement between the base and structure to the maximum static response of single degree of freedom systems while X axis represents the ratio of mechanical shock duration to natural period of the antenna structure (see Figure 4.4). Figure 4.4 shows relative displacement shock response spectrum of half sine for various damping ratios. It is should be noted that central difference method (see Section 3.2) is used to plot this shock response spectrum. In this plot, duration of the mechanical shock or natural period of the structure is considered as the independent variable. It can be seen from Figure 4.4 that when the duration of shock is much higher than the natural period of the antenna structure, this phenomenon is called as quasi-static case where dynamic effect of the mechanical shock on response may be neglected. In other words, static response dominates response of the antenna structure in that case. Secondly, the maximum load in the mechanical shock, which is applied as a distributed force throughout the structure, is used to find the maximum static response of the antenna structure. In the light of above mentioned information, the maximum relative displacement is estimated as follows

$$w_{\max} = \frac{A_{dyn}}{A_{stat}} x_{stat} \ , \tag{4.1}$$

where, $w_{\max}$ is the maximum relative displacement of the antenna structure, A_{dyn} / A_{stat} is obtained from the relative displacement shock response spectrum and x_{stat} is the maximum static deformation of the antenna structure. The maximum static deformation of the antenna structure is expressed as [43]

$$x_{stat} = \frac{\rho A a_{\max} l^4}{8EI} \ , \tag{4.2}$$

where, ρ and A are uniform density and cross section of the antenna structure, $a_{\max}$ is the maximum acceleration amplitude of the mechanical shock, l is the length and EI is the flexural rigidity of the antenna structure.

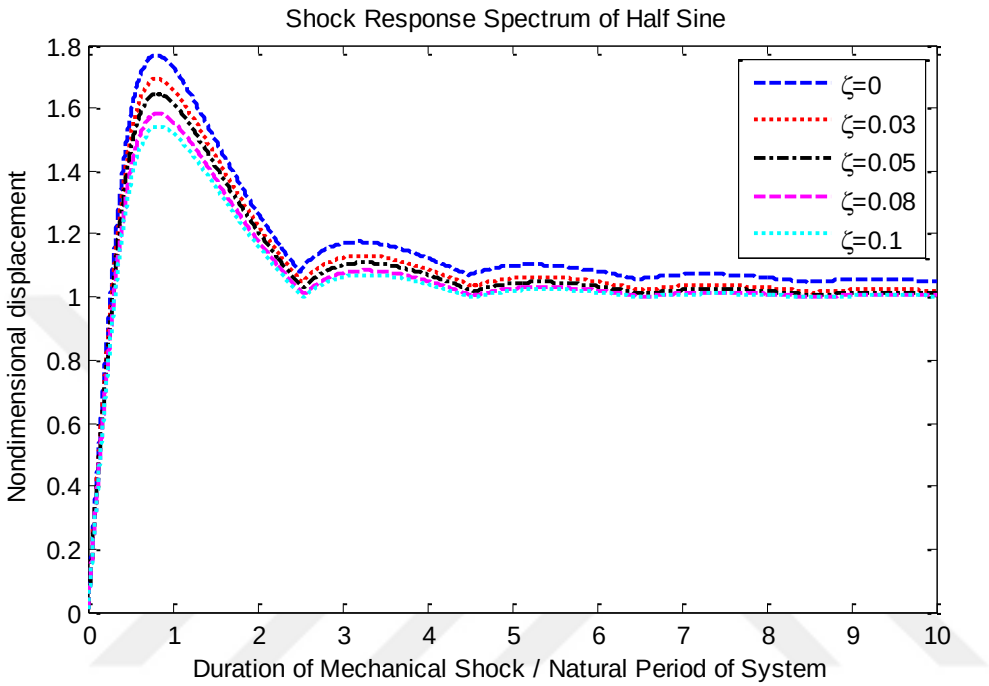

Figure 4.4 Relative displacement shock response spectrum of half sine mechanical shock

For instance, consider the antenna structure given in Figure 2.11 with uniform density and constant cross section. The maximum static deflection of the antenna structure is computed by using Eq. (4.2). Dynamic constant is calculated by using the relative displacement shock response spectrum. In this computation, natural period of the antenna structure is found by using an equivalent lumped mass system, where the natural period is computed as

$$T_{strucuture} = \frac{2\pi}{\omega_n} = 2\pi\sqrt{\frac{m_{eq}}{k_{eq}}}\ , \tag{4.3}$$

where, m_{eq} (see Eq. (2.7)) is the equivalent lumped mass and k_{eq} (see Eq. (2.6)) is the equivalent stiffness of the antenna structure. In the light of the above information, the maximum relative displacement of the tip point of the antenna structure is given

in Figure 4.5 for various shock amplitudes. In this example, damping ratio is taken as 0.05 and duration of the mechanical shocks are equal to 11ms.

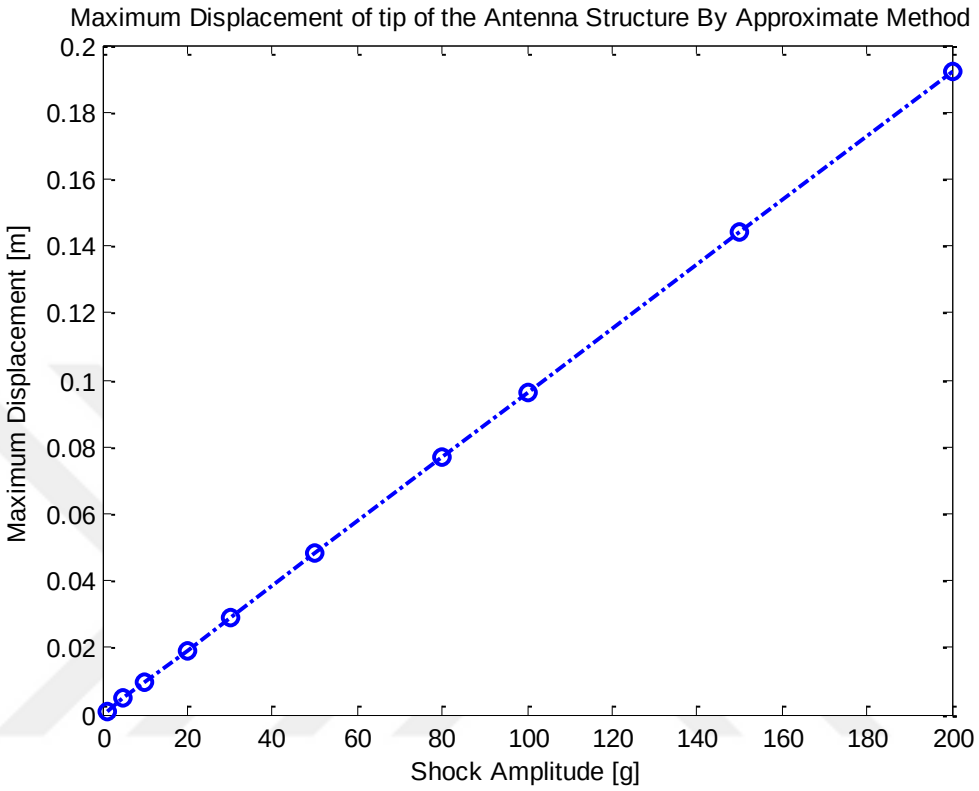

Figure 4.5 Maximum deformation of the antenna structure

In the case of shock response of the antenna structure including geometric nonlinearity, estimation of the maximum response is computationally more expensive than its linear counterpart [22]. Nevertheless, computation time is much less than the solution of the transient nonlinear equation of motion. For example, consider the equation of motion of the antenna structure under mechanical shock including nonlinearity defined by Eq. (2.31). Static response of the antenna structure is calculated by neglecting the time derivatives in Eq. (2.31). Therefore, equation of motion simplifies to a nonlinear differential equation as

$$\frac{\partial^4 w}{\partial x^4} = -\frac{\partial}{\partial x}\left(\frac{\partial w}{\partial x}\frac{\partial}{\partial x}\left(\frac{\partial w}{\partial x}\frac{\partial^2 w}{\partial x^2}\right)\right) + F_{non} \ , \tag{4.4}$$

where, w is the transverse displacement of the antenna structure, F_{non} is the nondimensional forcing parameter defined in Eq. (2.32). Consider a solution in the following form

$$w = \sum_{i=1}^{n} u_i \phi_i(x) \ , \tag{4.5}$$

where, u_i is a constant to be calculated. Substitute Eq. (4.5) into Eq. (4.4) and multiplying both sides by $\phi_j(x)$ and integrating from 0 to 1, the following result is obtained

$$\begin{aligned} &\sum_{i=1}^{n} u_i(t) \int_0^1 \phi_j(x) \phi_i''''(x) \, \mathrm{d}x = \\ &-\int_0^1 \phi_j \left(\begin{array}{l} \left(\sum_{i=1}^{n} u_i \phi_i'' \right)^2 + 4 \left(\sum_{i=1}^{n} u_i \phi_i' \right) \left(\sum_{i=1}^{n} u_i \phi_i'' \right) \left(\sum_{i=1}^{n} u_i \phi_i''' \right) \\ + \left(\sum_{i=1}^{n} u_i \phi_i' \right)^2 \left(\sum_{i=1}^{n} u_i \phi_i'''' \right) \end{array} \right) dx + \int_0^1 \phi_j(x) F_{non} a_{pulse} \end{aligned} \ . \tag{4.6}$$

The resulting system of nonlinear algebraic equations are solved by using "*fsolve*" command of MATLAB® 2015. Figure 4.6 shows the maximum approximate shock response of the antenna structure under the 11ms half sine mechanical shock for various amplitudes. As observed from Figure 4.6, the relation between shock amplitude and the maximum static deformation is not linear as expected.

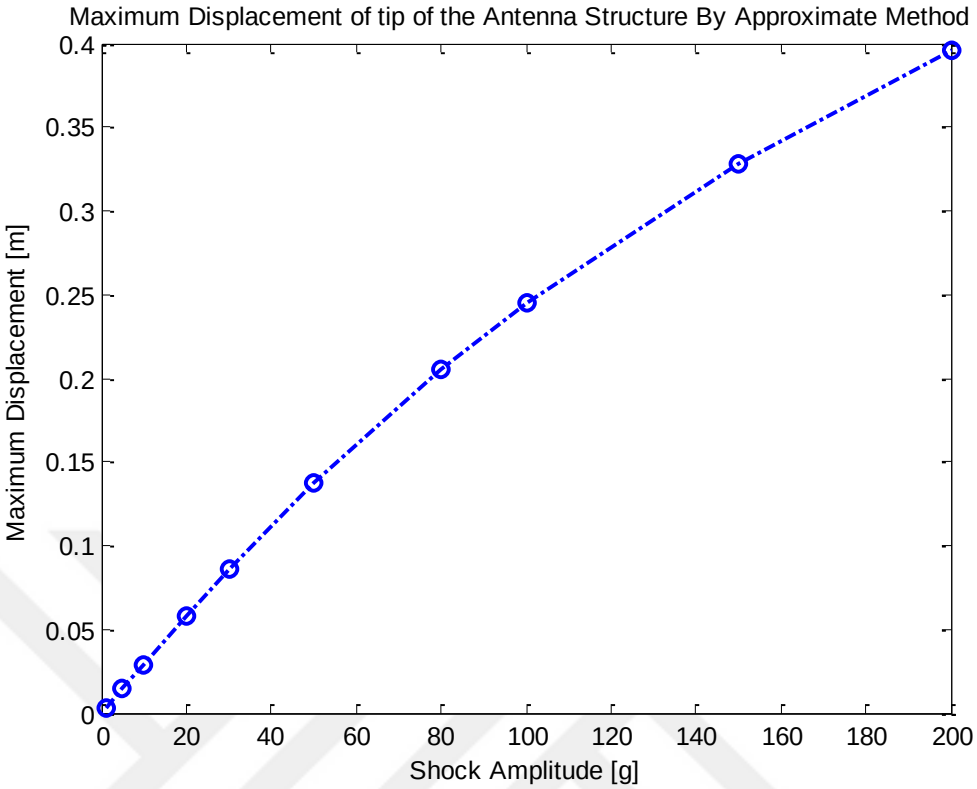

Figure 4.6 Maximum deformation of the antenna structure including geometric nonlinearity

One of the main drawbacks of the approximate methods based on static combination is that the maximum acceleration, which is crucial for antenna systems, cannot be estimated since static deformation reveals only the maximum displacement. Therefore, the approximate methods, which estimate acceleration response, is needed.

4.3 Approximate Methods based on Modal Combination

In this Section, approximate methods based on modal combination are introduced. In these methods, the maximum response of the antenna structure is estimated by a combination of mass normalized eigenfunction coefficient, modal participation factor and dynamic constant obtained from shock response spectrum. Moreover, mass normalized eigenfunction coefficient is obtained by using a mode shape function of the antenna structure at a desired location. Furthermore, the modal participation

factor shows effectiveness of a particular mode on the response [44] And it can be calculated as [33]

$$\Gamma_n = \rho A \int_0^L \phi_n(x)\,\mathrm{d}x \ , \tag{4.7}$$

where, Γ_n is the modal participation factor, ρ and A are uniform density and cross section of the antenna structure, respectively and $\phi_n(x)$ is the mass normalized mode shape of the n^{th} mode.

4.3.1 Absolute Sum Method (ABS)

In this method, the maximum response of all modes reveal at the same time. Therefore, the outcome is an upper bound to the maximum response estimation. According to absolute sum method, the maximum displacement and acceleration are written as

$$w(x)_{\max} \le \sum_{i=1}^{n} \left|\Gamma_i\right| \left|\phi_i(x)\right| \left|A_{dyn,i}\right| \ , \tag{4.8}$$

$$\ddot{w}(x)_{\max} \le \sum_{i=1}^{n} \left|\Gamma_i\right| \left|\phi_i(x)\right| \left|\ddot{A}_{dyn,i}\right| \ , \tag{4.9}$$

respectively [45]. Here, $w_{\max}(x)$ and $\ddot{w}_{\max}(x)$ are the maximum relative displacement and acceleration responses, respectively and Γ_i is the modal participation factor of the i^{th} mode, $\phi_i(x)$ is the mass normalized mode shape of the antenna structure at location x, $A_{dyn,i}$ is a constant obtained from the relative displacement shock response spectrum at the i^{th} natural frequency and $\ddot{A}_{dyn,i}$ is a constant obtained from the maximax acceleration shock response spectrum at the i^{th} natural frequency.

4.3.2 Square Root of the Sum of Squares Method (SRSS)

In this method, as the name implies, the maximum response is calculated by square root of the sum of squares of the maximum responses of all modes. In other words, the maximum relative displacement and acceleration are obtained as [45]

$$w(x)_{\max} = \sqrt{\sum_{i=1}^{n} \left(\Gamma_i \phi_i(x) \mathrm{A}_{dyn,i} \right)^2} \ , \tag{4.10}$$

$$\ddot{w}(x)_{\max} = \sqrt{\sum_{i=1}^{n} \left(\Gamma_i \phi_i(x) \ddot{\mathrm{A}}_{dyn,i} \right)^2} \ . \tag{4.11}$$

4.3.3 Naval Research Laboratories Summation Method (NRL)

In this method, maximum displacement and acceleration are estimated as [20]

$$w(x)_{\max} = \left| \Gamma_k \phi_k(x) \mathrm{A}_{dyn,k} \right| + \sum_{i=1, i \neq k}^{n} \sqrt{\left(\Gamma_i \phi_i(x) \mathrm{A}_{dyn,\mathrm{i}} \right)^2} \ , \tag{4.12}$$

where, the k^{th} mode has the largest $\left| \Gamma_k \phi_k(x) \mathrm{A}_{dyn,k} \right|$ value.

4.3.4 Complete Quadratic Combination Method (CQC)

In this method, the maximum displacement and acceleration are obtained as [46]

$$w(x)_{\max} = \sqrt{\left(\left| \sum_{i=1}^{n} \sum_{j=1}^{n} k \varepsilon_{ij} \left(\Gamma_i \phi_i(x) \mathrm{A}_{dyn,\mathrm{i}} \right) \left(\Gamma_j \phi_j(x) \mathrm{A}_{dyn,\mathrm{j}} \right) \right| \right)} \ , \tag{4.13}$$

where,

$$k = \begin{cases} 1 \text{ if } i = j \\ 2 \text{ if } i \neq j \end{cases}, \tag{4.14}$$

$$\varepsilon_{ij} = \frac{8(\zeta_i \zeta_j)^{1/2}(\zeta_i + \zeta_j)\mathrm{r}^{3/2}}{(1-\mathrm{r}^2)^2 + 4\zeta_i\zeta_j r(1+\mathrm{r}^2) + 4(\zeta_i^2 + \zeta_j^2)\mathrm{r}^2}, \tag{4.15}$$

$$r = \frac{\omega_j}{\omega_i}, \tag{4.16}$$

and, ζ is the damping ratio and ω is the natural frequency.

For instance, consider the antenna structure given in Figure 2.11 with uniform density, constant cross section and 0.05 damping ratio for all modes. The maximum relative displacement and acceleration responses of the antenna structure obtained by absolute sum square root of sum of squares, naval research laboratories and complete quadratic combination methods for a 11ms half sine mechanical shock are given in Figure 4.7 and Figure 4.8, respectively.

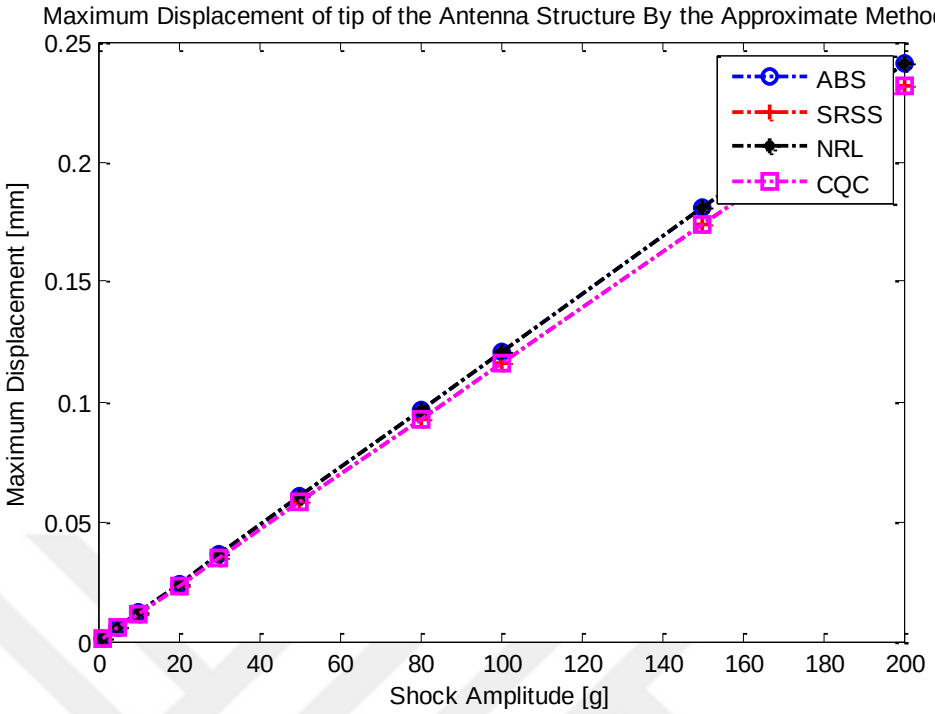

Figure 4.7 Maximum deflection of the antenna structure using modal combination methods

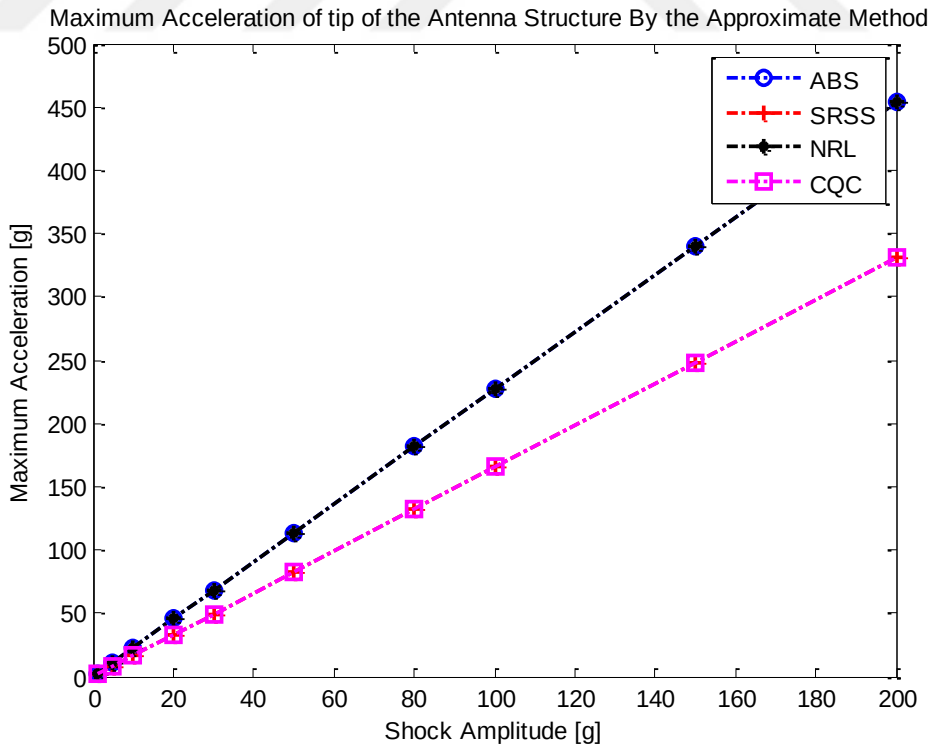

Figure 4.8 Maximum acceleration of the antenna structure using modal combination methods

It can be observed from the results that absolute summation method and naval research laboratories method give an upper bound.

In this chapter, several approximate methods are introduced. Firstly, the approximate methods based on static combination are presented to estimate both linear and nonlinear maximum relative displacement of the antenna structure. Secondly, the approximate methods based on modal combination are examined to predict both the linear maximum relative displacement and acceleration responses of the antenna structure.

CHAPTER 5

EXPERIMENTAL STUDIES

5.1 Introduction

In this chapter, experimental studies which consist of modal test and mechanical shock testing are introduced. Firstly, modal test of the antenna structure is carried out by using impact hammer in order to validate the test setup. Moreover, modal damping ratios are determined after modal testing. Secondly, mechanical shock is carried out by using drop table in order to validate both mathematical modelling and simulations.

5.2 Modal Testing of the Antenna Structure

In this section, modal testing of an antenna structure is detailed. Initially, experimental equipment's used in modal mechanical shock testing are introduced. Later, results obtained from modal testing are given.

Modal testing of the antenna structure is necessary, since natural frequencies are vital in order to validate the antenna model. In addition to this, damping ratio of each mode of the antenna structure is determined from modal testing. Therefore, modal testing should be done in order to validate the model that will be used shock testing.

As observed from Figure 5.1, accelerometer, miniature impact hammer, data acquisition system and test computer are used for modal testing. In the modal test, a triaxial miniature accelerometer, whose mass is 1 g is used. The measurement range of the accelerometer is about ±1000g and other physical and electrical properties of the accelerometers are given in Appendix-A. Modal testing of the antenna structure is done by using a hard tip impact hammer whose response curve is given in Figure

5.3. It can be observed from the figure that frequency range of the impact hammer is sufficient to reveal dominant mode of the antenna structure. Further properties of the miniature impact hammer are given in Appendix-A. Additionally, IOTECH WaveBook/516E is used for data acquisition. The technical paper for this system is given in Appendix-A. Test computer is used to store and examine the data collected from modal testing.

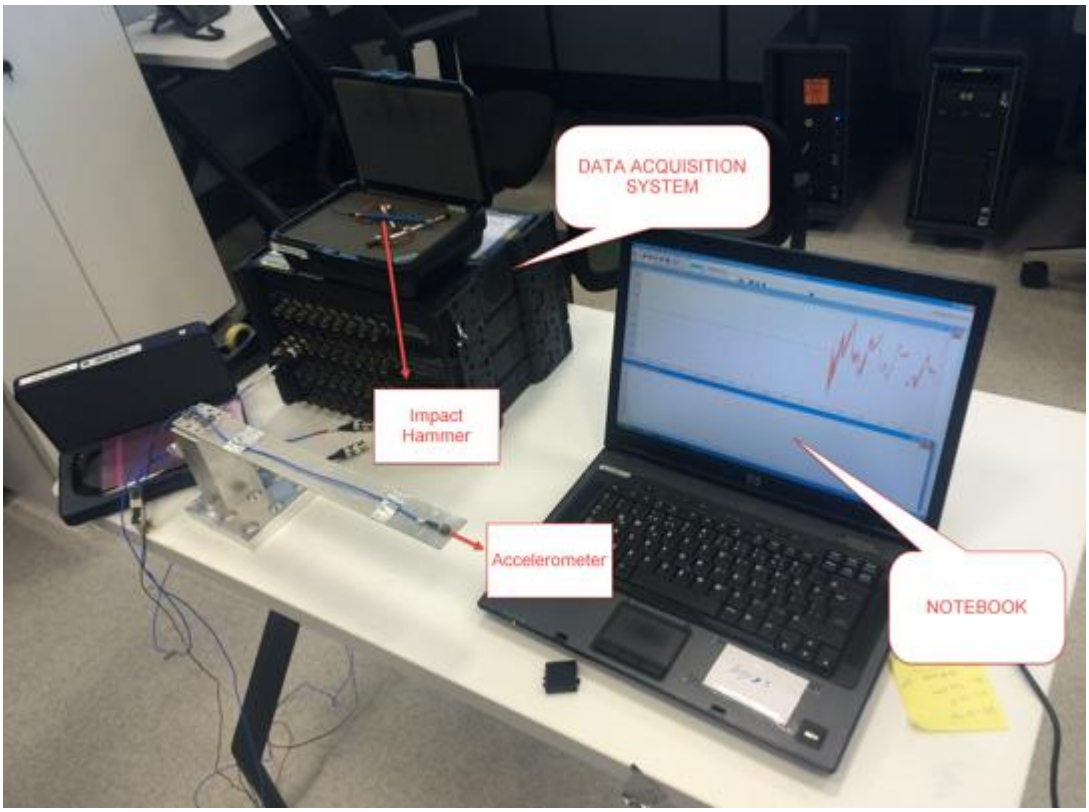

Figure 5.1 Test equipment

Figure 5.2 Miniature impact hammer and accelerometer

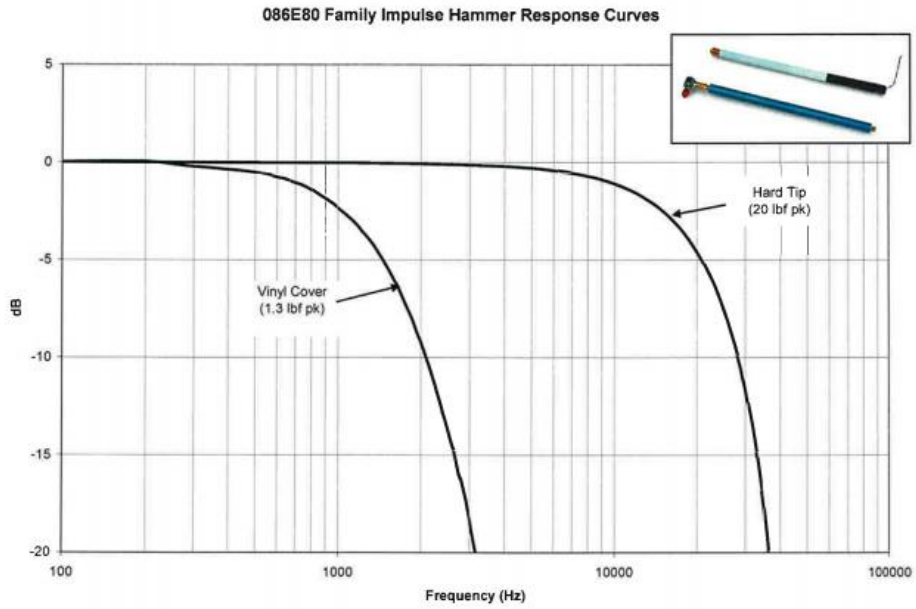

Figure 5.3 Response curve of the impact hammer [47]

In modal testing, eZ-Analyst software tool is used to obtain the frequency response function (FRF) of the antenna structure. Furthermore, analysis and sampling frequency is selected as 2000Hz and 5120 Hz, respectively. It is suggested that, in the modal testing where impact hammer is used, excitation (or reference) and response signals should be exposed to rectangular and exponential windows, respectively [48]. In addition to this, average of 10 tests is used in order to obtain a

proper FRF and coherence function. The modal test setup used in the experimentation is illustrated in Figure 5.4.

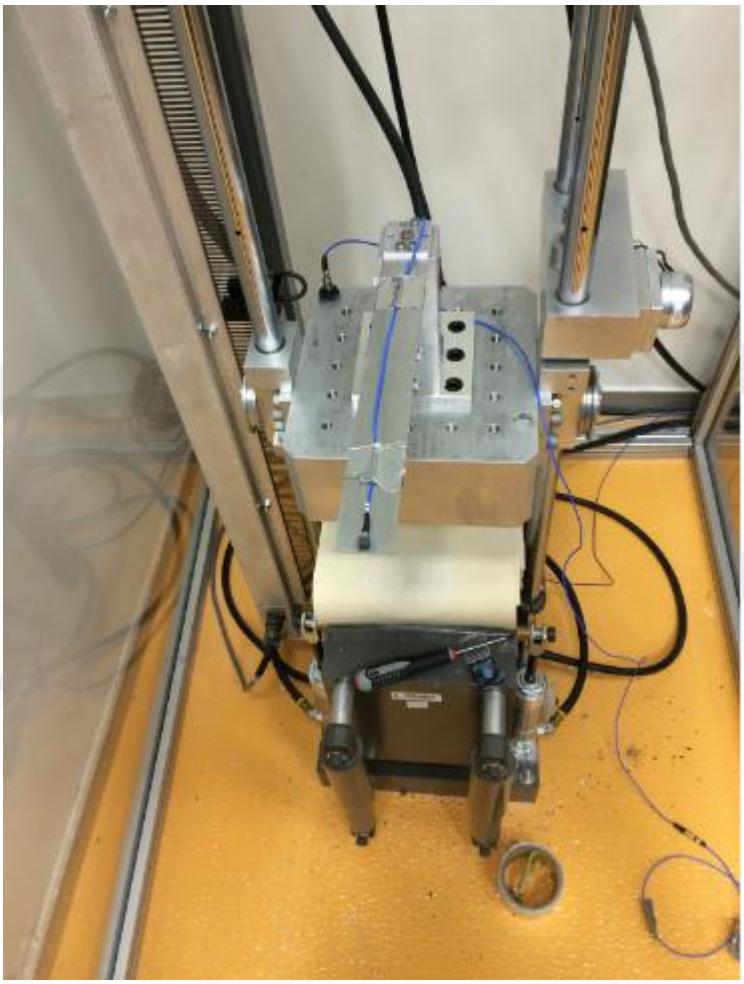

Figure 5.4 Modal and shock analyses test setup

In this experiment, 5754 –H26 series aluminum whose properties are listed in Table 5.1 is used as the material of the antenna structure. The length, width and thickness of the antenna structure are $350mm$, $40mm$ and $2mm$, respectively.

Table 5.1 Mechanical properties of 5754 H26 Aluminum [49]

Mechanical Properties of 5754 H26 Al	
Density	2670 kg/m
Ultimate Tensile Strength	290 MPa
Yield Tensile Strength	245 MPa
Modulus of Elasticity	70.3 GPa

In modal testing, both response measurement and force excitation locations are at the tip of the antenna structure which can be seen in Figure 5.4. After modal testing, frequency response function of the antenna structure is given in Figure 5.5. It is observed from the results that natural frequency of the first four modes are 12.5 Hz, 81.56 Hz, 228.4 Hz and 447.2 Hz, respectively. Furthermore, Table 5.2 summarizes natural frequencies of the antenna structure obtained from Euler-Bernoulli beam theory and experiments. The main reason of the difference between experimental and theoretical results is the weight of the accelerometer and cable used. However, it can be concluded from Table 5.2 that experimental results are in agreement with the theoretical results. Moreover, Table 5.2 shows the results obtained from finite element method with and without the effect of accelerometer mass. If the accelerometer mass is included to the model as a point mass, natural frequencies obtained are very close to the ones obtained from the experiment.

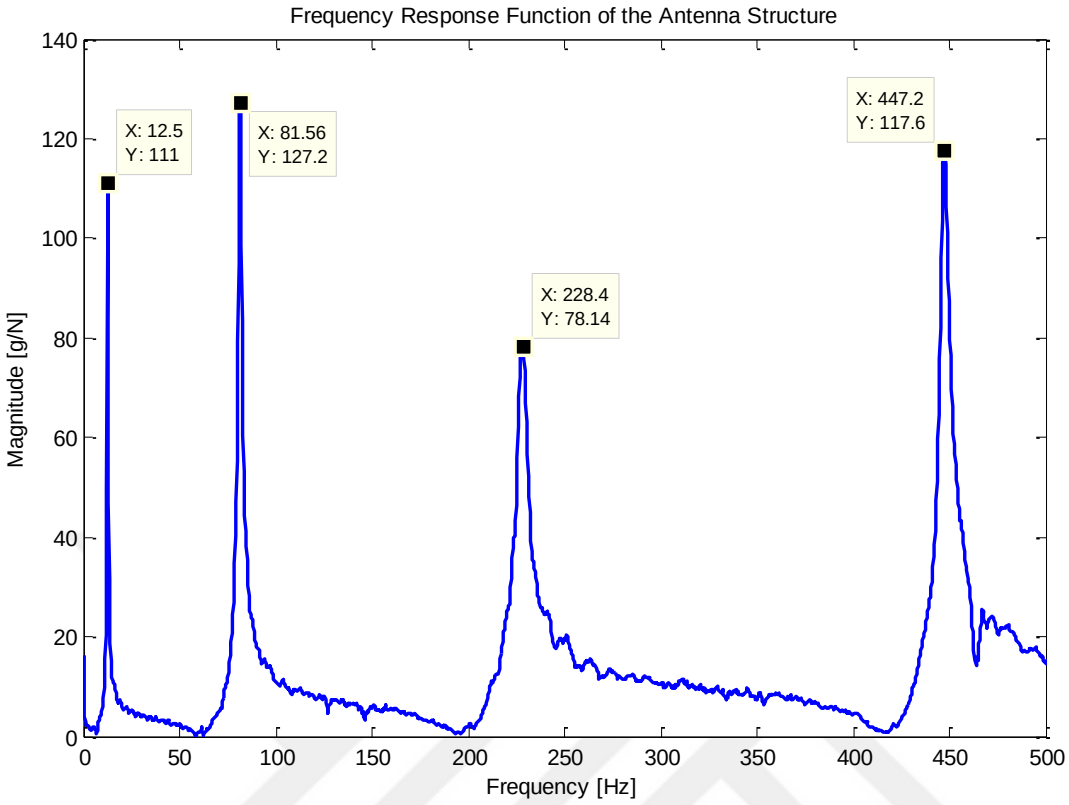

Figure 5.5 FRF of the antenna structure

Table 5.2 Natural frequencies of the antenna structure

Mode Number	Euler-Bernoulli Beam Theory [Hz]	Experiment Results [Hz]	ERROR (%)	FEM [Hz]	FEM with point mass [Hz]
1	13.53	12.5	7.61271	13.53	12.92
2	84.81	81.56	3.8321	84.8	81.25
3	237.5	228.4	3.83158	237.4	228.1
4	465.3	447.2	3.88996	465	447.9

Damping ratios of the antenna structure can be easily calculated from the frequency response function given in Figure 5.5 by using half power points. For instance, consider the first resonant frequency of the antenna structure in Figure 5.5. Magnitude of the frequency response function at the half power points is

$$X_1 = X_2 = \frac{1}{\sqrt{2}} X_{resonant} \ , \qquad (5.1)$$

where, X_1, X_2 and $X_{resonant}$ are magnitude of FRF at the first, second and resonant frequencies, respectively. The frequencies that correspond to X_1 and X_2 are called as half power frequencies. Then, for light damping, damping ratio of the that mode can be computed as

$$\zeta_i = \frac{\omega_i^{(2)} - \omega_i^{(1)}}{2\omega_i} \ , \tag{5.2}$$

where, $\omega_i^{(1)}$ and $\omega_i^{(2)}$ are the frequencies of the half power points and ω_i is the resonant frequency. Therefore, damping ratios of the antenna structure for the first four modes are given in Table 5.3.

Table 5.3 Modal damping ratios of the antenna structure

Mode Number	**Damping Ratio**
1	0.0220
2	0.0113
3	0.0121
4	0.0052

In this section, details on modal testing of the antenna structure are discussed. Main objective of modal testing is to

- Validate experimental model,
- Compute damping ratios of the antenna structure,

According to above information, experimental model is validated and damping ratios that can be used in Euler-Bernoulli reduced order model and finite element model are calculated.

5.3 Mechanical Shock Testing

In this section, mechanical shock testing is discussed. In military systems, most of the mechanical shock qualification tests are done on drop table, since many standards such as MIL-STD-810G enforces to use drop table for qualification test of ballistic shocks. The shock amplitude in such cases is very high; hence, it cannot be obtained by electrodynamic shakers. Figure 5.6 illustrates a simple drop table, where the test item is dropped and the amplitude of acceleration and duration of the impact are controlled. The programmer, usually known as pulse shaper as shown in the figure, is used for controlling the duration and type of shock pulse. The pulse shaper is generally made up of face seal that set duration and shape of shock pulse. In addition to this, specific shock level and duration is determined by a trial and error analysis, since these parameters are very sensitive to the weight of the tested equipment, drop height and thickness of face seal. Moreover, as can be seen from Figure 5.7, drop table position sensor and wireless controller prevent the second impact of the test equipment after the main fall.

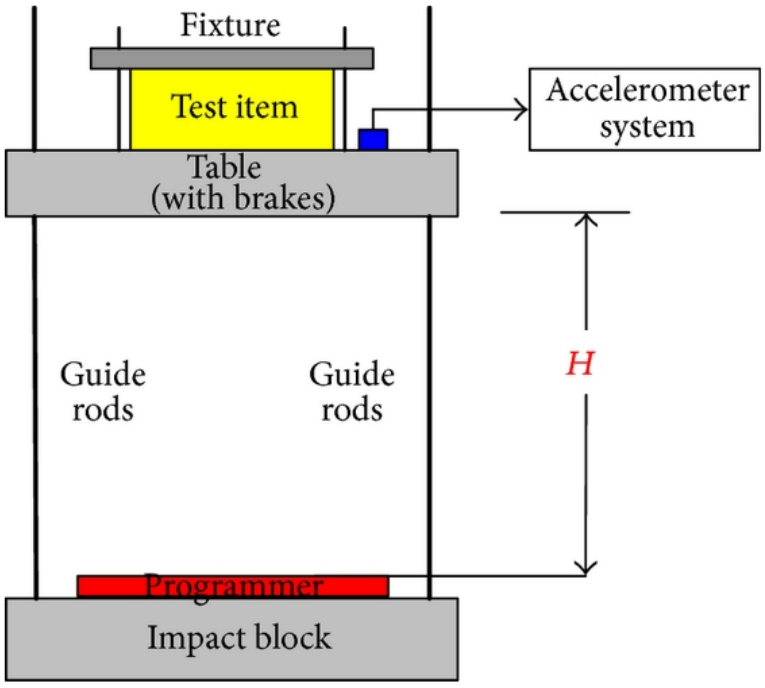

Figure 5.6 Drop table- [50]

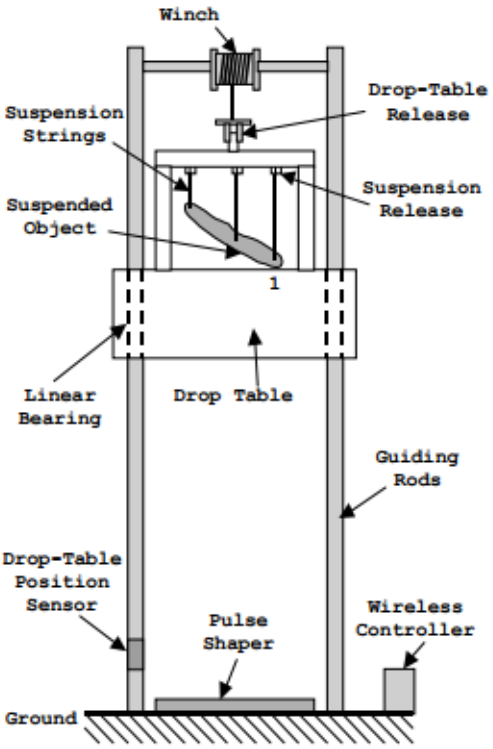

Figure 5.7 Drop table [51]

The pneumatic drop table used in the mechanical shock testing of the antenna structure is shown in Figure 5.7. Technical specifications of the pneumatic drop test table is given in Appendix-A.

In mechanical shock testing, one of the accelerometers is located on the table as shown in Figure 5.6, while the other one is located at tip of the antenna structure. In Figure 5.8 input shock time history is given whereas in Figure 5.9 shock response of the antenna structure is presented. Furthermore, Figure 5.10 illustrates the frequency content of the mechanical shock described in Figure 5.8.

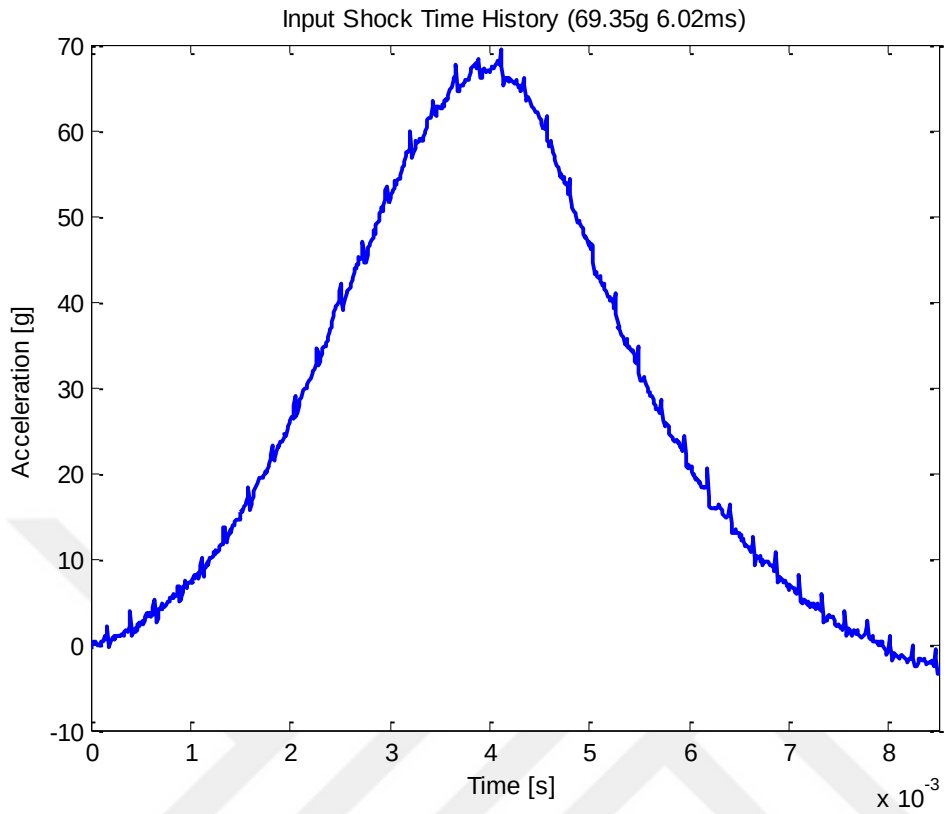

Figure 5.8 Time history of mechanical shock

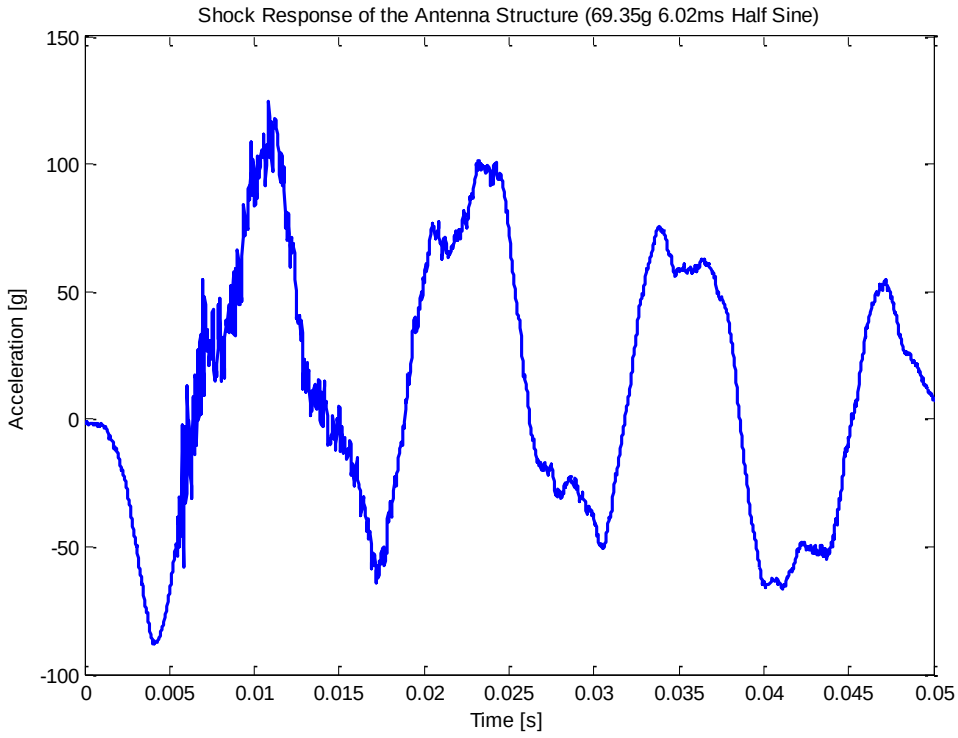

Figure 5.9 Shock response of the antenna structure

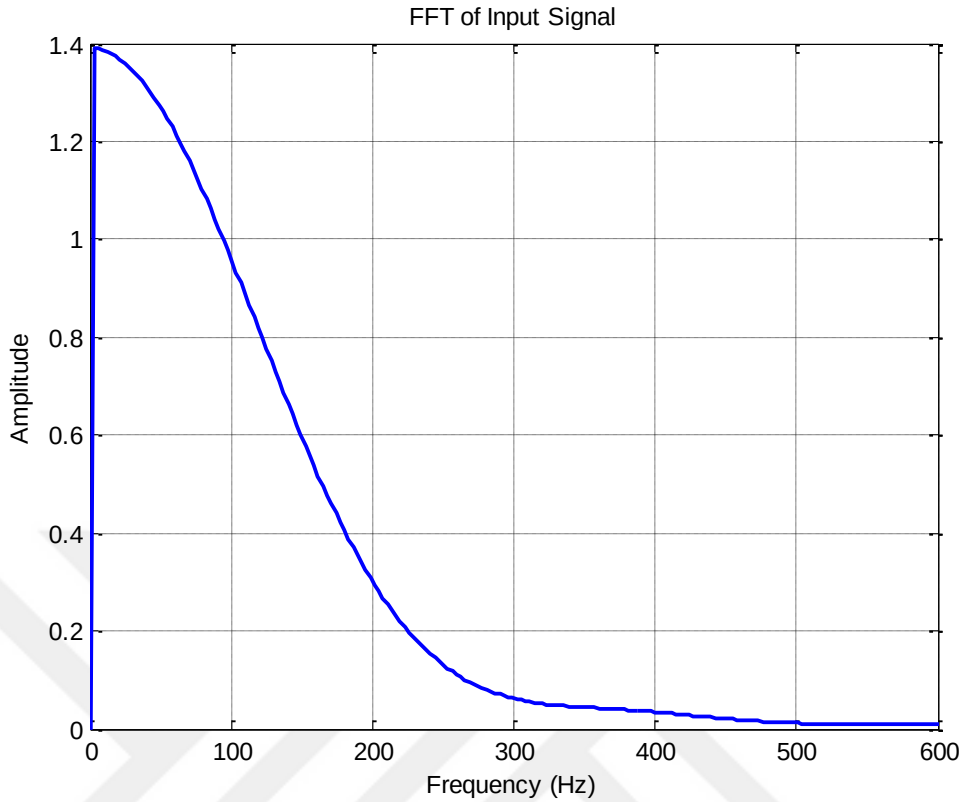

Figure 5.10 FFT of input mechanical shock

Moreover, as can be seen from Figure 5.11, shock response amplitude of the antenna structure before hitting the impact block is negligible compared to the shock amplitude after hitting the impact block, which is approximately 100 times larger than the former.

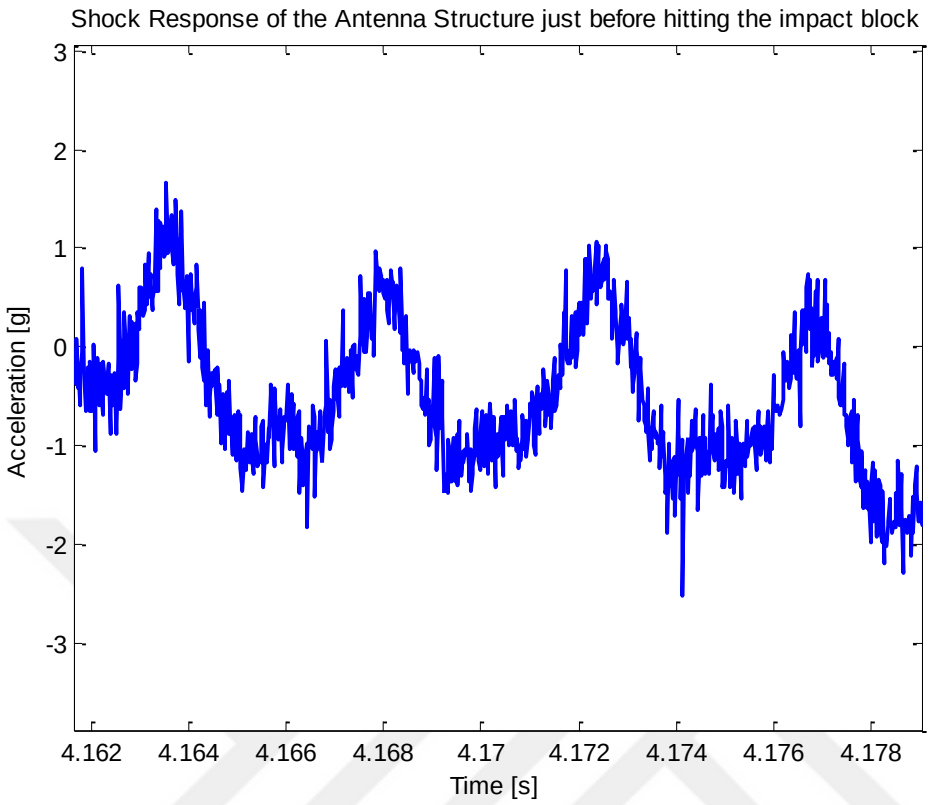

Figure 5.11 Shock response of the antenna structure just before hitting the impact block

CHAPTER 6

CASE STUDIES OF SHOCK RESPONSE OF THE ANTENNA STRUCTURE

In this chapter, responses of the antenna structure under the several types of shock phenomena are demonstrated. In Section 6.1, importance of half sine mechanical shock is discussed. In Section 6.2, several linear case studies are demonstrated and in Section 6.3, several nonlinear case studies are presented.

6.1 Importance of Half Sine Mechanical Shock

In this section, importance of half sine mechanical shock is introduced. Antenna structures in military systems survive after exposure of mechanical shocks such as transportation, ballistic shocks etc. Therefore, all antenna systems are tested at shock levels described in the standards. For instance, in MIL-STD-810G, shock levels are specified with respect to the nature of shock phenomena. According to MIL-STD-810G, during transportation, antenna structure experiences mechanical shock. The standard claims that if measured data is not available, the terminal peak sawtooth mechanical shocks given in Figure 1.5 are used as shock type for qualification tests [8]. Moreover, transportation shock is interpreted as 50g 11ms half sine mechanical shock for antenna structures in wheeled vehicles and aircrafts according to International Standard IEC-60068-2-27 [34] (see Figure 2.13). In addition to this, near miss under water explosion is simulated as double half sine mechanical shock for submarines and ships according to BV-043 (Building Specification for Ships of Federal Armed Forces) [52]. In this case, the shock amplitude depends on types of watercraft and distance from where explosion occurs. Figure 6.1 shows an example of a ballistic shock of a warship according to BV043 [52]. As can be seen from Figure 6.1, the first wave reaches the watercraft and it is responsible for the positive half sine. Moreover, the reflection of the first wave from water surface creates the negative shock. Therefore, the shock pulse is represented by double half sine.

Moreover, ballistic shocks have complex time history that cannot be reproduced for qualification. Therefore, shock response spectrum (SRS) is used as a tool for qualification tests. For example, mechanical shocks such as ballistic for combat vehicles and warships cannot be easily reproduced in order to carry out qualification tests. Therefore, an equivalent half sine mechanical shock can be calculated via shock response spectrum. Half sine mechanical shock is widely used in qualification of any type of mechanical shock, since it is easily produced by means of either mechanical shaker or drop table. Consider ballistic shock requirement of warships according to BV043 (see Figure 6.2). This double half sine mechanical shock cannot be reproduced by mechanical shakers or drop tables. Therefore, mechanical shocks having complex time history can be converted to half sine mechanical shock via SRS. For instance, equivalent half sine mechanical shock of double half sine shock described in Figure 6.1 is given in Figure 6.2

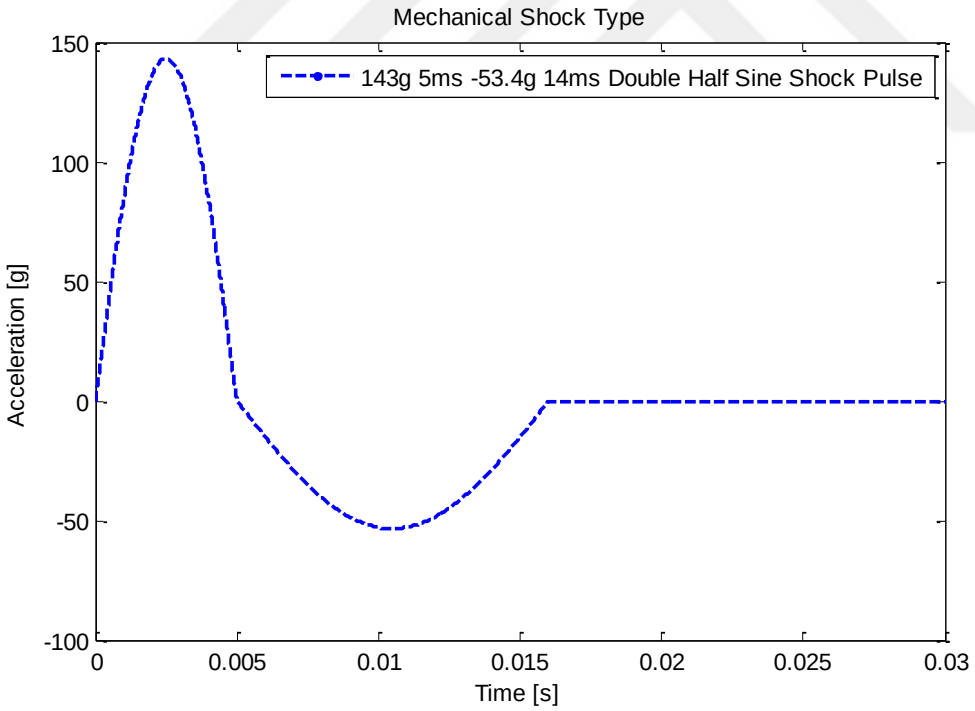

Figure 6.1 Ballistic shock requirement of the warship according to BV043

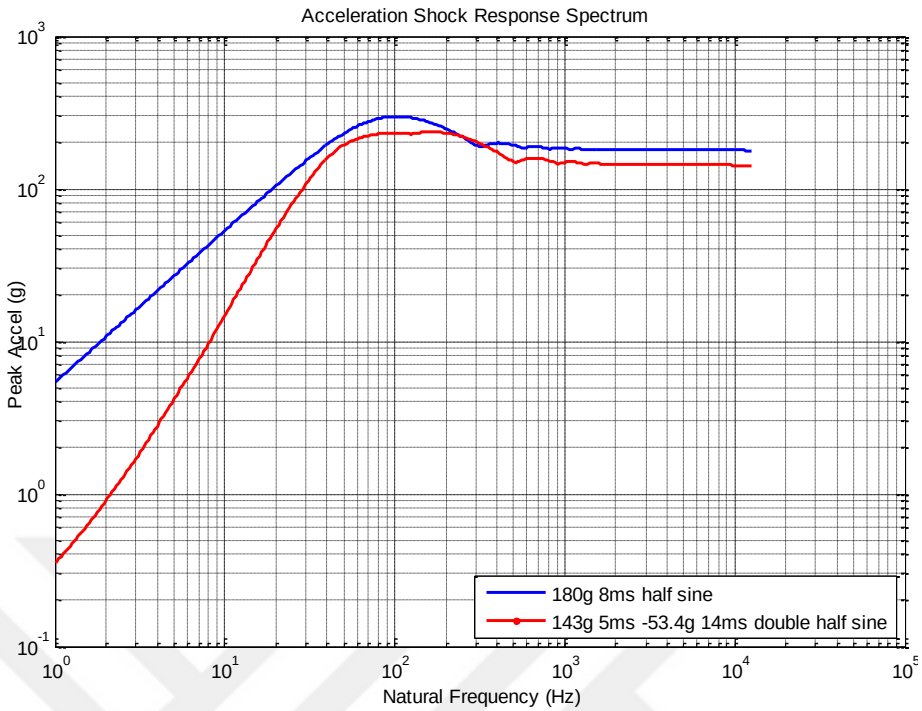

Figure 6.2 Equivalent half sine mechanical shock

6.2 Linear Case Studies

In this section, shock responses of the antenna structure are given for several cases by only linear theories.

Firstly, shock response of the antenna structure obtained from equivalent lumped mass model (see section 2.2) and reduced order continuous beam model (see section 2.3) are compared with each other. As an example, consider the antenna structure given in Figure 2.11 with uniform density and constant cross section. It is assumed to be exposed to transportation mechanical shock of 50g 11ms half sine, which is specified in IEC-60068-2-27 [34].The time step for all linear analysis is taken as 10^{-6} s which satisfies the requirements specified in [7] and [35]. Shock responses of the antenna structure under this shock are given in Figure 6.3 and Figure 6.4.

As can be seen from Figure 6.3 and Figure 6.4, equivalent lumped mass model, which is computationally efficient, cannot estimate both relative displacement and acceleration responses of the antenna structure correctly for this case. The main

reason behind this result can be easily understood by studying the frequency content of input signal given in Figure 6.5 and natural frequencies of the antenna structure [1]. . It is observed that the first two modes are dominant in the shock response of the antenna structure. Therefore, equivalent lumped mass model, which is based only the first mode information is insufficient to predict the shock response of the antenna structure for this special transportation shock. It should be noted that if one mode is used, although tip displacement response is estimated correctly, tip acceleration response cannot be estimated, since the contribution of the second mode increases due to damped natural frequency square term in the acceleration.

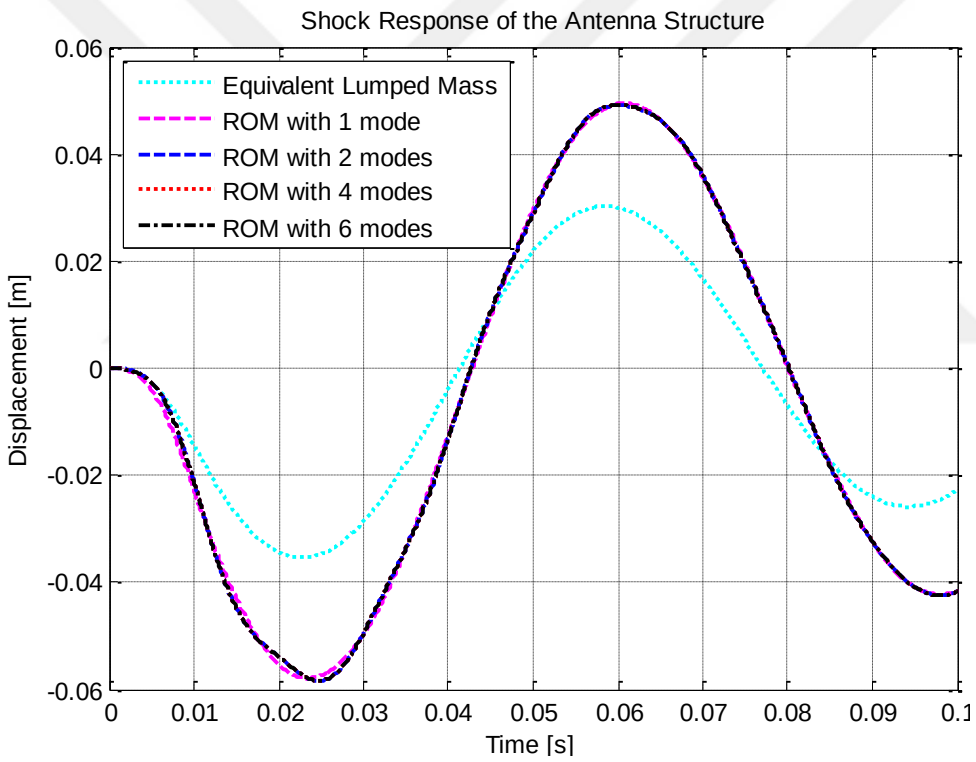

Figure 6.3 Displacement shock response of the antenna structure using linear models

[1] The natural frequencies of the antenna structure are 13.43 Hz, 84.16 Hz, 235.6 Hz, 461.8 Hz

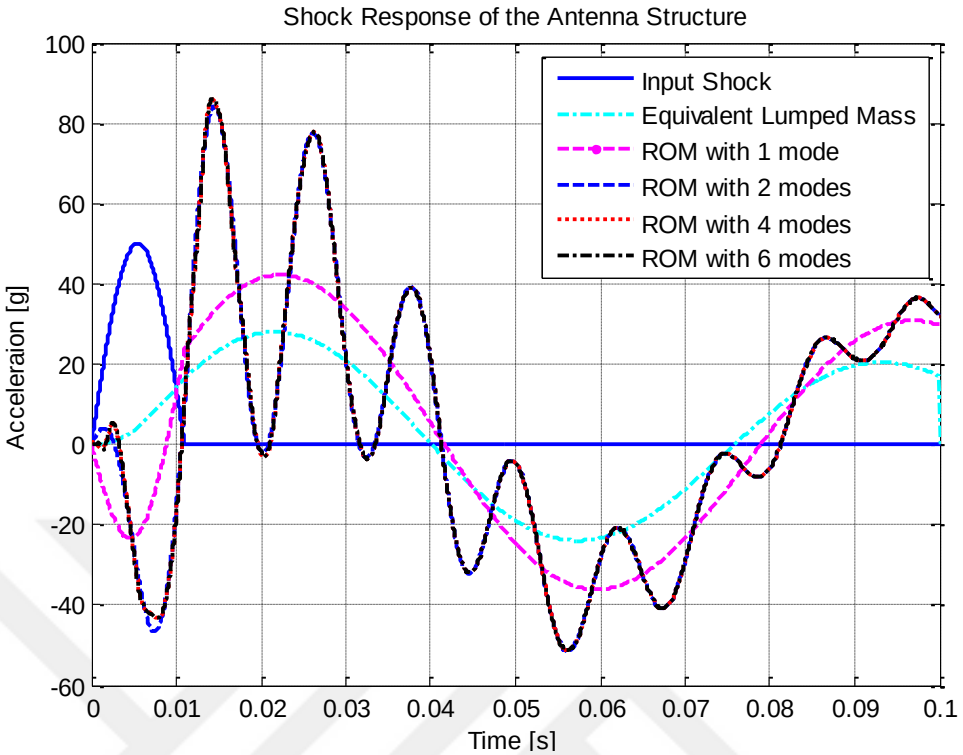

Figure 6.4 Acceleration shock response of the antenna structure using linear models

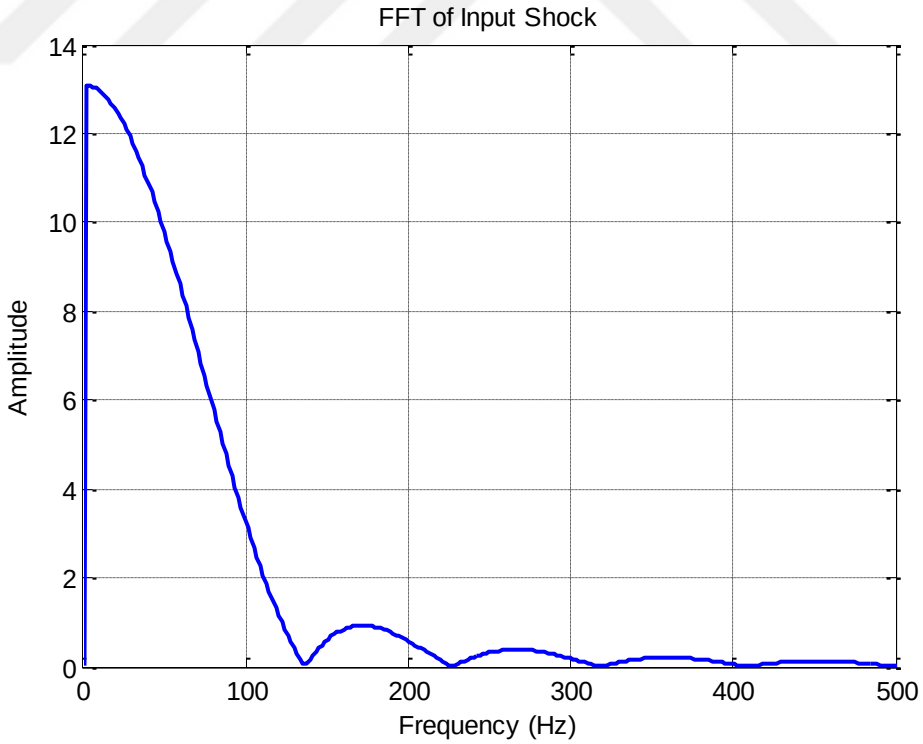

Figure 6.5 FFT of input 50g 11ms half sine shock

Furthermore, the minimum number of modes that is required to get shock response of the antenna structure is a crucial issue. Inherently, continuous models have an infinite number of modes; however, it is not possible to include all of them in dynamic response calculations. Therefore, reduced order models are extensively used to predict dynamic characteristics in the literature. Younis [30] claims that the first six modes are needed to get the dynamic response of systems, since higher modes have negligible effect on the response; while Tom [33] remarks that the dynamic response of a structure is represented accurately when the analysis includes the number of modes, whose effective total mass is at least 90 % of the actual mass. It should be noted that computational cost is proportional to number of modes included in the analysis; hence, optimum number of modes is required to get dynamic response of the antenna structure in practical times. Indeed, frequency content of the input shock signal determines the number of modes that are essential to get shock response of a structure.

The next linear case study the maximum response of an antenna structure is determined. Antenna structures can be broken down at the maximum relative displacement and acceleration due to the failure of PCB. Therefore, the maximum shock amplitude of an antenna structure is critical. In this case study, antenna structure given in Figure 2.11 with uniform density and constant cross section is considered. The structure is exposed to several mechanical shocks with 11ms duration. The maximum relative displacement and acceleration responses of the antenna structure obtained for different levels of shocks are given in Figure 6.6 and Figure 6.7.

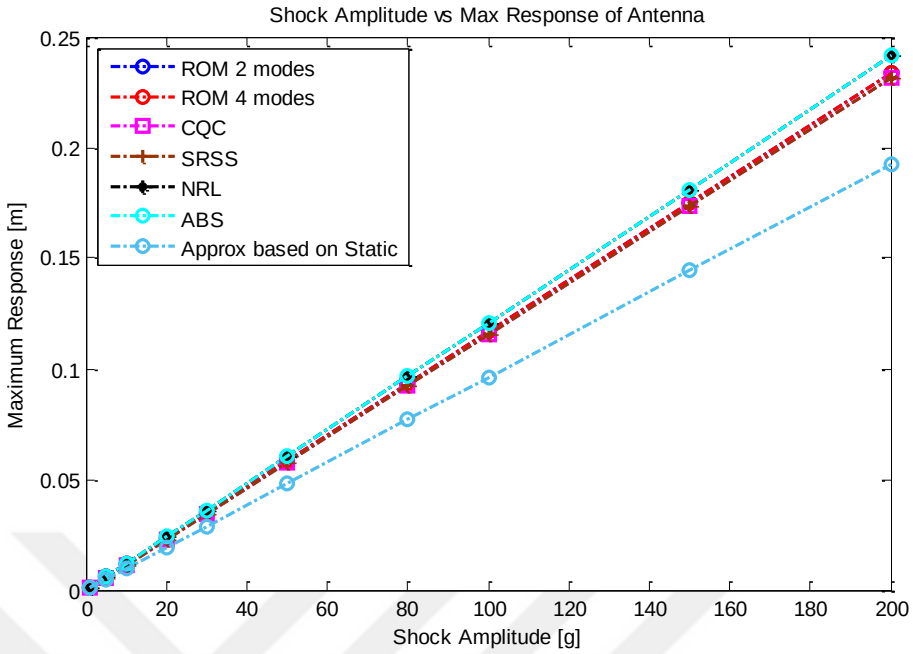

Figure 6.6 Maximum relative displacement of the antenna structure

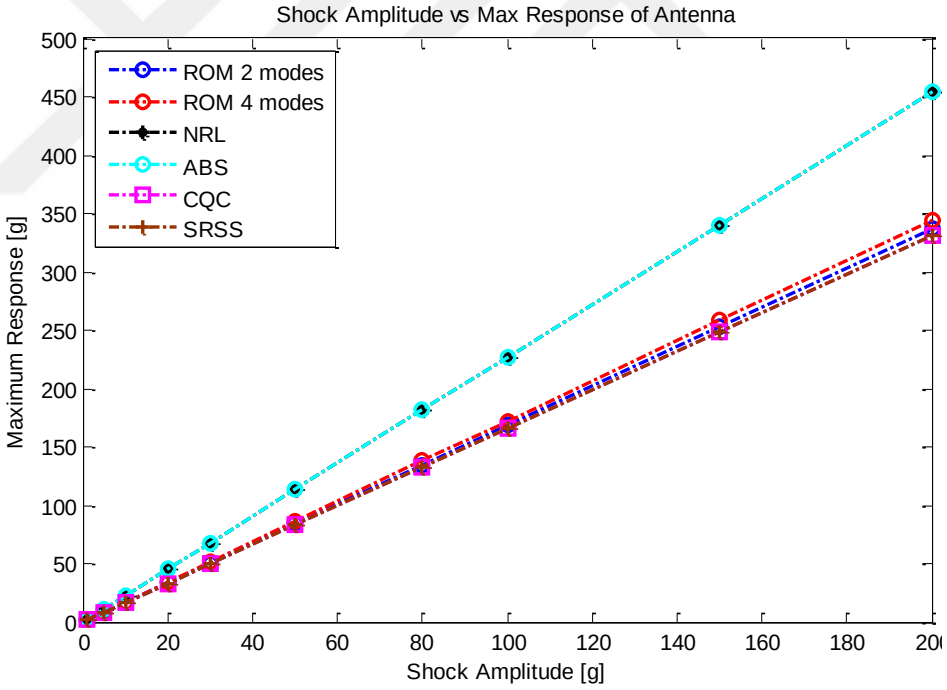

Figure 6.7 Maximum acceleration of the antenna structure

The approximate methods based on modal combination estimate precisely the maximum relative displacement of the antenna structure as can be seen from these figures. However, only CQC and SRSS types of approximate methods based on modal combination give good estimation of the maximum acceleration response of the antenna structure.

In another case study, the effect of gun fire shock on dynamic response of an antenna structure is studied. The antenna structure on an armored military vehicle may experience gun fire shock, which has high repetition rate, due to repetitive gunfire. The same antenna structure used in the previous case studies and given in Figure 2.11 is considered. The gun fire mechanical shock acting on the antenna structure contains five shots as shown in Figure 6.8. As can be seen from Figure 6.9 and Figure 6.10, for this case study, acceleration response of the antenna structure with five shots is significantly larger than the acceleration response of the antenna structure with one shot. Therefore, the gun fire shock needs to be analyzed carefully because of amplification of the acceleration response, which may be detrimental for antenna structures. On the other hand, the maximum relative displacement does not change significantly five shots compared to one shot. Frequency content of the gunfire mechanical shock is illustrated in Figure 6.11. As can be seen from the figure, the first two natural frequencies which are $13.43Hz$ and $84.16Hz$ are dominant frequencies of the input signal. Therefore, shock response of the antenna structure is amplified.

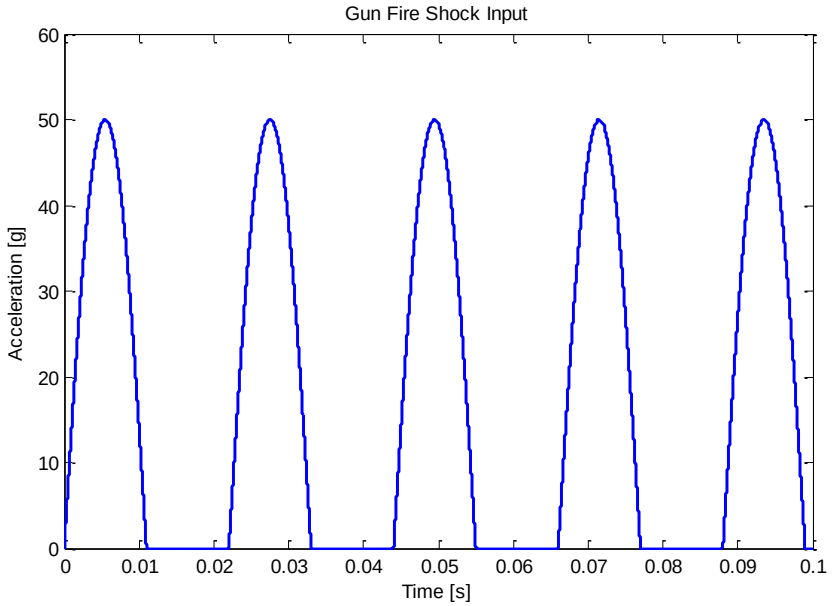

Figure 6.8 Gun fire mechanical shock with five shots

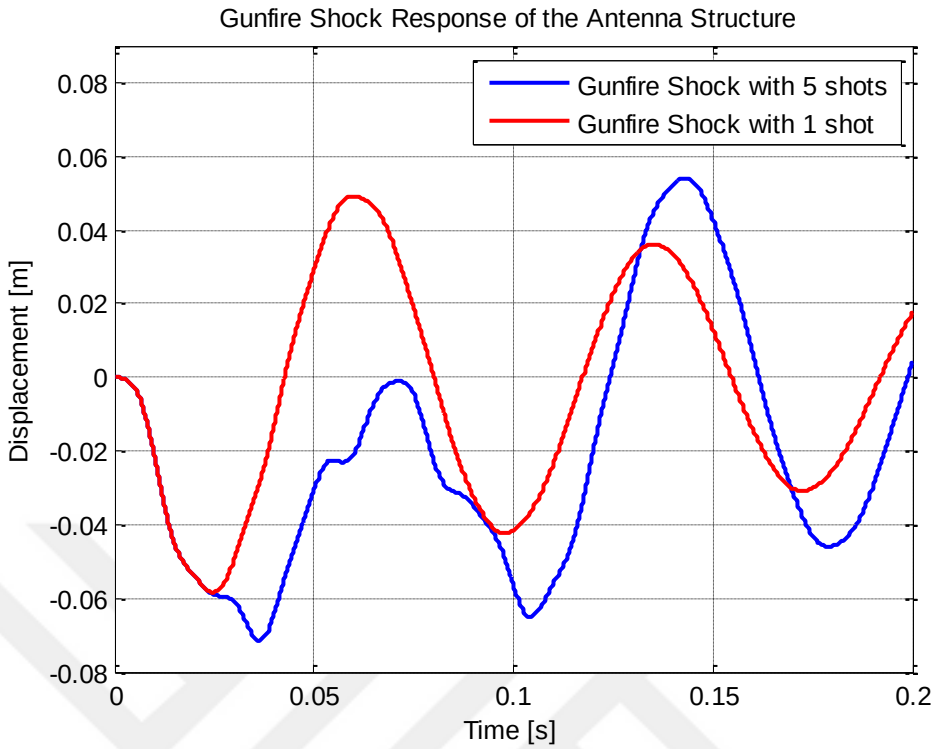

Figure 6.9 Relative displacement of the antenna structure exposed to gun fire shock

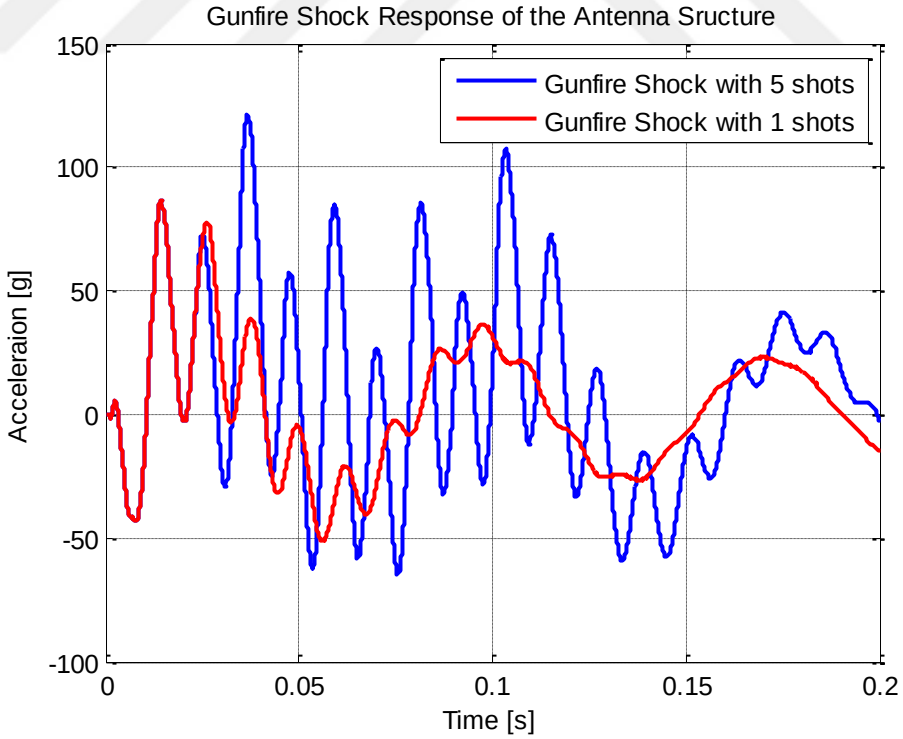

Figure 6.10 Acceleration response of the antenna structure exposed to gun fire shock

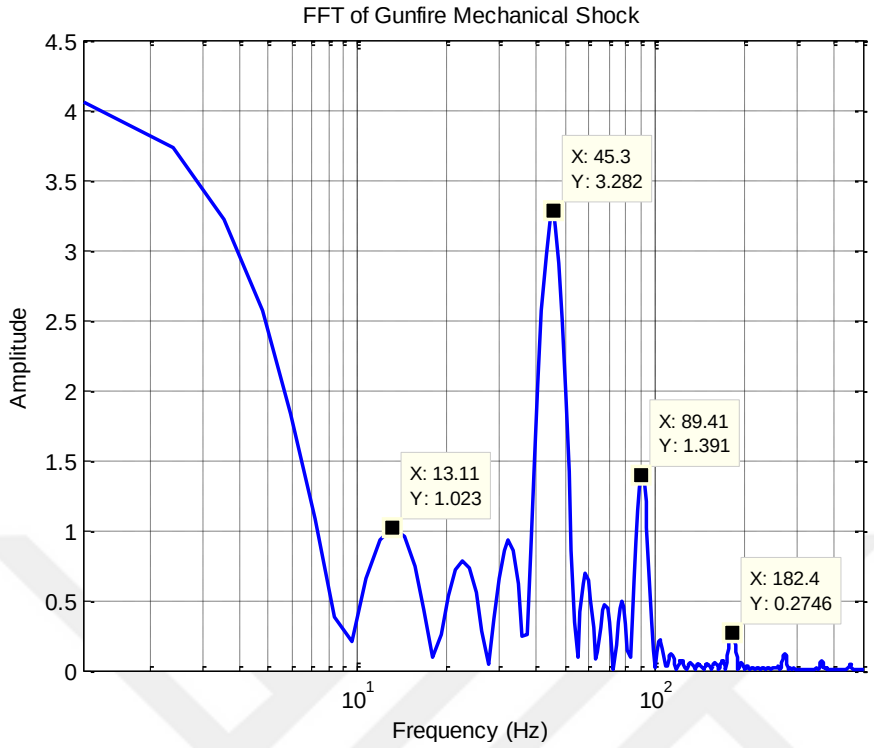

Figure 6.11 FFT of gunfire mechanical shock

In this section, linear methods to determine shock response of an antenna structure are presented with several case studies. Initially, results of equivalent lumped mass and reduced order continuous beam models are compared with each other. After that, the maximum relative displacement and acceleration responses of the antenna structure are compared utilizing transient solution. Moreover, the effect of gunfire shock on dynamic response of an antenna structure is discussed.

6.3 Nonlinear Case Studies

In this section, shock response of the antenna structure including geometric nonlinearity is examined by both reduced order Euler-Bernoulli beam model and finite element method and the results obtained are compared with the experiments carried out on a drop table.

The antenna structure used in the previous case studies and given in Figure 2.11 is considered here. Antenna structure is made up of aluminum with a density of

$70GPa$ and elastic modulus of $2700kg/m^3$ and damping ratio is assumed to be 0.05. The structure is exposed to 200g 11ms half sine mechanical shock. Time step is taken as 10^{-6} s which satisfies the requirements in given in [7]. Acceleration shock response of the antenna structure is presented in Figure 6.12. It is observed from the figure that nonlinearity dominates the shock response of the antenna structure significantly. In other words, the maximum acceleration shock response of the antenna structure is reduced due to geometric nonlinearity. Nayfeh [53] showed that nonlinear inertial terms have softening effect on structures. This softening effect reduces the amplitude of the shock response; therefore, the results of the nonlinear system are lower than the results obtained from linear model.

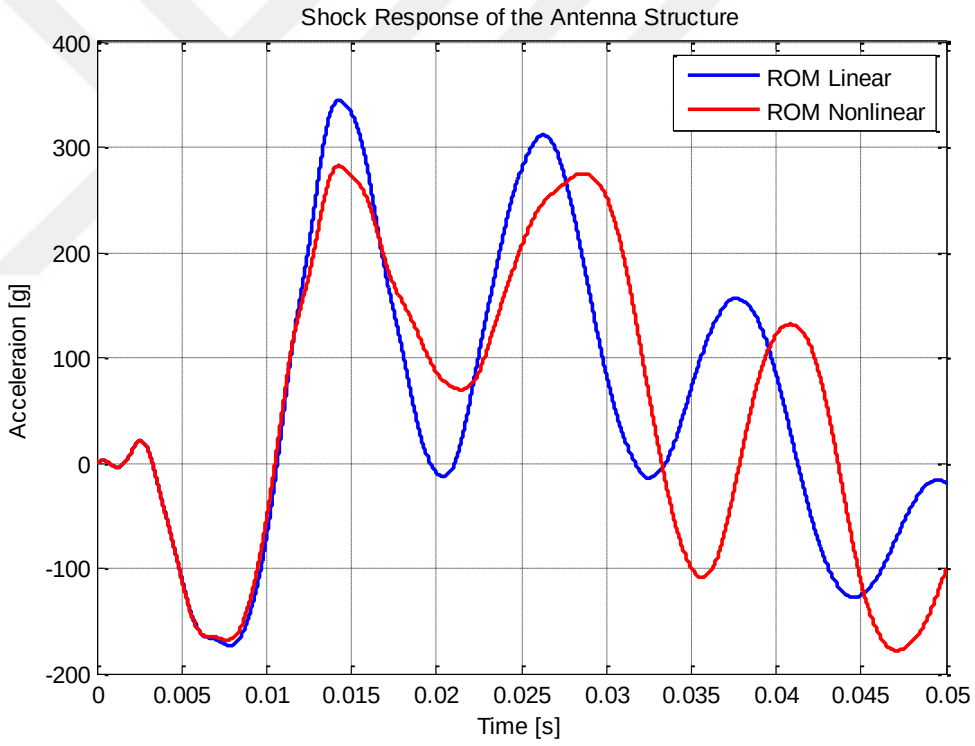

Figure 6.12 Shock response of the antenna structure including geometric nonlinearity

Furthermore, effect of the nonlinearity is studied on the experimental setup which is detailed given in Chapter 5. The antenna structure considered is made up of 5754 H26 series aluminum whose mechanical properties are given in Table 5.1 and damping ratios are obtained from modal tests (see Table 5.3). The antenna structure

is subjected to a 177.8g 5.13ms half sine mechanical shock given in Figure 6.13. Shock response of the antenna structure calculated by continuous reduced order model, finite element model and measured experimentally are given in Figure 6.14.

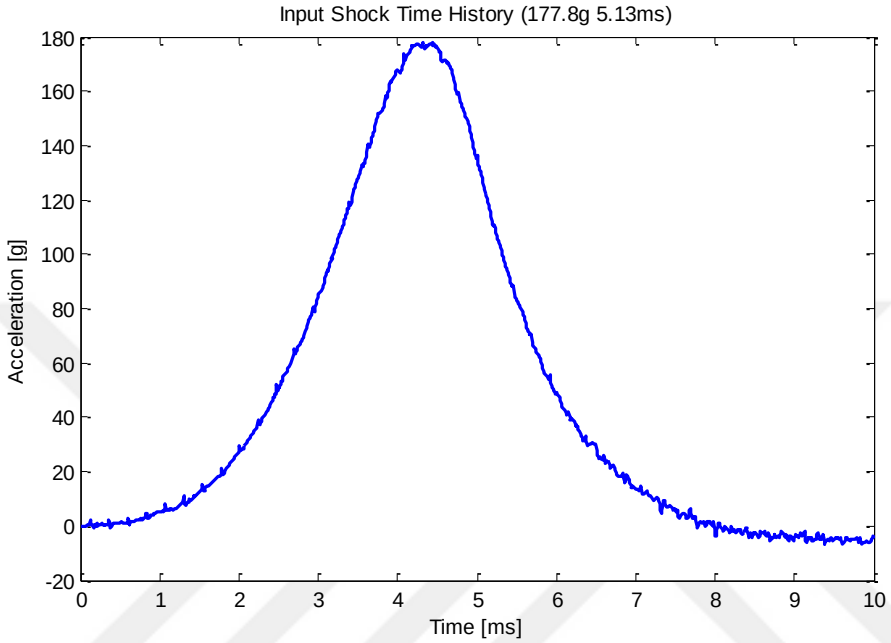

Figure 6.13 Time history of input mechanical shock

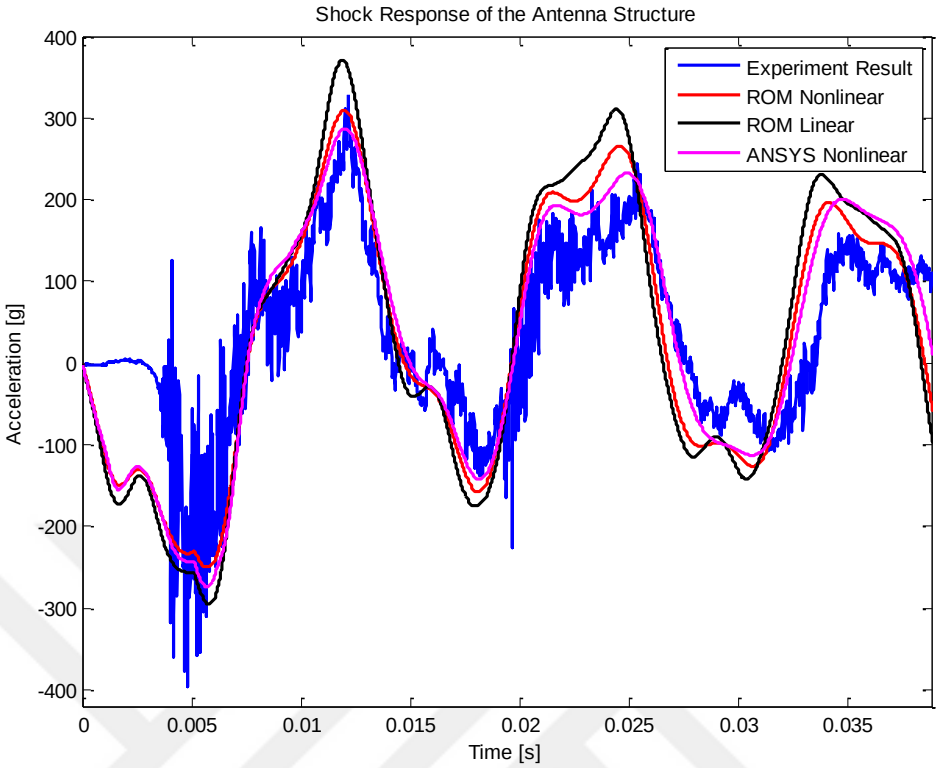

Figure 6.14 Shock response of the antenna structure

As can be seen from Figure 6.14, experimental study is in agreement with results of both nonlinear continuous reduced order model and finite element model.

In the next case study the maximum response of an antenna structure is considered. PCB is very sensitivity to acceleration amplitude; therefore, the maximum acceleration shock response amplitude of an antenna structure is critical. In this case study, the antenna structure given in Figure 2.11 with uniform density and constant cross section with a damping ratio of 0.05 is considered. The antenna structure is exposed to several mechanical shocks having a duration of 11ms. As can be seen from Figure 6.15, nonlinearity plays an important role on the shock response of the antenna structure, especially when the shock amplitude is above $100g$ in this case study. Furthermore, as can be seen from Figure 6.16, the maximum acceleration shock response amplitude of the antenna structure obtained from the continuous reduced order model and finite element model are in good agreement with the results obtained from the experiments for the half sine mechanical shock considered in this

case study. The amplitude and duration of the mechanical shocks in Figure 6.16 are given in Table 6.1. The reason of slight difference between the results of experimental and continuous reduced order model is due to experimental errors such as weight of accelerometer and cable.

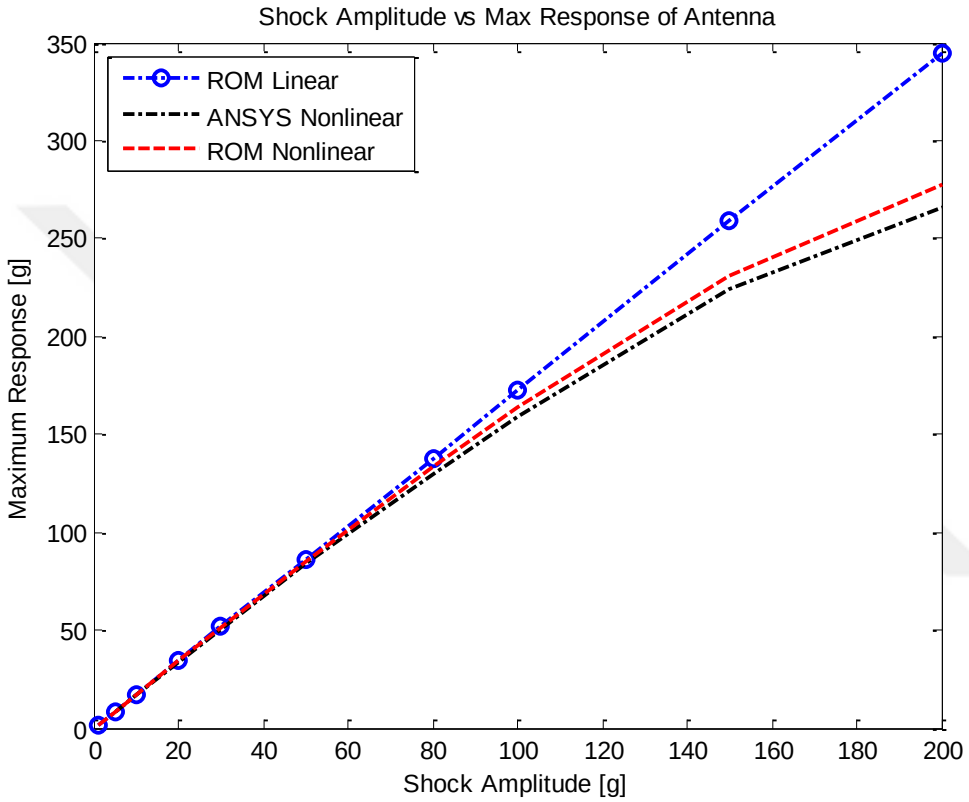

Figure 6.15 Maximum acceleration shock response of the antenna structure for $11ms$ half sine shocks with various shock amplitudes

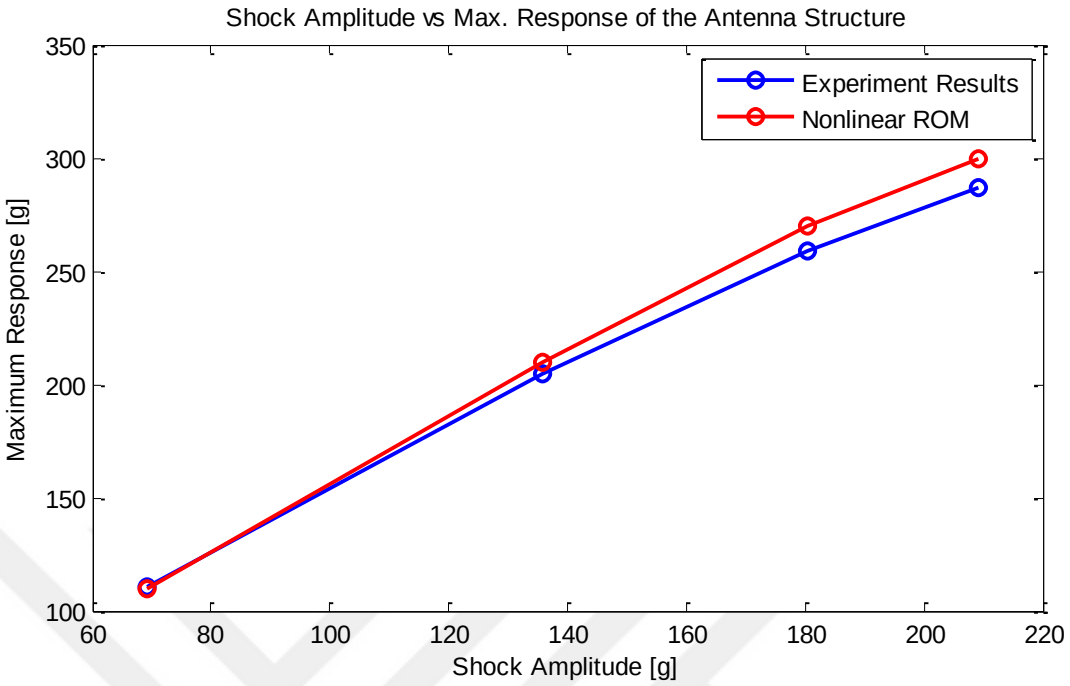

Figure 6.16 Experiment vs ROM results

Table 6.1 Shock amplitudes and durations used in the experiment

Shock Amplitude [g]	Shock Duration [ms]
69.35	6.02
135.64	5.68
180.38	5.45
209.15	5.62

In this section, dynamic characteristic of the antenna structure under mechanical shock is modeled by including geometric nonlinearity. The result of the mathematical model is compared with both experiment results and finite element method by using ANSYS, including nonlinear effects due to large deformation.

CHAPTER 7

DISCUSSION AND CONCLUSION

In this thesis, shock response of an antenna structure including geometric nonlinearity is investigated. Firstly, lumped mass model of an antenna structure is studied. Although lumped mass model is a fundamental and computationally efficient model, it is not applicable for case studies where contribution of higher modes cannot be neglected. Therefore, continuous beam model based on Euler-Bernoulli beam theory is used and the results obtained are highly accurate, since the effects of higher modes can as well be retained in the solution. Although both linear reduced order model (ROM) and finite element model are in agreement with each other, ROM is computationally very efficient compared to the finite element model, since fine mesh is required in order to capture the propagation of shock wave properly. As a result, this leads to increased solution times.

Furthermore, geometric nonlinearity plays an important role on shock response of an antenna structure, since many antenna structures have large dimension in longitudinal direction. It is interesting to note that geometric nonlinearity reduces both relative displacement and acceleration response, especially in the case of high shock acceleration because of the softening effect of nonlinear terms in the equation of motion. This statement is proved by the experimental results, and results of the nonlinear reduced order model and nonlinear finite element model. It is similar to the case where as if shock isolator is used. In other words, when the antenna structure is modeled properly including geometric nonlinearity, the response is similar to the case where an antenna structure is modeled by linear theory including a shock isolator. Therefore, nonlinear modeling can eliminate the need for a shock isolator. In addition to this, antenna structure is designed as simple as possible, since electromagnetic waves are affected by any components such as metallic isolator, bolt, screw, elastomer etc. In other words, when a bolt or any metallic or nonmetallic components are used even at the bottom of the antenna structure, electromagnetic waves are reflected or absorbed by these components. Thus, electromagnetic pattern

or antenna pattern is changed which affects the performance of the antenna structure in a negative way.

For the solution of the shock problem, MATLAB ODE solvers are not capable of solving the resulting set of nonlinear equations. Thus, Newmark and backward Euler methods are used in order to solve the nonlinear equations of motion. Furthermore, it can be concluded that approximate methods are inherently conservative methods and may be used as a starting point of shock analysis due to their short computation times.

REFERENCES

[1] Internet Live Stats, "Number of Internet Users (2014) - Internet Live Stats," 2014. [Online]. Available: http://www.internetlivestats.com/internet-users/. [Accessed: 01-Jun-2015].

[2] F. Wikipedia, "List of countries by number of mobile phones in use," *Notes*, 2011. [Online]. Available: https://en.wikipedia.org/wiki/List_of_countries_by_number_of_mobile_phones_in_use. [Accessed: 01-Jun-2015].

[3] R. A. Poisel, *Antenna Systems and Electronic Warfare Applications*. Norwood: Artech House, 2012.

[4] A. Solutions, F. O. R. The, and G. S. Environment, "Antenna Solutions for the Changing Global Security Environment | PCTEL," pp. 1–3, 2009.

[5] Y. Huang and K. Boyle, *Antennas: From Theory to Practice*, First Edit. John Willey and Sons Ltd, 2008.

[6] J. E. Alexander, "Shock Response Spectrum – A Primer," *Sound Vib.*, no. June, pp. 6 – 14, 2009.

[7] C. Lalanne, *Mechanical Shock: Mechanical Vibration and Shock Analysis, Volume 2*. John Willey and Sons Ltd, 2009.

[8] "Department of Defense Test Method Standard Environmental Engineering Considerations and Laboratory Tests," 2008.

[9] J. T. Klopcic, W. T. Robinson, D. W. Petty, and M. R. Sivack, "An Experiment, Analysis, and Model of Ballistic Shock.pdf," 1997.

[10] J. Eriksson and W. Kropp, "Measuring and Analysis of Pyrotechnic Shock," CHALMERS UNIVERSITY OF TECHNOLOGY, 1999.

[11] M. C. S. Reddy and J. Hussain, "Structural Analysis of Dipoloop Antenna Radome for Airborne Applications," *Int. J. Eng. Res. Technol.*, vol. 4, no. 03, pp. 724–735, 2015.

[12] A. V. Lopatin and E. V. Morozov, "Modal analysis of the thin-walled composite spoke of an umbrella-type deployable space antenna," *Compos. Strucute*, vol. 88, no. 1, pp. 46–55, 2009.

[13] H. Su, "Structural Analysis of Ka-Band gimbaled antennas," *COM DEV Ltd*, Ontario, p. 15.

[14] T. Sreekantamurthy, T. Mann, V. Behun, J. C. Pearson, S. Scarborough, A. Engineer, and S. Aerospace, "Nonlinear Structural Analysis Methodology and Dynamics Scaling of Inflatable Parabolic Reflector Antenna Concepts," *Am. Inst. Aeronaut. Astronaut.*, no. April, pp. 1–15, 2007.

[15] M. I. Younis, F. M. Alsaleem, R. Miles, and Q. Su, "Characterization of the performance of capacitive switches activated by mechanical shock," *J. Micromechanics Microengineering*, vol. 17, no. 7, pp. 1360–1370, 2007.

[16] G. X. Li and F. a. Shemansky, "Drop test and analysis on micro-machined

structures," *Sensors Actuators, A Phys.*, vol. 85, no. 1, pp. 280–286, 2000.

[17] M. I. Younis, R. Miles, and D. Jordy, "Investigation of the response of microstructures under the combined effect of mechanical shock and electrostatic forces," *J. Micromechanics Microengineering*, vol. 16, no. 11, pp. 2463–2474, 2006.

[18] M. I. Younis and H. N. Arafat, "Investigation of the Effect of Nonlinearities on the Response of Cantilever Microbeams under Mechanical Shock and Electrostatic Loading," *Soc. Exp. Mech.*, pp. 5–10, 2008.

[19] M. I. Younis, F. Alsaleem, and D. Jordy, "The response of clamped-clamped microbeams under mechanical shock," *Int. J. Non. Linear. Mech.*, vol. 42, no. 4, pp. 643–657, 2007.

[20] C. Liang, M. Yang, and Y. Tai, "Prediction of shock response for a quadrupod-mast using response spectrum analysis method," *Ocean Eng.*, vol. 29, no. 8, pp. 887–914, 2002.

[21] J. E. Alexander, "Nonlinear System Mode Superposition Given a Prescribed Shock Response Spectrum Input," *Proc. Int. Modal Anal. Conf. - IMAC*, no. 3, pp. 346–355, 2002.

[22] M. I. Younis, D. Jordy, and J. M. Pitarresi, "Computationally Efficient Approaches to Simulate the Dynamics of Microbeams Under Mechanical Shock," *IMECE 2006 2006 ASME Int. Mech. Eng. Conf. Expo.*, vol. 16, no. 3, pp. 628–638, 2006.

[23] A. Erturk and D. J. Inman, "On Mechanical Modeling of Cantilevered Piezoelectric Vibration Energy Harvesters," *J. Intell. Mater. Syst. Struct.*, vol. 19, no. 11, pp. 1311–1325, 2008.

[24] W. T. Thomson and M. D. Dahleh, *Theory of Vibration and Applications*, Fifth Edit. PEARSON EDUCATION, 1998.

[25] T. Irvine, "Rayleigh Method," no. 1. vibrationdata, pp. 1–18, 2010.

[26] T. Irvine, "Bending frequencies of beams, rods, and pipes," *Available on the web on site: http://www. vibrationdata.com*. pp. 1–61, 2012.

[27] S. S. Rao, *Mechanical Vibrations*, Fifth Edit., no. 3. Pearson, 2011.

[28] L. Majkut, "Free and Forced Vibrations of Timoshenko Beams Described by Single Difference Equation," *J. Theor. Appl. Mech.*, vol. 47, no. 1, pp. 193–210, 2009.

[29] S. S. Rao, *Vibration of Continuous Structures*. John Willey and Sons Ltd, 2007.

[30] M. I. Younis, *MEMS Linear and Nonlinear Statics and Dynamics*. Springer, 2011.

[31] J. K. Yee, H. H. Yang, and J. W. Judy, "Shock resistance of ferromagnetic micromechanical magnetometers," *Sensors Actuators, A Phys.*, vol. 103, no. 1–2, pp. 242–252, 2003.

[32] P. L. Gatti and V. Ferrari, *Applied Structural and Mechanical Vibrations*, First Edit. Taylor & Francis Group, 1999.

[33] T. Irvine, "Effective Modal Mass and Modal Participation Factors," *Vibrationdata*, no. 1, pp. 1–36, 2013.

[34] "International Standard-IEC 60068-2 -27." Basic Safety Publication, p. 80, 2008.

[35] "ANSYS 15 Help Viewer," 2014.

[36] H. A. Saieni, "Non-linear vibrations of tensegrity structures," Royal Institute of Technology, 2012.

[37] D. Roy and M. K. Dash, "Explorations of a family of stochastic Newmark methods in engineering dynamics," *Comput. Methods Appl. Mech. Eng.*, vol. 194, no. 45–47, pp. 4758–4796, 2005.

[38] N. M. Newmark, "A Method of Computation for Structural Dynamics," *J. Eng. Mech. Div.*, vol. 85, no. 7, pp. 67–94, 1959.

[39] "Ordinary Differential Equations - MATLAB & Simulink," *MATLAB*, 2015. [Online]. Available: http://www.mathworks.com/help/matlab/math/ordinary-differential-equations.html. [Accessed: 01-Jul-2015].

[40] T. Liu, C. Zhao, Q. Li, and L. Zhang, "An efficient backward Euler time-integration method for nonlinear dynamic analysis of structures," *Comput. Struct.*, vol. 106–107, pp. 20–28, 2012.

[41] A. K. CHOPRA, *Dynamics of Structures*, Forth Edit. Pearson.

[42] B. T. Irvine, "An introduction to the shock response spectrum," pp. 1–69, 2002.

[43] F. P. Beer, E. Russell Johnston Jr, J. T. DeWolf, and D. F. Mazurek, *Mechanics of Materials*, SIXTH EDIT. New York: Mc Graw Hill, 2012.

[44] E. H. Abed, D. Lindsay, and W. a. Hashlamoun, "Thechnical Report On participation factors for linear systems," *Automatica*, vol. 36, no. 10, pp. 1489–1496, 1999.

[45] T. Irvine, "SHOCK RESPONSE OF MULTI DEGREE OF FREEDOM SYSTEMS," *vibrationdata*, pp. 1–25, 2010.

[46] R. W. Clough, "A Replacement for the Stress Method in Seismic Analysis," *Earthq. Eng. Struct. Dyn.*, vol. 9, pp. 187–194, 1981.

[47] "PCB Piezotronics." [Online]. Available: http://www.pcb.com/products.aspx?m=086E80. [Accessed: 01-Jan-2015].

[48] M. Celik, "IOTECH WAVEBOOK VERİ TOPLAMA CİHAZI KULLANIM KILAVUZU," 2003.

[49] "MATWEB 5754-H26 Aluminum." [Online]. Available: http://www.matweb.com/search/DataSheet.aspx?MatGUID=b9183da49f3d417ca447dfe45b66d71b&ckck=1. [Accessed: 09-Jan-2015].

[50] C. Chen, C. Wu, and H. Lee, “Determination of Optimal Drop Height in Free-Fall Shock Test Using Regression Analysis and Back-Propagation Neural Network,” vol. 2014, 2014.

[51] S. Goyal and E. K. Buratynski, “Methods for realistic drop-testing,” *Int. J. Microcircuits Electron. Packag.*, vol. 23, no. 1, pp. 45–52, 2000.

[52] “BUILDING SPECIFICATION for SHIPS OF FEDERAL ARMED FORCES.” Federal Board of Defence Engineering and Acquisition, 1984.

[53] A. H. Nayfeh and P. F. Pai, *Linear and Nonlinear Structural Mechanics*, vol. 40, no. 2. 2005.

[54] “PCB Piezotronics.” [Online]. Available: http://www.pcb.com/products.aspx?m=356A01. [Accessed: 01-Jan-2015].

[55] “User’s Manual Wavebook.” [Online]. Available: http://www.mccdaq.com/pdfs/manuals/wavebook_series.pdf. [Accessed: 01-Jan-2015].

APPENDICES

APPENDIX A

In this part, some properties of the equipment's that are used for both modal and shock testing are introduced. In figure A1, some properties of the accelerometers are given. Some properties of the miniature hammer impact are given in figure A2.

Performance	**ENGLISH**	**SI**	
Sensitivity(± 20 %)	5 mV/g	0.51 mV/(m/s²)	
Measurement Range	± 1000 g pk	± 9810 m/s² pk	
Frequency Range(± 5 %)(y or z axis)	2 to 8000 Hz	2 to 8000 Hz	
Frequency Range(± 5 %)(x axis)	2 to 5000 Hz	2 to 5000 Hz	
Frequency Range(+1 dB)(x axis)	≥ 8 kHz	≥ 8 kHz	
Resonant Frequency	≥ 50 kHz	≥ 50 kHz	
Broadband Resolution(1 to 10,000 Hz)	0.003 g rms	0.03 m/s² rms	[1]
Non-Linearity	≤ 1 %	≤ 1 %	[3]
Transverse Sensitivity	≤ 5 %	≤ 5 %	
Environmental			
Overload Limit(Shock)	± 10,000 g pk	± 98,100 m/s² pk	
Temperature Range(Operating)	-65 to +250 °F	-54 to +121 °C	[2]
Temperature Response	See Graph	See Graph	[1][2]
Electrical			
Excitation Voltage	18 to 30 VDC	18 to 30 VDC	
Constant Current Excitation	2 to 20 mA	2 to 20 mA	
Output Impedance	≤ 200 Ohm	≤ 200 Ohm	
Output Bias Voltage	7 to 12 VDC	7 to 12 VDC	
Discharge Time Constant	0.24 to 1.0 sec	0.24 to 1.0 sec	
Settling Time(within 10% of bias)	<3 sec	<3 sec	
Spectral Noise(1 Hz)	1200 µg/√Hz	11,772 (µm/sec^2)/√Hz	[1]
Spectral Noise(10 Hz)	300 µg/√Hz	2943 (µm/sec^2)/√Hz	[1]
Spectral Noise(100 Hz)	100 µg/√Hz	981 (µm/sec^2)/√Hz	[1]
Spectral Noise(1 kHz)	30 µg/√Hz	294 (µm/sec^2)/√Hz	[1]
Physical			
Sensing Element	Ceramic	Ceramic	
Sensing Geometry	Shear	Shear	
Housing Material	Titanium	Titanium	
Sealing	Hermetic	Hermetic	
Size (Height x Length x Width)	0.25 in x 0.25 in x 0.25 in	6.35 mm x 6.35 mm x 6.35 mm	
Weight(without cable)	0.04 oz	1.0 gm	[1]
Electrical Connector	Integral Cable	Integral Cable	
Electrical Connection Position	Side	Side	
Cable Length	5 ft	1.5 m	
Cable Type	034 4-cond Shielded	034 4-cond Shielded	
Mounting	Adhesive	Adhesive	

Figure A1 Properties of the accelerometers [54]

	ENGLISH	SI	
Performance			
Sensitivity (±20 %)	100 mV/lbf	22.5 mV/N	[1]
Measurement Range	50 lbf pk	222 N pk	
Resonant Frequency	≥100 kHz	≥100 kHz	
Non-Linearity	≤1 %	≤1 %	[2]
Electrical			
Excitation Voltage	20 to 30 VDC	20 to 30 VDC	
Constant Current Excitation	2 to 20 mA	2 to 20 mA	
Output Impedance	<100 Ohm	<100 Ohm	
Output Bias Voltage	8 to 14 VDC	8 to 14 VDC	
Discharge Time Constant	≥100 sec	≥100 sec	[2]
Physical			
Sensing Element	Quartz	Quartz	
Sealing	Epoxy	Epoxy	
Hammer Mass	0.17 oz	4.8 gm	[3]
Head Diameter	0.25 in	6.3 mm	
Tip Diameter	0.10 in	2.5 mm	
Hammer Length	4.2 in	107 mm	[3]
Electrical Connection Position	Side	Side	
Extender Mass Weight	0.044 oz	1.25 gm	
Electrical Connector	5-44 Coaxial	5-44 Coaxial	[4]

Figure A2 Properties of the miniature impact hammer [47]

Technical properties of the IOTECH Wavebook/516E is given in Figure A3.

WaveBook/516A Front Panel

Note: /516 & /512A Front Panels also have this appearance.

WaveBook/516A Rear Panel

Note: The /512A Rear Panel also has this appearance. The /516 Rear Panel has a Printer Pass-Thru Port instead of two SYNC Ports.

WaveBook/516E Front Panel

WaveBook/516E Rear Panel

WaveBook Product Comparison

Analog Input	/512A	/516, /516A, /516E
A/D resolution	12-bit	16-bit
A/D speed	1 MHz	1 MHz
Sample rate	1 µs/channel	1 µs/channel
Ranges Unipolar (Note 2) Bipolar	0 to +10V, 0 to +4V, 0 to +2V (Note 2) ±10V, ±5V, ±2V, ±1V	0 to +10V, 0 to +4V, 0 to +2V (Note 2) ±10V, ±5V, ±2V, ±1V
A/D accuracy	±0.03 % FS	±0.012% FS
20-kHz low-pass filter	Yes	Yes
Analog input channels	8 DE	8 DE
Differential amplifiers	8 (1 per analog input)	8 (1 per analog input)
PGAs (Option)	1 (shared by all 8 inputs)	1 (shared by all 8 inputs)
Maximum capacity	72 Channels	72 Channels
FIFO depth	64K samples	64K samples
Total Harmonic Distortion 10Hz to 20Khz, Typical[1]	-70dB	-84dB
Signal to Noise and Distortion (SINAD)[1]	-70dB	-74dB
High-Speed Digital Inputs		
Digital I/O	16	16
External Clock / Frequency Input		
32-Bit Period Measurement	Yes	Yes
Trigger		
Single and multi-channel	Yes	Yes
Digital Pattern	Yes	Yes
Pulse	Yes	Yes
Synchronization		
	2 SYNC Ports	2 SYNC Ports (/516A & /516E Only)
Ethernet Connection		
	Via a WBK25 Interface or a connection to a WaveBook/516E	/516E – Direct connection to Ethernet /516 and /516A – via WBK25 Interface or a connection to a WaveBook/516E
Parallel Expansion Ports		
	No*	/516 and /516A – No* /516E – Yes, 3 expansion ports

[1] The THD and SINAD values apply to the -10 to +10 V range.

[2] Unipolar mode does not apply when a WBK11A, WBK12A, or WBK13A is installed.

* Three parallel expansion ports are available to the WaveBook/512A, /516, and /516A when the unit is connected to a WBK25 Ethernet Interface option.

Figure A3 Technical specification of the data acquisition system [55]

Technical specification of the Lansmont the model 23 pneumatic drop test table is given in Figure A4.

The Model 23D Shock Test System is a high-performance version of the Model 23 Shock Test System. The multi-sided magnesium shock carriage generates nearly ideal half-sine shock pulses and allows for mounting test items in multiple orientations simultaneously.

The Model 23D is outfitted standard with a TouchTest™ Shock II Table Top Control Console which will communicate seamlessly with Test Partner Data Acquisition Systems.

PERFORMANCE SPECIFICATIONS

TABLE DIMENSIONS

Front Face	9.06 x 9.06 in. (23 x 23 cm)
Top Face	6.0 x 9.06 in. (15.2 x 23 cm)

TEST CAPABILITIES

Max. Acceleration	2000g
Min. Pulse Duration	0.25 msec (half sine)
Max. Velocity Change	24 – 32 ft./sec (7.3 – 9.7 m/sec)
Pulse Waveforms	Half Sine
**with Optional Programmers*	Trapezoidal*
	Terminal Peak Sawtooth*
MAXIMUM PAYLOAD	40 lbs. (18 kg)

MACHINE SPECIFICATIONS

MACHINE ENVELOPE DIMENSIONS

Height	96 – 120 in. (244 – 305 cm)
Side to Side	21 in. (53 cm)
Front to Back	24 in. (61 cm)

POWER REQUIREMENTS

Machine	200 – 240 VAC/3Φ/50 – 60 Hz: 4 amp min.
	380 – 480 VAC/3Φ/50 – 60 Hz: 2 amp min.
Controller	100 – 120 VAC/1Φ/50 – 60 Hz: 1 amp min.
	200 – 240 VAC/1Φ/50 – 60 Hz: 1 amp min.

PNEUMATIC REQUIREMENTS

Nitrogen	1000 -2000 psi (69 – 138 bar)
Plant Air*	90 psi (6.2 bar)

**for optional DB Programmer*

Figure A4 Technical specification of the drop table

APPENDIX B – Conference Paper

SHOCK RESPONSE OF AN ANTENNA STRUCTURE CONSIDERING GEOMETRIC NONLINEARITY

Yunus Emre Ozcelik, Ender Cigeroglu, Mehmet Caliskan
Department of Mechanical Engineering, Middle East Technical University, Ankara 06800, Turkey

ABSTRACT

Antenna structures used in electronic warfare, radar, naval, satellite, spacecraft systems encounter mechanical shock from various sources such as near miss under water explosion, pyrotechnic and ballistic shocks. Since most of the antenna structure has larger dimension in longitudinal direction and experience high frequency, high amplitude shock energy, geometric nonlinearity become crucial to predict dynamic behavior in real life. In this study, the antenna structure is modeled by Euler-Bernoulli beam theory including geometrical nonlinearity. The resulting partial differential equations of motion are converted into a set of nonlinear ordinary differential equations by using Galerkin's Method, which are solved by Newmark. The results for the linear system obtained from time integration and approximate methods such as Absolute Method, Naval Research Method, and Shock Response Spectrum Method (SRS) are compared to the nonlinear ones. Moreover, these results are compared with the ones obtained from commercial Finite Element software

Keywords: Antenna Structure, Mechanical Shock, Nonlinear Dynamic Analysis, Finite Element Method

1. Introduction

In all around the world, approximately 40 % of the total world population uses internet [1], and cell phones are used by around 97 people out of every 100 people [2], which can provide a valid evidence for the idea that wireless communication is used worldwide. These infrastructures communicate with each other via antennas. In other words, the Internet and cell phones services are not functional without antennas. Thus, it can be said that the antenna structure is an irreplaceable and vital component of such electronic systems. IEEE defines what antenna does as "transmitting or receiving electromagnetic waves". In other words, the antenna structure converts electrical signal into electromagnetic or electrical signal. For military applications, antenna structures are used in electronic warfare (EW), radar, naval, satellite and spacecraft systems so that devices and vehicles associated with these systems can communicate with each other. Common antenna types used in civil and military systems are dipole antennas, monopoles antennas (see Fig. 1), loops antennas, helix antennas etc. As can be seen from Fig. 1, most of these antenna structures have inherently cantilever beam type configuration since one end is connected to the antenna hub, while the other end is free to receive or transmit electromagnetic wave, known as radio frequency (RF). Moreover, these antenna structures are generally made up of high conductive materials since the performance of an antenna structure is proportional to conductivity of the material [4]. Table 1 summarizes the most widely used materials in antenna structures. Copper and aluminum are the most widely used materials because of cost and weight concerns.

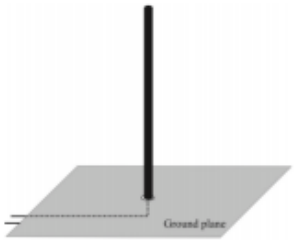

Fig. 1 Monopole antenna structure [3]

Table 1 Conductivity of the some common materials [4]

Material	Conductivity (S/m)	Material	Conductivity (S/m)
Silver	6.30E+07	Zinc	1.70E+07
Copper	5.80E+07	Brass	1.00E+07
Gold	4.10E+07	Phosphor Bronze	1.00E+07
Aluminum	3.50E+07	Tin	9.00E+06
Tungsten	1.80E+07	Lead	5.00E+06

However, antenna structures used in military and civil systems can encounter many mechanical shocks from various sources such as near miss underwater explosion, ballistic shock due explosion of mine, pyrotechnic shock, dropping of an antenna structure and so forth. Mechanical shock can be described as "a sudden and violent change in the state of motion of the component parts or particles of a body or medium resulting from sudden application of a relatively large external force, such as a blow or impact" according to first Shock and Vibration Symposium in 1947 [5]. Generally mechanical shocks contain high amplitude and rich spectral energy since the duration of mechanical shock is measured in milliseconds and the amplitude may be as high as 1000 G (see Fig. 2). Therefore, even if only one of the antennas in the electronic warfare and communication systems is broken down due to a mechanical shock, the whole system will be unable to function properly. For example, a printed circuit board (PCB), printed on the antenna structure, may be damaged due to exposure of a high level of mechanical shock, and as a result of this, the system becomes dysfunctional. Therefore, antenna structures must be designed to withstand mechanical shock types, which are explained briefly below, to ensure their reliability.

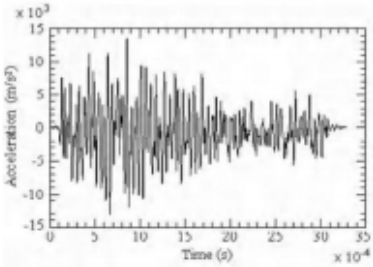

Fig. 2 Time history of mechanical shock [6]

Transportation and handling shock is received by electronic and mechanical systems used in military and civil applications as a result of transportation and human errors in handling of materials. For instance, while a military armored vehicle is running over a bump at unwary speed, all systems including antennas are exposed to mechanical shocks. Furthermore, ballistic shock is another type of mechanical shock containing high amplitude and high frequency content which is mainly caused by the impact of non-perforating mine blast, projectiles or ordnances on armored vehicle [7]. In addition to that pyroshock which is the response of a system to high-frequency stress waves one example of mechanical shock. Generally, pyroshock is generated as a result of explosive charges in order to separate two stages of a rocket [8]. Moreover, gunfire shock is a repetitive wave originated from artillery shooting of military vehicle. Consequently, the antenna structure should withstand these mechanical shocks originating from various environmental effects.

In literature, studies on the nonlinear dynamic characteristics of antenna structures exposed to mechanical shocks are limited since most researchers have investigated modal and random vibrations analyses of the antenna structure. Concerning the linear dynamic analyses of antenna structure, the simulations were performed by commercial finite element programs such as ABAQUS® and NASTRAN®. Static and dynamic analyses of dipoloop antenna radome were simulated by a linear finite element analysis by Reddy and Hussain [9]. Mechanical shock analysis was conducted on ABAQUS®. In this study, only stresses were evaluated on the dipoloop antenna radome. Lopatin and Morozov [10] studied the free vibration of thin-walled composite spoke of an umbrella-type deployable space antenna. The composite spoke of the deployable space antenna was

modeled as a cantilever beam via including effects of transverse shear. On the other hand, the nonlinear dynamic response of the antenna structure under dynamic loads is characterized by limited number of researchers. Random and modal analyses of a gimbaled antenna including gap nonlinearity resulting from small clearances in the joints are studied by Su [11] where the nonlinearity is linearized and then the resulting linear systems is solved commercial finite element software. Moreover, Sreekantamurthy et al. [12] investigated static and dynamic loads such as inflation pressure, gravity and pretension loads on a parabolic reflector antenna by using commercial finite element software. In their work, geometric nonlinearity was included into the model, since the deformation of parabolic reflector antenna was large.

Inherently, antenna structures has a larger dimension in longitudinal direction. When they receive high mechanical shock such as ballistic and pyrotechnical shocks, nonlinear effects play an important role on shock response of antenna structures.
Although the nonlinear dynamic characteristics of antenna structure, under mechanical shock is different from the linear ones, there appears almost no study on this specific topic. However, especially in micro and nanoscale areas, many researchers investigated the dynamics response of micro electro mechanical systems, micro beams, micro switches and so forth which are under mechanical shock even by considering the nonlinear effects. As an initial attempt, some authors used single degree of freedom assumption to get a rough estimation of the dynamic response of micro systems. For example, Younis et al. [13] studied the performance of capacitive switches modeled as a single degree of freedom (SDOF) system under mechanical shock through including the effects of squeeze-film damping and electrostatic forces. Moreover, Li and Shemansky [14] treated the micro-machined structure as a single degree of freedom system as well as a distributed parameter model. For more accurate analysis, many authors used continuous beam models to simulate the response of micro systems to a mechanical shock. As an example, Younis et al. [15] investigated the simultaneous effects of mechanical shock and electrostatic forces on microstructures simulated as cantilever and clamped-clamped beams. In this particular study, reduced order model results based on Galerkin's Method were compared with the ones obtained from commercial finite element software. Due to the large deformation of micro systems resulting from the applied mechanical shock, some researchers included nonlinearity to the models to predict the dynamic behavior in real life. For instance, Younis and Arafat included both geometric and inertia nonlinearities into their studies while analyzing the response of the cantilever microbeam activated by mechanical shock and electrostatic forces [16]. In their work, they analyzed the effects of cubic geometric and inertia nonlinearities on the cantilever microbeam by using reduced order model which is based upon Galerkin's Method. In another study of Younis et al. [17], the response of the clamped-clamped microbeam was investigated through using four modes in the Galerkin based reduced order model including geometric nonlinearity. Moreover, Younis et al. [17] studied the effects of shape of shock pulse and package on the response of microbeam and validated the results via commercial finite element software. Furthermore, some researchers employed approximate solutions to the response of systems under mechanical shock through frequency domain approaches rather than time domain approach which is computationally expensive. As an example, Liang et al. [18] estimated shock response of the mast in ships using frequency domain method such as square root of the sum of squares (SRSS), complete quadratic combination method (CQC), naval research laboratory method (NRL) and absolute summation method (ABS). Alexander [19] mentioned the frequency domain methods which are applied to the nonlinear systems as well. Younis and Pitarresi [20] emphasized synthetic methods utilizing the static response and shock spectrum based on maximum responses of many single degree of freedom systems. In this study [20], linear and nonlinear response of microbeam found in synthetic method and Galerkin-based reduced order method employing six modes were compared in terms of different values of shock amplitude.
Mechanical shock excitation is inherently applied to the base of structures. In literature, mechanical shock was simulated for continuous systems by base excitation which is either applied to the fixed boundary condition ([21, 22]) or distributed force applied through the structure ([15, 16, 17, 20]).

Antenna structures, which are used for military and civil applications, are vital component of the many the electronic systems. These antenna structures are subjected to mechanical shock from various environments such as transportation, ballistic, pyrotechnic shocks. Therefore, correct modeling of dynamic characteristic of the antenna structure under mechanical shock is needed because of the need to accurately predict the performance of the antenna structure. Inherently, most of the antenna structures have slender shape and larger dimension in longitudinal direction. Moreover, they are subjected to high frequency, high amplitude mechanical shocks. Thus, mathematical modeling of the antenna structure through linear theory can yield incorrect results, since antenna structures experience large deformation, where nonlinear effects become dominant. In other words, nonlinearities due to large deformation must be included in order to predict dynamic behavior accurately.

2. Mathematical Modeling

In this section, antenna structure is modeled by equivalent lumped mass model, Euler-Bernoulli Beam Theory, finite element method and approximate methods.

2.1 Equivalent Lumped Mass Model

In this section, the antenna structure is treated as a single degree of freedom system utilizing an equivalent lumped mass model. Basically, most of the antenna structures such as monopole antennas (see Fig. 3) have a cantilever beam structure since one end is fixed to the antenna hub while the other end is free to transmit or receive electromagnetic waves.

Fig. 3 Cantilever beam type the antenna structure

Equivalent mass and stiffness of the antenna structure described in Fig. 3 is given as [23].

$$m_{eq} = 0.2427mL\,, \tag{1}$$

$$k_{eq} = \frac{3EI}{L^3}\,, \tag{2}$$

where m is the mass per unit length of the antenna structure, l is the length of the antenna structure and E is Young's modulus of the antenna's material. Therefore, the antenna structure shown in Fig. 3 is reduced to a single degree of freedom system as shown in Fig. 4.

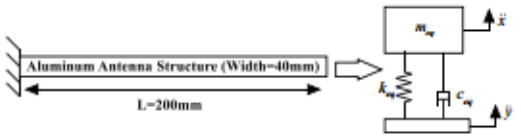

Fig. 4 Equivalent lumped mass model of the antenna structure

2.2 Linear Continuous Model

In this part, the antenna structure is modeled by Euler-Bernoulli beam theory, which is widely used in literature, in order to predict dynamic characteristic of slender beam like structure [13, 15, 16, 17, 20, 21]. However, due to inherent assumptions of the theory, accuracy of the results is poor when the thickness to length ratio is larger than 10%. In such cases Timoshenko beam model is applied to get accurate results [24]. In this paper, Euler-Bernoulli beam theory is used to model the antenna structure, since most of the antenna structures naturally have thickness to length ratio much less than 10%.

Consider the antenna structure, whose length, density, cross sectional area and flexural rigidity are represented as l, ρ, A and EI, respectively. As can be seen in Fig. 5, the transverse deflection of the antenna structure is defined as $w(x,t)$, where x is the axial position, t represents time and $F(x,t)$ is the distributed force that is applied through the length of the antenna structure. Equation of motion of the antenna structure is given as [25]

$$\frac{\partial^2}{\partial x^2}\left(EI\frac{\partial^2 w(x,t)}{\partial x^2}\right) + c\frac{\partial w(x,t)}{\partial t} + \rho A\frac{\partial^2 w(x,t)}{\partial t^2} = F(x,t)\,. \tag{3}$$

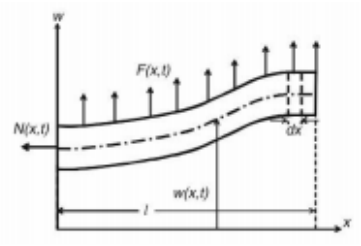

Fig. 5 Nomenclatures of the antenna structure in bending direction [25]

In this paper, mechanical shock is applied as distributed force through the length of the antenna structure (see Fig. 5). Hence, equation of motion of the antenna structure subjected to mechanical shock can be given as

$$\frac{\partial^2}{\partial x^2}\left(EI\frac{\partial^2 w(x,t)}{\partial x^2}\right)+c\frac{\partial w(x,t)}{\partial t}+\rho A\frac{\partial^2 w(x,t)}{\partial t^2}=-(\rho A a_{max})a_{pulse}(t), \tag{4}$$

where, a_{max} is the maximum value of mechanical shock and a_{pulse} is a unit mechanical shock profile such as half sine, terminal peak sawtooth and so forth. The equation of motion given by Eq. (4) can be nondimensionalized by using following non dimensional parameters

$$\hat{x}=\frac{x}{l},\ \hat{w}=\frac{w}{l},\ \hat{t}=\frac{t}{T}, \tag{5}$$

where T is the time scale parameter. Substituting Eq. (5) into Eq. (4), the outcome is

$$\frac{\partial^4 w(x,t)}{\partial t^4}+c_{non}\frac{\partial w(x,t)}{\partial t}+\frac{\partial^2 w(x,t)}{\partial t^2}=F_{non}a_{pulse}(t), \tag{6}$$

where, nondimensional damping and forcing terms are as follows

$$c_{non}=\frac{cl^4}{EIT},\ F_{non}=\frac{-\rho A a_{max} l^3}{EI}. \tag{7}$$

The nondimensional force given in Eq.(7) implies that effects of the mechanical shock increases sharply with increasing length and decreasing thickness of the antenna structure. This is in agreement with the experimental findings available in the literature [26].

The resulting partial differential equation of motion can be converted into a set of ordinary differential equations by using Galerkin's method. In this method, the following form of solution is assumed

$$w(x,t)=\sum_{i=1}^{n}a_i(t)\phi_i(x), \tag{8}$$

where, $\phi_i(x)$ is a comparison function which satisfies both geometric and natural boundary conditions as well as differentiable at least to the order of the partial differential equation. $a_i(t)$ is generalized coordinate to be determined, and n is the number of modes used in the analysis [27]. After substituting Eq. (8) into Eq. (6), multiplying the resulting equation with ϕ_j and integrating from 0 to 1, the following result is obtained

$$\sum_{i=1}^{n} u_i(t)\left(\int_0^1 \phi_j(x)\phi_i^{iv}(x)\,dx\right)+c_{non}\sum_{i=1}^{n}\dot{u}_i(t)\left(\int_0^1 \phi_j(x)\phi_i(x)\,dx\right)+\sum_{i=1}^{n}\ddot{u}_i(t)\left(\int_0^1 \phi_j(x)\phi_i(x)\,dx\right)=\int_0^1 \phi_j(x)\,F_{non}\,a_{pulse}(t)\,dx\,. \tag{9}$$

If orthogonal comparison functions are used, Eq. (9) is reduced to an uncoupled form as follows

$$\ddot{u}_j(t)+2\zeta_j\omega_{non,j}\dot{u}_j(t)+\omega_{non,j}{}^2u(t)=\int_0^1 \phi_j(x)\,F_{non}\,a_{pulse}(t)\,dx\,, \tag{10}$$

where, ζ_j is the modal damping ratio of the j^{th} mode and it is given by

$$\zeta_j=\frac{c_{non}}{2\omega_{non,j}}\,. \tag{11}$$

2.3 Nonlinear Continuous Model

In this section, shock response of an antenna structure considering geometric and inertia nonlinearities is analyzed. In real life, response of almost all systems to any forcing is nonlinear, where superposition property of linear systems does not hold. For simplicity, many engineering systems are treated as linear which is a valid assumption in most cases. For instance, in order to obtain linear equation of motion of an antenna structure under mechanical shock, small deformation is assumed. This assumption gives accurate results if the deformations in the real case is small with respect to the thickness of the antenna structure. However, if the deformation is large, small deformation assumption results in highly inaccurate results. Therefore, linear modeling may result in a design which is not optimum and hence, increases weight and cost. In addition to this, estimated acceleration of a PCB on the antenna structure is not accurate. Since mechanical shocks result in large deformations, antenna structure needs to be modeled by including nonlinearities.

Nonlinearities common in structures are geometric nonlinearity, damping nonlinearity, inertia nonlinearity, curvature nonlinearity, material nonlinearity and boundary condition nonlinearity. Since, the antenna structure experiences large deformation due to its long and slender structure, curvature and inertia nonlinearities are included into the model.

In the light of above mentioned information, equation of motion of the antenna structure, which has uniform density and constant cross section, under mechanical shock including geometric curvature and inertia nonlinearities is given as [25]

$$EI\frac{\partial^4 w}{\partial x^4}+c\frac{\partial w}{\partial t}+\rho A\frac{\partial^2 w}{\partial t^2}=-EI\frac{\partial}{\partial x}\left(\frac{\partial w}{\partial x}\frac{\partial}{\partial x}\left(\frac{\partial w}{\partial x}\frac{\partial^2 w}{\partial x^2}\right)\right)-\frac{1}{2}\rho A\frac{\partial}{\partial x}\left(\frac{\partial w}{\partial x}\int_L^x\left(\frac{\partial^2}{\partial t^2}\int_0^x\left(\frac{\partial w}{\partial x}\right)^2 dx\right)dx\right)-(\rho A a_{max})a_{pulse}(t)\,. \tag{12}$$

Eq. (12) is converted into a set of nonlinear ordinary differential equations by using Galerkin's method. Similar to the previous case, substituting Eq. (8) into Eq. (12) multiplying the result by ϕ_j and integrating from 0 to 1 the following result is obtained

$$\begin{aligned}&\sum_{i=1}^{n} u_i(t)\int_0^1 \phi_j(x)\phi_i^{iv}(x)\,dx+c_{non}\sum_{i=1}^{n}\dot{u}_i(t)\int_0^1 \phi_j(x)\phi_i(x)\,dx+\sum_{i=1}^{n}\ddot{u}_i(t)\int_0^1 \phi_j(x)\phi_i(x)\,dx=\\&-\int_0^1\phi_j\left(\left(\sum_{i=1}^{n}u_i\phi_i'\right)^2+4\left(\sum_{i=1}^{n}u_i\phi_i'\right)\left(\sum_{i=1}^{n}u_i\phi_i''\right)\left(\sum_{i=1}^{n}u_i\phi_i'''\right)+\left(\sum_{i=1}^{n}u_i\phi_i'\right)^2\left(\sum_{i=1}^{n}u_i\phi_i^{iv}\right)\right)dx\,,\\&-\alpha_{in}\int_0^1\phi_j\left(\frac{\partial}{\partial x^2}\left(\left(\sum_{i=1}^{n}u_i\phi_i'\right)\int_1^x\left(\frac{\partial^2}{\partial t^2}\int_0^x\left(\sum_{i=1}^{n}u_i\phi_i'\right)^2 dx\right)dx\right)\right)dx+\int_0^1\phi_j(x)\,F_{non}\,a_{pulse}\end{aligned} \tag{13}$$

where nondimensional damping, inertia and forcing parameters are given as

$$c_{non}=\frac{cl^4}{EIT}\,,\ \alpha_{in}=\frac{l^4\rho A}{2T^2EI}\,,\ \mathrm{F}_{non}=\frac{-\rho A a_{max}l^3}{EI}\,. \tag{14}$$

Eq. (13) can be represented in matrix form, where in this study MUPAD® available in MATLAB® is used for the symbolic calculations.

2.4 Finite Element Simulation by ANSYS

In this section, shock response of an antenna structure is obtained by using ANSYS, which is commonly used commercial finite element software. In this paper, the antenna structure is modeled by 3-D 2 Node beam elements known as BEAM188 (see Fig. 6). This element type is used to analyze slender beam like structures. Moreover, this element has six degrees of freedom which are three translational degrees of freedom in X, Y and Z directions and three rotational degrees of freedom about X, Y and Z axes. In addition to that, the element is suitable for the consideration of stress stiffening and large deformation effects. The theory behind this element is Timoshenko beam theory, which includes shear deformation [28].

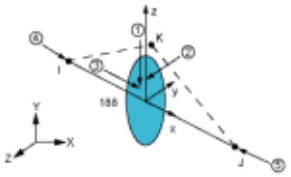

Fig. 6 Geometry of BEAM188 [28]

ANSYS Workbench does not have a tool for mechanical shock simulation, since mechanical shocks are applied to a structure from its base. In literature, Application Customization Toolkit exists for transient base excitation analysis. However, this toolkit is applicable for only linear transient analysis. As a result of that, ANSYS Parametric Design Language (APDL) is used to simulate mechanical shock. The APDL code which is embedded into "Transient Structural" module is written by "ACCEL" command. This command gives acceleration to the selected nodes. Furthermore, Rayleigh damping is used to model damping which is defined as

$$[C]=\alpha_m[M]+\beta_m[K], \tag{15}$$

where, α and β are mass and stiffness constants, respectively. In this example, the first two modes are used in order to find these damping coefficient, which is implemented into ANSYS Transient Structural.

2.5 Approximate Methods

In this part, approximate methods based on modal combination is introduced. In these methods, the maximum response of the antenna structure is estimated by combination of mass normalized eigenfunction coefficient, modal participation factor and dynamic constant obtained from shock response spectrum. Moreover, mass normalized eigenfunction coefficient is obtained by using a mode shape function of the antenna structure at a desired location. Furthermore, the modal participation factor shows effectiveness of a particular mode on the response [29]. Thus, the modal participation factor, Γ_n, of the antenna structure is given as [30]

$$\Gamma_n=\rho A\int_0^L \phi_n(x)\,dx, \tag{16}$$

where, ρ and A are uniform density and cross sectional area of an antenna structure, respectively and $\phi_n(x)$ is the mode shape of the n^{th} mode.

Absolute sum (ABS), square root of sum of squares (SRSS), naval research (NRL) and complete quadratic combination methods are examples of approximate methods. These methods are used to get maximum shock response of an antenna structure. The main advantage of these methods is their computational efficiency compared to transient analysis. Moreover,

these methods are conservative compared to transient analysis, since modal maximum responses are assumed to act simultaneously and have the same sign.

3 Case Studies

In this section, several case studies are conducted in order to analyze shock response of the antenna structure in detail. Moreover, linear and nonlinear ordinary differential equations are solved by Newmark method, which is also used in finite element software ANSYS.

Firstly, finite element method is compared with the linear continuous model. Consider the antenna structure given in Fig. 3 with constant cross section and uniform density. The antenna structure has 350mm length, 40mm width and 2mm thickness. Moreover, the antenna structure is made up of aluminum, the density and Young's modulus of which are $2700 kg/m^3$ and $70 GPa$, respectively. In addition to that, the antenna structure is subjected to 50G 11ms half sine mechanical shock which is the transportation shock for wheeled vehicle and aircraft according to International Standard IEC-60068-2-27 [31]. Acceleration responses of the antenna structure to the given input mechanical shock using reduced order model and finite element simulation are given in Fig. 7. It is observed that the result of ROM is in agreement with the result of the finite element method.

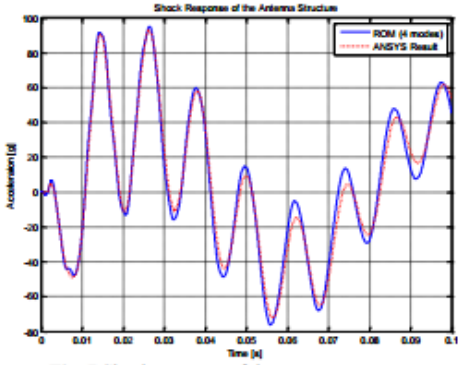

Fig. 7 Shock response of the antenna structure

In nonlinear finite element analysis, there are some drawbacks which affect shock response of an antenna structure. One of them is Rayleigh damping, which depends on mass and stiffness matrices as seen from Eq. (15). Using constant β_m leads to undesirable results in the nonlinear analysis, since ANSYS updates stiffness matrix for each iteration. Therefore, β_m constant can not be used in nonlinear analysis. In this case study, damping is assumed to be zero and artificial damping is introduced as 0.5.In Newmark method, the amount of numerical dissipation is controlled by artificial damping. Furthermore, this damping leads to reduction of numerical errors. Linear and nonlinear shock responses of the antenna structure are compared in Fig. 8. According to the results obtained, nonlinearity reduces the shock response of the antenna structure significantly.

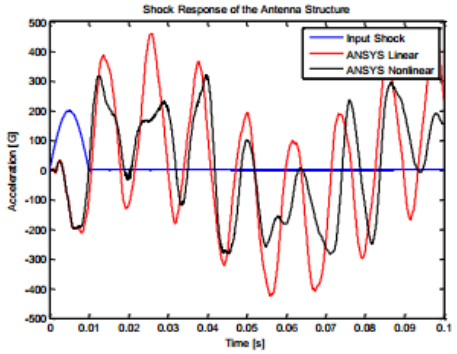

Fig. 8 Linear and nonlinear shock response of the antenna structure

Nonlinear mathematical model used in this study is validated by Ref. [16]. Younis et al. [16] studied nonlinear analysis of the cantilever MEMS under mechanical shock. The maximum nondimensional deflection versus shock amplitude graph given in [16] is used to validate the nonlinear mathematical model used in this study. Consider the cantilever MEMS, whose length, thickness and width are $L = 100\mu m$, $h = 0.1\mu m$ and $b = 10\mu m$, respectively. The cantilever MEMS is made up of silicon, whose density and Young's modulus are $2332 kg/m^3$ and $169 GPa$, respectively. The results obtained are compared with the ones given in [16] in Fig. 9 and Fig. 10b. The results obtained is in well agreement with the ones given in [16]; hence, the nonlinear model and the solution method used are validated.

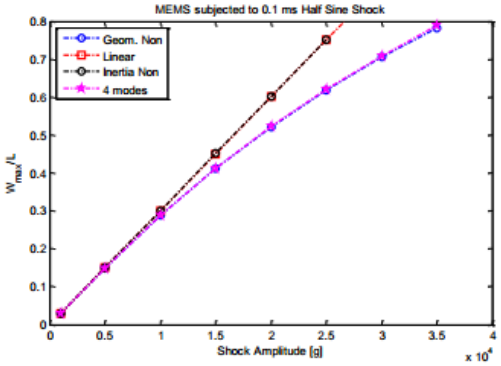

Fig. 9 Calculated shock response of the cantilever MEMS

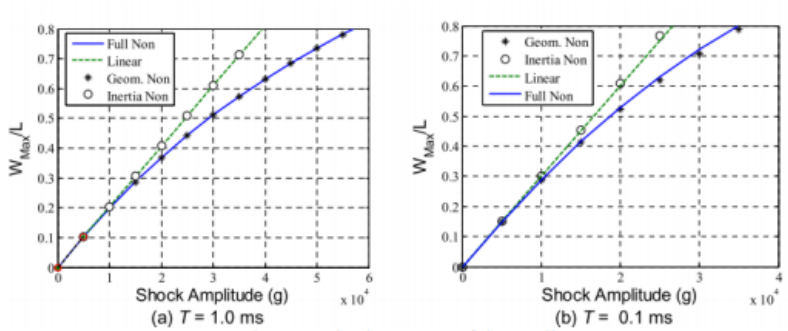

Fig. 10 The paper shock response of the cantilever [16]

The maximum relative displacement and acceleration tip response of an antenna structure is critical for design, since PCB, which is placed on the tip of an antenna structure, is sensitivity to the amplitude of the mechanical shock. Therefore, plot of the maximum response of the antenna structure vs. shock amplitude gives a better idea in terms of durability of the antenna structure. It can be observed from Fig. 11 and Fig. 12, both acceleration and relative displacement responses of the antenna structure is reduced when geometric nonlinearity is considered. Moreover, approximate methods can be used as a starting point of shock analysis of an antenna structure. Although approximate methods give conservative results compared to linear transient counterparts, computation time is significantly reduced. Furthermore, equivalent lumped mass model leads to enormous error in this case study, since the second, the third and the fourth modes also contribute to the shock response of the antenna structure in addition to the first mode. In other words, acceleration response of the antenna structure is composed of the first, the second, the third and the fourth modes of the structure which can be deduced from Fig 13.

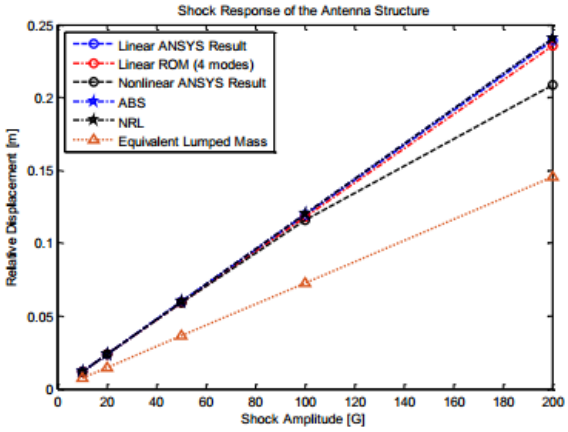

Fig. 11 Maximum acceleration response of the antenna structure

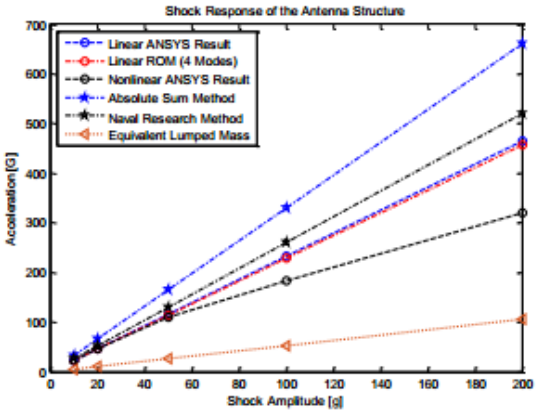

Fig. 12 Maximum relative displacement of the antenna structure

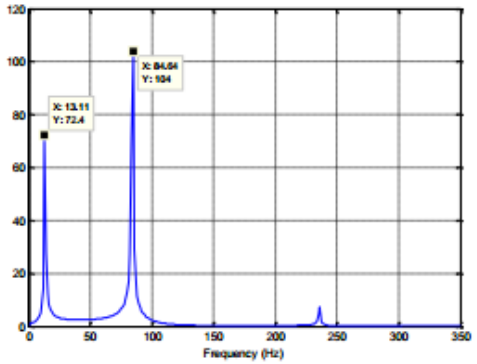

Fig 13 Frequency content of acceleration response of the antenna structure

4 Conclusion

In this study, shock response of an antenna structure including geometric nonlinearity is investigated. Firstly, lumped mass model of an antenna structure is studied. Although lumped mass model is a fundamental and computationally efficient model, this is not applicable for case studies where contribution of the modes higher than the first mode cannot be neglected. Therefore, modeled continuous beam model by using Euler-Bernoulli beam theory results in highly accurate results due to the fact that the effects of higher modes can as well be retained in the solution. Although both linear reduced order model (ROM) and finite element model are in agreement with each other, ROM is computationally very efficient, since a fine mesh is required in order to capture the propagation of shock wave properly. However, this leads to increased solution times. Furthermore, geometric nonlinearity plays an important role on shock response of an antenna structure, since many antenna structures have larger dimension in longitudinal direction. It is interesting to note that geometric nonlinearity reduces both relative displacement and acceleration response, especially in the case of high shock acceleration. It is similar to the case where as if shock isolator is used. In other words, when the antenna structure is modeled properly including geometric nonlinearity, response is similar to the case where an antenna structure is modeled by linear theory including shock isolator. Therefore, nonlinear modeling can eliminate the usage of shock isolator. It can be concluded that approximate methods are inherently conservative methods and may be used as a starting point of shock analysis due to their little computation time.

References

[1] Internet Live Stats, "Number of Internet Users (2014) - Internet Live Stats," 2014. [Online]. Available: http://www.internetlivestats.com/internet-users/. [Accessed: 01-Jun-2015].
[2] F. Wikipedia, "List of countries by number of mobile phones in use," Notes, 2011. [Online]. Available: https://en.wikipedia.org/wiki/List_of_countries_by_number_of_mobile_phones_in_use. [Accessed: 01-Jun-2015].
[3] R. A. Poisel, Antenna Systems and Electronic Warfare Applications. Norwood: Artech House, 2012
[4] Y. Huang and K. Boyle, Antennas: From Theory to Practice, First Edit. John Willey and Sons Ltd, 2008.
[5] J. E. Alexander, "Shock Response Spectrum – A Primer," Sound Vib., no. June, pp. 6 – 14, 2009.
[6] C. Lalanne, Mechanical Shock: Mechanical Vibration and Shock Analysis, Volume 2. John Willey and Sons Ltd, 2009.
[7] "Department of Defense Test Method Standard Environmental Engineering Considerations and Laboratory Tests," 2008.
[8] J. Eriksson and W. Kropp, "Measuring and Analysis of Pyrotechnic Shock," CHALMERS UNIVERSITY OF TECHNOLOGY, 1999.
[9] M. C. S. Reddy and J. Hussain, "Structural Analysis of Dipoloop Antenna Radome for Airborne Applications," Int. J. Eng. Res. Technol., vol. 4, no. 03, pp. 724–735, 2015.
[10] A. V. Lopatin and E. V. Morozov, "Modal analysis of the thin-walled composite spoke of an umbrella-type deployable space antenna," Compos. Strucute, vol. 88, no. 1, pp. 46–55, 2009.
[11] H. Su, "Structural Analysis of Ka-Band gimbaled antennas," COM DEV Ltd, Ontario, p. 15.
[12] T. Sreekantamurthy, T. Mann, V. Behun, J. C. Pearson, S. Scarborough, A. Engineer, and S. Aerospace, "Nonlinear Structural Analysis Methodology and Dynamics Scaling of Inflatable Parabolic Reflector Antenna Concepts," Am. Inst. Aeronaut. Astronaut., no. April, pp. 1–15, 2007
[13] M. I. Younis, F. M. Alsaleem, R. Miles, and Q. Su, "Characterization of the performance of capacitive switches activated by mechanical shock," J. Micromechanics Microengineering, vol. 17, no. 7, pp. 1360–1370, 2007.
[14] G. X. Li and F. a. Shemansky, "Drop test and analysis on micro-machined structures," Sensors Actuators, A Phys., vol. 85, no. 1, pp. 280–286, 2000.
[15] M. I. Younis, R. Miles, and D. Jordy, "Investigation of the response of microstructures under the combined effect of mechanical shock and electrostatic forces," J. Micromechanics Microengineering, vol. 16, no. 11, pp. 2463–2474, 2006.
[16] M. I. Younis and H. N. Arafat, "Investigation of the Effect of Nonlinearities on the Response of Cantilever Microbeams under Mechanical Shock and Electrostatic Loading," Soc. Exp. Mech., pp. 5–10, 2008.
[17] M. I. Younis, F. Alsaleem, and D. Jordy, "The response of clamped-clamped microbeams under mechanical shock," Int. J. Non. Linear. Mech., vol. 42, no. 4, pp. 643–657, 2007.
[18] C. Liang, M. Yang, and Y. Tai, "Prediction of shock response for a quadrupod-mast using response spectrum analysis method," Ocean Eng., vol. 29, no. 8, pp. 887–914, 2002.
[19] J. E. Alexander, "Nonlinear System Mode Superposition Given a Prescribed Shock Response Spectrum Input," Proc. Int. Modal Anal. Conf. - IMAC, no. 3, pp. 346–355, 2002.
[20] M. I. Younis, D. Jordy, and J. M. Pitarresi, "Computationally Efficient Approaches to Simulate the Dynamics of Microbeams Under Mechanical Shock," IMECE 2006 2006 ASME Int. Mech. Eng. Conf. Expo., vol. 16, no. 3, pp. 628–638, 2006.
[21] A. Erturk and D. J. Inman, "On Mechanical Modeling of Cantilevered Piezoelectric Vibration Energy Harvesters," J. Intell. Mater. Syst. Struct., vol. 19, no. 11, pp. 1311–1325, 2008.
[22] W. T. Thomson and M. D. Dahleh, Theory of Vibration and Applications, Fifth Edit. PEARSON EDUCATION, 1998.
[23] T. Irvine, "Bending frequencies of beams, rods, and pipes," Available on the web on site: http://www. vibrationdata.com. pp. 1–61, 2012.
[24] L. Majkut, "Free and Forced Vibrations of Timoshenko Beams Described by Single Difference Equation," J. Theor. Appl. Mech., vol. 47, no. 1, pp. 193–210, 2009.
[25] M. I. Younis, MEMS Linear and Nonlinear Statics and Dynamics. Springer, 2011.
[26] J. K. Yee, H. H. Yang, and J. W. Judy, "Shock resistance of ferromagnetic micromechanical magnetometers," Sensors Actuators, A Phys., vol. 103, no. 1–2, pp. 242–252, 2003
[27] P. L. Gatti and V. Ferrari, Applied Structural and Mechanical Vibrations, First Edit. Taylor & Francis Group, 1999
[28] "ANSYS 15 Help Viewer," 2014
[29] E. H. Abed, D. Lindsay, and W. a. Hashlamoun, "Thechnical Report On participation factors for linear systems," Automatica, vol. 36, no. 10, pp. 1489–1496, 1999.
[30] T. Irvine, "Effective Modal Mass and Modal Participation Factors," Vibrationdata, no. 1, pp. 1–36, 2013
[31] "International Standard-IEC 60068-2 -27." Basic Safety Publication, p. 80, 2008.